DIFFERENTIAL IDENTIFICATION OF GENES RELATED TO IMPLANTATION PROCESS VIA USE OF CRISPR/Cas9

by

Gizem SÖYLER

A Dissertation Submitted to the
Graduate School of Health Sciences in Partial
Fulfillment of the Requirements for the Degree

of

Doctor of Philosophy
in
Reproductive Medicine

KOÇ ÜNİVERSİTESİ

January 29, 2024

DIFFERENTIAL IDENTIFICATION OF GENES RELATED TO IMPLANTATION PROCESS VIA USE OF CRISPR/Cas9

Koc University

Graduate School of Health Sciences

This is to certify that I have examined this copy of a doctoral dissertation by

Gizem Söyler

and have found that it is complete and satisfactory in all respects,
and that any and all revisions required by the final
examining committee have been made.

Committee Members:

Assist. Prof. Dr. Serçin Karahüseyinoğlu (Advisor)

Prof. Dr. Özgür Öktem

Prof. Dr. Ceyda Açılan Ayhan

Prof. Dr. Sevinç İnan

Assoc. Prof. Dr. Şule Ayla

Date: January 29, 2024

To all Phoenixes on the way of science

“Sometimes you just have to die a little inside
in order to be reborn and rise again
as a stronger and wiser version of yourself!”
-Erica Coppola

ABSTRACT

Differential Identification of Genes Related to Implantation Process via Use of CRISPR/Cas9

Gizem SÖYLER
Doctor of Philosophy in Reproductive Medicine
January 29, 2024

Implantation failure occurs when chorionic gonadotropin secreted by trophoectoderm cells is not produced during the invasion of the embryo into the endometrium, or if it is produced, it cannot form the gestational sac. Even in spontaneous pregnancies where assisted reproductive techniques are not applied, the probability of implantation failure on the first attempt varies between 25-40%. This project aims to elucidate the activity, interactions, temporal and cell type-dependent variability of genes affecting implantation, changes in *in vitro* conditions, and their effects on implantation using the efficient CRISPR/Cas9 genome editing method.

To achieve this goal, samples were collected at 24 and 72 hours from blastocysts incubated in *in vitro* three-dimensional culture environment in different experimental groups. RNA sequence analysis was performed on these samples and active genes were revealed. For each identified active gene, silencing was performed separately on endometrial epithelial cells and endometrial stroma cells using the CRISPR/Cas9 method. In vitro implantation parameters were examined for each group.

The study focused on Hmga2 in endometrial epithelial cells, Uxs1 genes in stromal cells, and Gm15452 genes (a pseudogene) in both epithelial and stromal cells. Knockout of these genes using the CRISPR/Cas9 method caused significant changes in the relevant genes identified as adhesion, invasion, and developmental and functional implantation parameters.

Knockout of Hmga2 in epithelial cells revealed significant changes in E-Cadherin, Fibronectin, LIF, Mmp9, and Wnt4 genes at different time groups. Knocking out of Gm15452 in epithelial cells led to significant changes in E-Cadherin and LIF expressions. Uxs1 knockout in stroma cells affected the expressions of E-Cadherin, LIF,

and Mmp9, while Gm15452 knockout in stroma cells significantly affected the expressions of E-Cadherin, LIF, and Mmp9.

Keywords: Implantation, CRISPR/Cas9, 3D culture, Mouse, RNA sequence

ÖZETÇE

İmplantasyon Süreciyle İlgili Genlerin CRISPR/Cas9 Kullanımıyla Diferansiyel Tanımlaması

Gizem SÖYLER
Üreme Tıbbı Doktora Programı
Ocak 29, 2024

İmplantasyon başarısızlığı, embriyonun endometriyuma invazyonu sırasında trofoektoderm hücreleri tarafından salgılanan koryonik gonadotropinin üretilmemesi veya üretildiği takdirde gebelik kesesini oluşturamaması durumunda ortaya çıkar. Yardımcı üreme teknikleri uygulanmayan spontan gebeliklerde bile ilk denemede implantasyonun başarısızlıkla sonuçlanma olasılığı % 25-40 arasında değişmektedir. Bu proje, etkili CRISPR/Cas9 genom düzenleme yöntemini kullanarak implantasyonu etkileyen genlerin aktivitesini, etkileşimlerini, zamansal ve hücre tipine bağlı değişkenliğini, in vitro koşullardaki değişiklikleri ve bunların implantasyon üzerindeki etkilerini açıklamayı amaçlamaktadır.

Bu amaca ulaşmak için farklı deney gruplarında *in vitro* üç boyutlu kültür ortamında inkübe edilen blastokistlerden 24. ve 72. saatlerde örnekler toplandı. Bu numuneler üzerinde RNA dizi analizi yapıldı ve aktif genler ortaya çıkarıldı. Tanımlanan her aktif gen için, CRISPR/Cas9 yöntemi kullanılarak endometriyum epitel hücreleri ve endometriyum stroma hücreleri üzerinde ayrı ayrı susturma gerçekleştirildi. Her grup için *in vitro* implantasyon parametreleri incelendi.

Araştırmada endometriyum epitel hücrelerinde Hmga2'ye, stroma hücrelerde Uxs1 genlerine ve hem epitel hem de stroma hücreleinrde Gm15452 genlerine (bir psödogen) odaklanıldı. Bu genler için genomun CRISPR/Cas9 yöntemi kullanılarak düzenlenmesi, adezyon, invazyon ve gelişimsel ve fonksiyonel olmak üzere implantasyon parametreleri olarak tanımlanan ilgili genlerde önemli değişikliklere neden oldu.

Epitel hücrelerinde Hmga2 nakavtının, farklı zaman gruplarında e-kaderin, fibronektin, LIF, Mmp9 ve Wnt4 genlerinin farklı zaman gruplarında anlamlı olarak değiştiği; epitel hücrelerinde Gm15452 nakavtının, e-kaderin ve LIF ifadelerinde önemli değişikliklere yol açtığı; stroma hücrelerinde Uxs1 nakavtının, e-kaderin, LIF ve Mmp9

ekspresyonlarını etkilerken, stroma hücrelerinde Gm15452 nakavtının, e-kaderin, LIF ve Mmp9 ekspresyonlarını önemli ölçüde etkilediği belirlenmiştir.

Anahtar Kelimeler: İmplantasyon, CRISPR/Cas9, 3B Kültür, Fare, RNA dizileme

ACKNOWLEDGMENTS

I would like to thank everyone who supported me throughout my PhD education adventure and thesis study.

First of all, I would like to thank my thesis advisor Dr. Serçin Karahüseyinoğlu. I am grateful for accepting me as a member of her team, giving me the opportunity to do this thesis, and allowing me to grow not only academically but also as a person. Her problem-solving approach, hardworking personality, and commitment to life will always be exemplary behavior for me in the future.

I would like to express my sincere gratitude to Prof. Dr. Özgür Öktem and Prof. Dr. Ceyda Açılan Ayhan, who were on my thesis monitoring committee, as well as Prof. Dr. Sevinç İnan and Assoc. Prof. Dr. Şule Ayla, my thesis committee members, for their valuable contributions and comments to improve my study.

The study was supported under TUBITAK 1001 support as project number 118S676 and I would like to thank TUBITAK for this financial support. This support is one of the important investments made not only for me but also for the advancement of scientific research.

I would like to express my sincere gratitude to Assoc. Prof. Dr. Ali Cihan Taşkın and Ahmet Kocabay, and then to Nilhan Coşkun and her team Muhammed Reşat Oğuzkan Yaralı, Mustafa Demir, Emre Uğur and Elif Abla, for their unwavering support in animal studies.

I would like to thank KUTTAM for the infrastructure and equipment provided. I would also like to thank Uğur Çerez, Güven Ayvaz and Ergün Başoğlu. I am grateful to them for their sympathetic attitude and immediate support with a cheerful approach whenever needed. I would also like to thank our kitchen staff, Fatma Abla, for her pleasant conversation and motherly approach.

I would like to thank the doctor of molecular biology, Dr. Alişan Kayabölen, and the king of sorting, Dr. Özgür Albayrak, for sharing their knowledge, experience, and help during the study.

I owe a special debt of gratitude to my teammates. I would like to thank Yağmur Ergün for sharing cell culture knowledge and techniques and Aylin Seren Güller for her kind attitude. I would like to thank the best teammate I've ever worked with, Mehmet Yunus Çomar, not only for his support in my thesis study but also for the fun times we spent

together. I would like to sincerely thank my last term teammates, İpek Yılmaz Düzgün, Ariana Sivaslıoğlu, Mehmet Eren Çiftçi, and Rüya Sera Polat, for giving me the best team ever and for all the support that they have made.

My companion, Alihan Erdağı, and I sometimes cried together, sometimes laughed together, and sometimes worked together. I am grateful for his support in both good and bad times.

I would like to sincerely thank my dear siblings I made after I turned 30, Canan Bayraktar and Arda Odabaş, not only for their knowledge and support during my doctoral education, but also for always being there for me, good or bad, and for all the fun moments we have had.

I am grateful to Kardelen Yangın for her friendship, which started as an event friend and turned into a huge friendship. Her warm heart always deserves to be happy. I am sure that new routes will be created for us in the future.

I would like to thank Begüm Durkut for her sage tea talks, kitchen activities, and unconditional help in the lab. I would like to thank Burak Sarıbaş for deep book conversations and absurd sense of humor, which kept us on the floor laughing for hours. My good-hearted, positive friend Özen Leylek, even though we could not spend much time in the lab, she was always on the other side of the phone, I would also like to thank her for her moral support. I thank Mükrime Altun, whom I had the opportunity to meet recently, for her sympathetic attitude, and helpful and thoughtful approach. I want to thank my former homemate, Hilal Dilşad Arabacı, for making the challenging times of the pandemic more enjoyable. I also would like to thank Sercan Güloğlu, Ghazal Nariman, İrem Akbulak, Hümeyra Nur Kaleli, Dilara Aydemir, Hacer Begüm Saka, Ceyda Nur Altınışık and Ömer Can Ergül, for the happy memories they left behind. I would like to spend more time if I had the opportunity.

I am grateful to my unfading timeless friends Merve Yalçındağ and Meryem Betmezoğlu, for their support in every situation and condition.

And I am eternally grateful to my parents and brother who provided all kinds of financial and moral support. It's almost like they did a thesis study with me. Without them, this journey would have been much more challenging. Expressing my gratitude to them is only partially possible with words.

TABLE OF CONTENTS

LIST OF TABLES

LIST OF FIGURES

ABBREVIATIONS

ART	Assisted Reproductive Technology
BSA	Bovine Serum Albumin
Cas9	CRISPR Associated Protein 9
CK18	Cytokeratin 18
CRISPR	Clustered Regularly Interspaced Short Palindromic Repeats
crRNA	CRISPR RNA
CT	Cycle Threshold
DEGs	Differentially Expressed Genes
DMEM	Dulbecco's Modified Eagle's Medium
DPBS	Dulbecco's Phosphate Buffered Saline
DSB	Double Strand Break
E2	Estradiol
ECM	Extracellular Matrix
EDTA	Ethylenediamine Tetraacetic Acid
ER	Estrogen Receptor
FACS	Fluorescence-Activated Cell Sorting
FBS	Fetal Bovine Serum
FCS	Fetal Charcoal Stripped Serum
FMC	Fluorescent mCherry
GAPDH	Glyceraldehyde 3-Phosphate Dehydrogenase
GFP	Green fluorescent protein
HB-EGF	Heparin-Binding EGF-like Growth Factor
HBSS	Hanks' Balanced Salt Solution
hCG	Human Chorionic Gonadotropin
HDR	Homology-Directed Repair
Hoxa10	Homeobox Protein A10
IF	Immunofluorescent Staining
IGF	Insulin Like Growth Factor
IGFBP	Insulin-like Growth Factor-Binding Protein
IL	Interleukin
IVF	*in vitro* Fertilization
i.p.	Intraperitoneal Injection
i.u.	International Unit
KO	Knock Out
LB	Luria-Bertani
LIF	Leukemia Inhibitory Factor
LV	Lentivirus
MMP	Matrix Metalloproteinase
MOI	Multiplicity of Infection
MUC	Mucin

NFDM	Non-Fat Dry Milk
NHEJ	Non-Homologous End-Joining
NK	Natural Killer
NT	Non-Targeted
PAM	Protospacer Adjacent Motif
PEG	Polyethylene Glycol
PFA	Paraformaldehyde
PMSG	Pregnant Mare Serum Gonadotropin
P4	Progesterone
PR	Progesterone Receptor
PRL	Prolactin
PS	Protamine Sulphate
PURO	Puromycin
qRT – PCR	Real Time Polymerase Chain Reaction
RIF	Recurrent Implantation Failure
RNA Seq	RNA Sequencing
RT	Room Temperature
SDS–PAGE	Sodium Dodecyl Sulfate-Polyacrylamide Gel Electrophoresis
sgRNA	Single Guide RNA
uNK	Uterine Natural Killer
Vim	Vimentin
Wnt4	Wnt Family Member 4
WOI	Window of Implantation
ZP	Zona Pellucida
2D	Two Dimensional
3D	Three Dimensional

Chapter 1
INTRODUCTION

1.1 Structural Features of The Uterus

The quickly developing morula leaves the uterine tube and reaches the uterus. This journey is necessary for every successive stage of fetal and embryonic development that will take place inside the uterus. The uterus is a muscular, pear-shaped, hollow organ with thick walls in the pelvis between the rectum and the bladder. The organ is 7.5 cm in length, 5 cm in width at its superior aspect, 2.5 cm in thickness, and 30–40 g in weight in a fertile woman. Because it is mobile, its position varies with the distension of the bladder, and the rectum also undergoes dramatic increases in size and development as a result of possible pregnancies [1],[2].

Two parts anatomically characterize the uterus. Firstly, the muscular body, constituting the superior two-thirds, extends from the fundus to the cervix. The fundus, located above the attachment of the uterine tubes, defines the upper, rounded region of the uterine body. Secondly, the cervix forms the cylindric inferior one-third of the uterus. The cervical canal, a component of the cervix, exhibits a constricted opening at each end. Principally, the internal os connects with the uterine cavity, while the external os opens into the vagina [2],[3].

The uterine wall is composed of three distinct layers. The innermost layer, the endometrium, constitutes the mucosal lining of the uterus. Adjacent to the endometrium is the myometrium, a robust muscular layer that seamlessly extends into the uterine tube and vagina. The myometrium is characterized by three loosely defined smooth muscle layers, inner and outer longitudinal or oblique, and central circular. To accommodate the growing fetus, the undergoing of the myometrium to hypertrophy and hyperplasia is crucial during pregnancy. The outermost layer, the perimetrium, represents a peritoneal layer firmly adhered to the myometrium. This serous layer forms a continuous connection with the pelvic and abdominal peritoneum and comprises mesothelium and a thin layer of loose connective tissue. While the perimetrium envelops the entire posterior surface of the uterus, it partially covers the anterior surface, with the

remaining portion characterized by connective tissue, or adventitia. Both the myometrium and endometrium undergo cyclic alterations with the menstrual cycle, to prepare the uterus for potential implantation [2]–[4].

1.2 Structure of The Endometrium

The endometrium is the region surrounding the innermost part of the uterus close to the lumen and is important for embryo implantation and subsequent development. The structure and characteristics of the endometrium vary depending on the uterine cycle. If an unfertilized oocyte is encountered at the end of each menstrual cycle, it is shed (menstruation) and rebuilt at the beginning of the new cycle[2],[4].

A completed normal endometrium is 4-5 mm thick and the surface facing the uterine cavity is lined by a single-layer columnar epithelium. The cells on the epithelial surface are observed in two different ways: ciliated or secretory. The lamina propria part is accompanied by a large quantity of fibroblast cells, type III collagen fibers, and ground substance. There are also tubular uterine glands located in the region [3],[5].

Throughout the reproductive period, in terms of structure and function, the endometrium is divided into two layers or two regions: the functional layer, which forms the upper two-thirds, close to the lumen, and the basal layer, which forms the lower third. The functional layer has a spongy structure and is rich in ground substance. It is the part where the uterine glands are elongated and getting denser. The thickness of the endometrium varies from 1 mm to 6 mm during the menstrual cycle, and this occurs due to expansion of the glands and increase in the vascularity of the functional layer related to hormone expression and active/dense secretion. It is the layer that is shed if implantation does not take place. The basal layer is close to the myometrium and forms the dense, cellular lamina propria. It not only contains the deep basal endings of the uterine glands, but also forms the area where the main blood vessels feeding the endometrium enter. For this reason, the basal layer serves as the regeneration source of the functional layer at the beginning of the new cycle and its size almost does not change during menstruation [2],[5].

1.3 Preimplantation Embryo Development

Starting from the formation of the zygote, the embryo undergoes a series of rapid division and cellular proliferation, called as the cleavage divisions, while it moves along

the uterine tube and is carried to the uterus (Figure 1)[6]. From the early stages of cleavage until the 8-cell stage, the embryo develops in the environment where pyruvate and lactate are concentrated in the uterine tubes. After 8-cell stage, the embryo needs a glucose-rich environment, and the uterus plays an active role in providing it with this opportunity. Likewise, cells formed up to the 8-cell stage are essentially spherical in structure, loosely interconnected, and lack intercellular junctional complexes and significant extracellular matrix. Starting from the 8-cell stage, the embryo begins to form a compacted structure. Cells become flatter, as intercellular gaps and tight junctions begin to form. When it reaches the 16-cell stage, compartmentalization occurs between the cells; some cells form the outer cell mass, while the others are assigned to form the inner cell mass. When the embryo reaches 32 cells, compartmentalization becomes completed. Tight junctions between cells in the outer polar region are increased and can be structurally distinguished from the inner group. At this stage, fluid begins to collect into the structure formed and the transition from the morula stage to the blastocyst stage begins. When the blastocyst stage is completed, the trophoblastic cells formed by the outer cell mass and the embryoblasts formed by the inner cell mass can be distinguished. At the same time, a new compartmentalization has occurred in the trophoectodermal region. The trophoblasts close to the inner cell mass form polar trophoblasts, which will also take part at the beginning of implantation and are in contact with embryoblasts, while the remaining part forms mural trophoblasts [3].

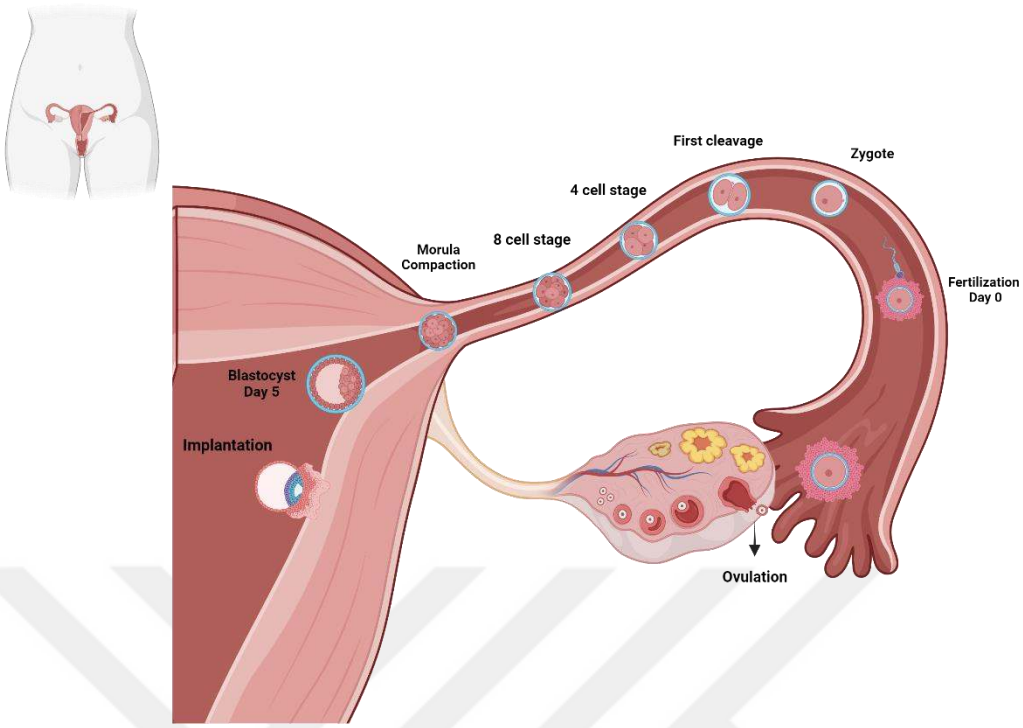

Figure 1. Visual demonstration of embryo development. (Generated via BioRender.com)

1.4 Implantation, Stages, and Necessary Elements

Implantation is a fundamental process in embryonic development that comprises sequential events such as apposition, adhesion, and invasion into the endometrium[7]. The blastocyst initiates apposition by establishing a suitable location for contact with the endometrial luminal epithelium, and a robust physical bond forms between the two. The initial loose connection during apposition transitions into a more secure attachment. This attachment enables the trophoblastic cells to adhere firmly to the uterine epithelium, facilitating the subsequent invasion. The invasion process would be crucial for the continued growth, development, and nourishment of the blastocyst which begins to invade the uterine stroma until successful implantation occurs within the endometrium. The implantation process requires effective bidirectional interaction between the embryo and the endometrium, which is supported by a series of morphological, biochemical, and genetic modifications orchestrated by hormones, cytokines, growth factors, and adhesion molecules (Figure 2)[8].

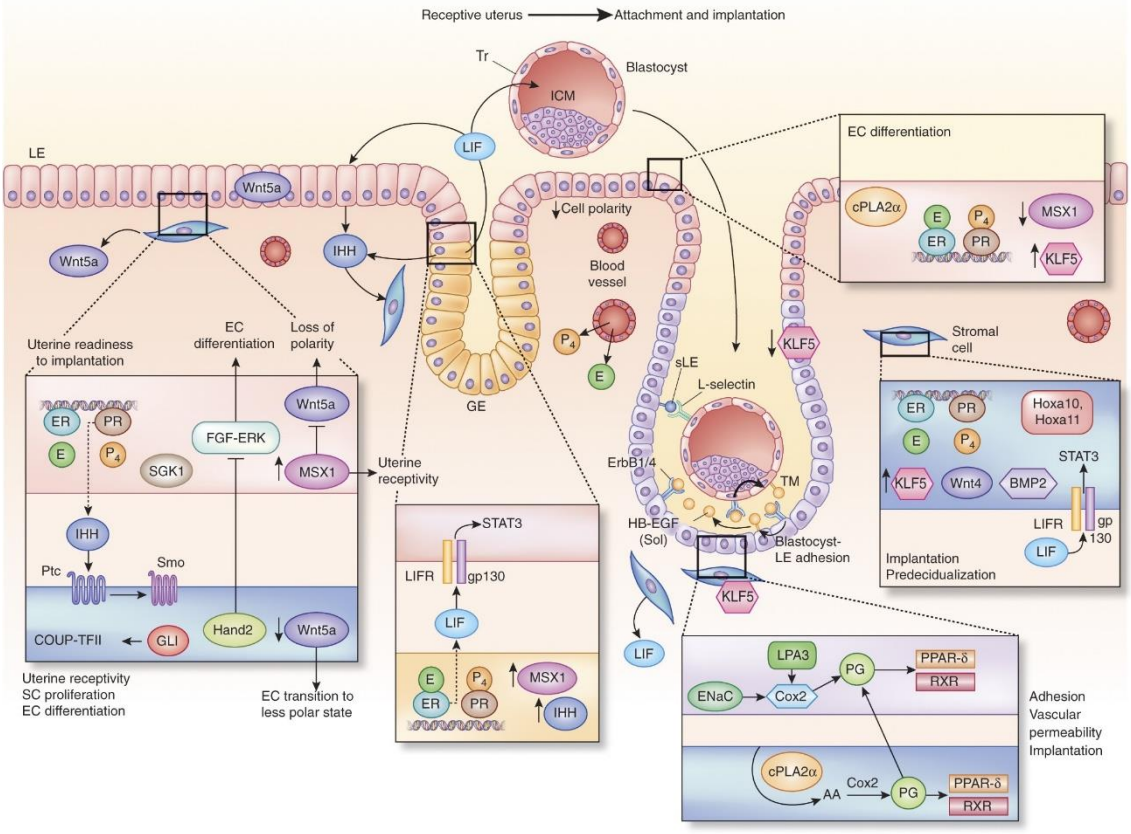

Figure 2. Signaling network for uterine receptivity and implantation. Expression of molecules for uterine receptivity, implantation, and decidualization are shown[9].

1.4.1Blastocyst Competency

Early embryo enters the uterine cavity in the morula stage and reaches the 32- to 256-cell blastocyst. Implantation begins with hatching, known as the loss of the zona pellucida. The active blastocyst undergoes structural changes. Just before the time of hatching, epiblast signals promote differentiation of the polar trophectoderm. Trophoblastic cells lose the cell cycle genes, and primitive syncytiotrophoblast markers begin to be expressed. Consequently, human embryos are oriented for the polar trophectoderm attached to the endometrial epithelium[10],[11].

1.4.2Window of Implantation

During the proliferative phase, estrogen levels are increased by the ovarian follicles, and this rise promotes the increasing thickness of the endometrium. Throughout the secretory phase of the endometrium, which also coincides with the luteal phase of the ovary, progesterone secretion increases. The release of the progesterone hormone

facilitates changes in the endometrium, that makes it possible for the embryo to get implanted. In the fertile women, implantation occurs 7–10 days after ovulation; this limited time for implantation to occur is called the window of implantation (WOI)[12]–[14].

1.4.3 Endometrial Receptivity

The physiological condition in which the endometrial epithelium permits the trophoblast cells to adhere and infiltrate into the uterine stroma is known as endometrial receptivity. The endometrium is only receptive for a certain time, thus the embryo must arrive on time[15]. Structural and functional modifications of the uterus is necessary for successful implantation. Estrogen and progesterone are two major hormones mediating these changes[16]. During WOI, cellular changes as decidualization, the transformation of the fibroblast-like endometrial stromal cells into larger and rounder decidual cells, take place. The secretory phase of the endometrium can be distinguished by using the Noyes criterion. Histologically, this phase is marked by the glands taking on a sawtooth appearance and establishing highly irregular patterns. The uterine stroma becomes more edematous and softer as vacuolization progresses, giving the structure thicker appearance. The emergence of large apical protrusions (pinopodes), formation of microvilli on the luminal epithelium, is the observable marker of receptivity. Membrane projection is formed by the fusion of pinopodes, and this increases the surface area between the endometrium and the blastocyst[17].

1.4.4 Decidualization

An essential step in the implantation and the embryonic development cascade is the decidualization process in the endometrium. Although progesterone plays a critical role in maintaining decidual gene expression, it is not enough to start the differentiation process on its own[18]. Several vascular changes, including vascular leakage, angiogenesis, and the recruitment of immune cells, are indicative of this complex transition. The decidualization of stromal cells plays a key role in orchestrating the transformation of natural killer (NK) cells into uterine NK (uNK) subsets, which exhibit intrinsic tolerance to the invading trophoblast cells and contribute significantly to vascular remodeling through the secretion of cytokines and angiogenic factors. Morphologically, decidualized stromal cells undergo distinct changes as, transitioning

from a spindle-shaped form to an enlarged, polygonal, or round, polyploid, epithelioid style. Increases in organelles like ribosomes, lysosomes, mitochondria, and microfilaments as well as the accumulation of lipids and glycogen in the cytoplasm are examples of the ultrastructural alterations. Significant changes occur in both proteomic and genetic mechanisms during this transition. Prolactin (PRL) and insulin-like growth factor binding protein (IGFBP) are two indicators of the molecular changes linked to the upregulated decidualization. Decidualized stromal cells also actively contribute to the remodeling of the extracellular matrix (ECM) by secretion of important constituents such as collagen IV, fibronectin, laminin, and alpha-smooth muscle actin.

1.4.5 Molecules and Structures Involved in Implantation

During implantation, some proteins, molecules, and structures are formed through the regulations of estrogen and progesterone, in a cycle-dependent manner. Many of these formations show an increase in expression, which eventually plays a prominent role during the process.

Leukemia Inhibitory Factor (LIF): Leukemia inhibitory factor (LIF), a member of IL-6 cytokine family, plays a pivotal role in multiple aspects of embryo implantation, such as embryo invasion, stromal differentiation, proliferation, and invasion via various signaling pathways[19]. In mice, LIF peaks in the endometrial glands during ovulation, ensuring the transformation of the endometrium for implantation and mediating endometrial receptivity. LIF-deficient female mice show signs of unsuccessful implantation. The absence of LIF causes an increase in glycocalyx and implantation failure[20]. In humans, LIF expression is prominent in the mid-luteal phase and uterine luminal fluid during this phase. Furthermore, LIF regulates immune responses, impacting uterine leukocyte subpopulations. In terms of embryo-endometrial interaction, LIF aids in pinopode formation and induces the expression of adhesion molecules like JAM-2[21],[22].

Insulin-like Growth Factor Binding Protein 1: Endometrial stromal cells produce insulin-like growth factors I and II (IGF-I and IGF-II) and high-affinity IGF-binding proteins (IGFBPs). All six high-affinity IGFBPs are expressed in human endometrium, with IGFBP-1 being the most abundant. IGFBP-1 is secreted by pre-decidualized

endometrial stromal cells under the influence of progesterone[23]. This protein serves as both a marker for decidualization and a paracrine/autocrine factor involved in the cascade of events from implantation to normal fetal outcome. Insulin-like growth factor binding protein-1 (IGFBP-1) plays a versatile role in human female reproductive physiology, contributing to various stages from menstrual cycles to fetal growth[24]. During the endometrial stromal differentiation process, insulin-like growth factor binding protein-1 (IGFBP-1) is produced by the decidualized endometrium and it inhibits the action of IGF-I, which causes estrogen-induced proliferation of endometrium by limiting its binding to the receptor[25]. IGFBP-1 also exhibits IGF-independent actions by interacting with α5β1 integrin on the cell surface, stimulating cell migration and adhesion[26].

Mucin-1: In the apposition phase of implantation, the blastocyst establishes loose physical contact with the receptive endometrium before firmly adhering to its surface [27]. Membrane-associated MUC1, a glycoprotein abundant during the implantation window, serves as a biochemical marker for endometrial receptivity. It has higher expression in fertile women compared to infertile counterparts, localized in both glandular and luminal epithelium. MUC-1 acts as a scaffold for L-selectin ligands, facilitating loose contact and blastocyst rolling over the endometrial surface[19].

2L-Selectin: Selectins are cell surface glycoproteins found on endothelial cells, leukocytes, and platelets, with roles in immune cell trafficking and various physiological and pathological processes. L-selectin is expressed on T and B lymphocytes and guides cells to secondary lymph nodes in adaptive immunity[28]. During the implantation, L-selectin ligands are significantly expressed in the endometrium. These ligand expression peaks occur during the receptive phase, contributing to the blastocyst-endometrium interaction. After the implantation process, L-selectin is detected in the cytotrophoblasts projecting into the decidua, and ligands shift to decidual cells, suggesting a role in cytotrophoblast penetration[29],[30].

Integrin & Fibronectin: Adhesion competence refers to the embryo's ability to adhere to the endometrial lining, which is a crucial step in the implantation process. Integrins, especially integrin α5β1 subunits on the surface of the blastocyst, play a crucial role in

this adhesion[31]. Expression of these integrins is increased at the apical surface of adhesion-competent blastocysts, facilitating a stronger interaction with fibronectin. Fibronectin, an extracellular matrix protein, promotes adhesion by acting as a bridge between integrins on the blastocyst and integrins on the endometrium. IGF1 has been found to positively affect this process by increasing apical fibronectin expression in blastocysts and increasing their binding to endometrial cells. The integrin-fibronectin axis regulated by IGF1 is emerging as a key mechanism affecting the adhesion competence of the blastocyst during implantation[32].

Entactin (Nidogen): Nidogen, also known as entactin, is a glycoprotein found in almost all basement membranes[33]. Two isoforms, nidogen-1 and nidogen-2, coexist in mammals[34]–[36]. Nidogen-1 participates in the assembly of basement membranes by acting as a bridge between laminin-1 and type IV collagen[37]. It has been shown to play a role in various cellular processes, including cell attachment, neutrophil chemotaxis, trophoblast growth, and angiogenesis[38]–[41]. During decidualization, implantation, and embryogenesis, both nidogen-1 and nidogen-2 are co-expressed in various uterine tissues. Nidogen-1 has been shown to protect laminin-1 against proteolytic cleavage and increase basement membrane stability. Immunolocalization studies show that nidogen-1 and nidogen-2 play a crucial role in the attachment of the blastocyst to the uterine luminal epithelium. Their expression coincides with the onset of decidualization, and they are involved in the removal of the basement membrane of the uterine epithelium during early pregnancy. Removal of nidogens from the basement membrane is suggested as a first step towards its degradation. Additionally, nidogen-1 and nidogen-2 are expressed in developing embryos, indicating their potential role in embryogenesis[42].

E-Cadherin: E-cadherin (E-cad) emerges as a key protein in maintaining integrity and plays a crucial role in the biogenesis of the uterine epithelium. Mice lacking Cdh1 (the gene encoding E-Cad) display disorganized uterine epithelium, highlighting the developmental necessity of E-Cad[43]. Dynamic changes in E-Cad expression occur during the menstrual cycle. Changes noted in the endometrial epithelium of infertile women reveal its importance in the adult endometrium[44],[45]. Beyond its role in epithelial biogenesis, E-Cad also contributes to the apicobasal polarity of the

epithelium, which is a prerequisite for directional secretory and absorptive functions. Stage-dependent changes are observed in the apico-lateral sequence of E-Cad. While widespread distribution is observed in the proliferative phase, lateral ordering is observed in the secretory phase and the expression is mediated by the steroid hormones. During embryo implantation, the endometrium undergoes extensive changes in response to mid-cycle estrogen increases and embryonic factors. While some studies report loss of E-Cad at the implantation site, others have found increased expression or higher apical sorting[46]–[48].

Pinopodes: Pinopodes are 5–10 μm cellular protrusions on the apical plasma membrane of uterine epithelial cells that are uniquely large compared to other epithelial protrusions and are particularly notable during the Window of Implantation (WOI)[49],[50]. Pinopodes are evolutionarily conserved structures found in mice, rats, and humans, and their formation has been associated with successful implantation[51],[52]. Ovarian steroid hormones estrogen and progesterone play a crucial role in regulating pinopode development[53]. Pinopodes undergo morphological changes during the menstrual cycle and are classified as developing, mature, and regressive. Their occurrence, which typically occurs around days 20-22 of the natural menstrual cycle, occurs during the luteal/secretory phase, which coincides with WOI[54]–[56].

Heparin-Binding Epidermal Growth Factor: The blastocyst and the maternal environment undergo complex communication during the implantation process, and HB-EGF (heparin-binding EGF-like growth factor) becomes involved in this conversation. Before attachment, HB-EGF expression is seen in the uterine luminal epithelium, demonstrating its critical function in preparing the maternal environment for eventual attachment. HB-EGF promotes trophoblast outgrowth, suggesting its involvement in trophoblast invasion during implantation. HB-EGF is identified as a mitogen for fibroblasts and smooth muscle cells, existing in both transmembrane and soluble forms. HB-EGF induces implantation-like responses, including increased vascular permeability and decidualization[57].

Homeobox A10: Homeobox A10 (HOXA10) emerges as a crucial regulator in the endometrium and implantation process, exerting its influence on various aspects of gene

expression and cellular functions. HOXA10, a DNA-binding transcription factor, plays a vital role in implantation, with its expression fluctuating throughout the menstrual cycle and peaking in the middle of the secretory phase[58]. Decreased HOXA10 expression is observed in the context of diseases associated with endometrial receptivity damage, such as endometriosis, adenomyosis, and hydrosalpinx[59]–[61]. In particular, HOXA10 has been found to regulate the expression of endometrial receptivity biomarkers, including integrin αvβ3 and insulin-like growth factor binding protein 1 (IGFBP1). The relationship between HOXA10 and E-cadherin was also investigated. It revealed lower expression levels of both HOXA10 and E-cadherin in patients with recurrent implantation failure (RIF) and unexplained recurrent miscarriages, and a positive correlation between the two. Also, the studies have revealed that during implantation, HOXA10 can directly bind to the E-cadherin gene promoter and thus regulate E-cad expression[62].

Wnt Signaling: Wnt signaling emerges as a critical player in both the endometrium and the complex implantation process, orchestrating important events in early pregnancy and embryonic development. During preimplantation embryonic development, Wnt ligands and receptors are present. Canonical Wnt signaling is indispensable for blastocyst formation. Non-canonical pathways are potentially important. Canonical Wnt signaling, particularly mediated by Wnt4, is central to blastocyst activation and successful implantation, influencing important aspects such as anterior-posterior axis formation and trophoblast lineage specification[63],[64]. Additionally, Wnt4 and Wnt6 in particular play specific roles in regulating epithelial differentiation, stromal cell proliferation, and survival during decidualization[65],[66]. Information from human studies highlights the relevance of Wnt signaling, with altered expression patterns associated with recurrent implantation failure and miscarriage[67],[68].

1.4.6 Experimental Designs and Technologies to Investigate Embryo-Maternal Interaction

A variety of experimental designs and technologies have been used to investigate embryo-maternal interaction, particularly with a focus on implantation (Figure 3). Animal models, including knockout mice, provide *in vivo* insights into molecular mechanisms. For example, one study generated Esr knockout mouse models and

identified ERα as the primary mediator of E2 function in endometrial cells[69],[70]. On the other hand, *in vitro* culture systems and three-dimensional (3D) models such as endometrial organoids and blastoids provide controlled environments in which endometrial responses to hormonal cues can be studied[71],[72]. A variety of culture conditions have been used in studies, including the use of different substrates such as uncoated tissue culture plastic plates, plates coated with collagen, laminin, or fibronectin, and co-culture with uterine monolayers or other somatic cells such as fibroblasts and Vero cells[73]–[76]. For example, the endometrial and trophoblast cell co-culture model involves co-culturing embryonic stem cells and trophoblast stem cells and allows the study of embryo cavitation, axis morphogenesis, and implantation[77]. Information from other studies indicates that experimental designs involving the Ishikawa cell line and rodent embryos have been used to investigate embryo-mother interaction, especially at the early stages of implantation[78]. The formation of blastoids from human pluripotent stem cells is an alternative model for studying early human development, including embryo-maternal interactions. Extracellular matrix (ECM) is also used in implantation research, and the use of ECM plays an important role in the preparation of endometrial organoids and establishing 3D endometrial culture. Matrigel is one of the widely used ECM material[79],[80]. Microfluidic systems, such as endometrium-on-a-chip, recreate tissue architecture for detailed studies[81],[82]. Endometrial populations combine different cell types for a more realistic model. Genetic screening and editing, as well as drug screening, identify key factors and compounds that influence implantation[83]. Single-cell RNA sequencing is another technique that offers detailed transcriptomic profiling[84].

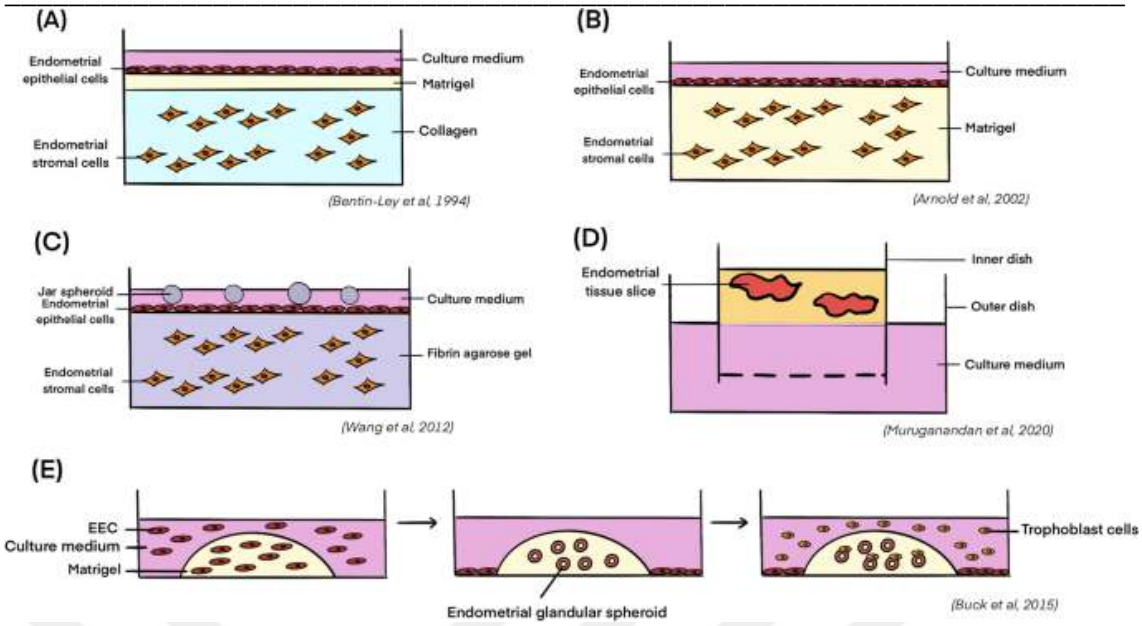

Figure 3. Established *in vitro* 3D culture models of the endometrium. A) Stromal cells suspended in collagen by a coating of Matrigel with epithelial cells seeded on top. B) Stromal cells resuspended in Matrigel with directly seeded Ishikawa epithelial cells. C) Endometrial stromal cells resuspended in fibrin-agarose gel, covered with epithelial cells, and using JAR cell-derived spheroids as trophoblast carriers. D) Combined 2D/3D model combining endometrial glandular spheroids, 2D monolayer of endometrial epithelial cells, and trophoblasts to study trophoblast invasion. E) 3D culture model using human endometrial slices suspended in a collagen matrix in a double-dish culture plate[72].

1.5 Female Infertility

Infertility is a medical condition that has significant effects on many aspects of well-being. Defined as the inability to achieve a clinical pregnancy after 12 or more months of regular, unprotected sexual intercourse, it poses psychological, physical, mental, spiritual, and medical challenges[85]. Globally, approximately 15% of reproductive-age couples, equivalent to 48.5 million couples, encounter difficulties in conceiving[86]. Female infertility constitutes 35% of cases. According to a World Health Organization study, 37% of infertile couples in developed countries exhibit female factor infertility, and 35% manifest both male and female related factors. Common identifiable female factors include ovulatory disorders (25%), endometriosis (15%), pelvic adhesions (12%), tubal blockage (11%), other tubal abnormalities (11%), and hyperprolactinemia (7%)[87].

1.5.1 Recurrent Implantation Failure (RIF)

The term "implantation failure" encompasses patients who either lack quantifiable signs of implantation, such as increased hCG levels or exhibit elevated hCG production without subsequent ultrasound evidence of a gestational sac[88]. This description applies to individuals undergoing assisted reproductive technology (ART) and those attempting conception without fertility treatment. Maternal age, embryo quality, and the stage of transfer (cleavage or blastocyst) are factors considered by different authors in defining RIF[89],[90]. A more comprehensive definition, proposed by Coughlan et al., involves the failure of clinical pregnancy after four good-quality embryo transfers and at least three IVF cycles and applies to women under 40[88]. In spontaneous conception, approximately 30% of pregnancies are lost before implantation, and 10% result in clinical pregnancy losses. It's essential to acknowledge that achieving spontaneous pregnancy on the first attempt is only seen in only around 30% of normal fertile couples, with success often occurring in subsequent attempts[91],[92].

1.5.2 Factors that affect implantation failure

Recurrent implantation failure can be caused by several factors. Maternal age is a critical factor because increasing age is associated with higher rates of aneuploidy and decreased pregnancy success[93],[94]. Obesity (BMI > 25 kg/m^2) is associated with higher implantation failure and lower implantation rates in ART by affecting oocyte quality and follicular development[95]. Smoking negatively impacts pregnancy outcomes, leading to increased miscarriage risk and decreased live birth rates[96]. Elevated cortisol levels which indicate stress, may increase the chance of miscarriage shortly after conception[97]. However, the impact of psychological stress on ART outcomes is debated. Although some studies suggest minimal effects in the first treatment cycle, they show higher rates of anxiety and depression after IVF failure[98]. Recurrent implantation failure (RIF) also involves the multifaceted interaction of immunological, genetic, and physiological factors. High levels of natural killer cells, both peripherally and in the uterus, are associated with an increased risk of miscarriage[99],[100]. Autoimmune antibodies, hereditary thrombophilias, and chronic endometritis contribute to implantation challenges, with Lactobacillus-dominated endometrium favoring successful outcomes[101]–[104]. Chromosomal abnormalities particularly translocations,

are more prevalent in RIF, prompting recommendations for parental karyotyping[105],[106].

1.5.3 Assisted reproductive techniques to overcome implantation failure

Various therapeutic interventions aim to improve outcomes for individuals experiencing RIF during IVF. Selection of the appropriate embryo stage for transfer (blastocyst or embryos at the cleavage stage) increases the implantation success rate. The use of frozen embryo transfer is gaining popularity over fresh transfer as it may increase endometrial receptivity[90]. Different methods of embryo transfer, including ultrasound-guided transfer, catheter type, and cervical mucus removal, can impact clinical pregnancy and live birth rates[88]. Controlled ovarian stimulation protocols, particularly the use of GnRH agonists versus antagonists, have been investigated. It has been determined that lower pregnancy rates are achieved with antagonists. In some new approaches for RIF patients, the dual use of GnRH agonists and antagonists are used more effectively in final follicle maturation[107]. The use of progesterone supplementation, especially dydrogesterone, provides benefits in increasing birth rates, and its oral administration is considered to be non-inferior to vaginal progesterone in IVF[108].

1.6 Crispr Cas9 Systems

Gene editing technology advanced significantly with the discovery of Clustered regularly interspaced short palindromic repeats (CRISPR) in Escherichia coli in 1987[109],[110]. Subsequently, the DNA splicing function of the CRISPR system was developed by Jennifer Doudna and Emmanuelle Charpentier[111],[112]. The system includes the Cas9 protein for DNA cutting and crRNA/tracrRNA for targeting specific DNA sequences. This system causes double strand breaks in target DNA sequences, thus the CRISPR/Cas9 system has been widely used in gene knockout, genome screening, and modeling. Other CRISPR systems, such as Cas12 and Cas13a, have also been applied to RNA imaging and rapid nucleic acid detection. The CRISPR system is divided into two categories based on its composition as an effector of the prokaryotic immune system. The first of these categories, the CRISPR/Cas system category, contains multiple effector proteins, including three types: type I, III, and IV. The other category includes single multidomain protein effectors commonly used in current

research and consists of types II, V, and VI. The widely used CRISPR/Cas9 system belongs to the type II category. The CRISPR system has been divided into six types, with ongoing modifications and applications in various fields of research. The CRISPR/Cas9 system mainly includes the Cas9 protein for cutting DNA and crRNA (CRISPR-derived RNA) and tracrRNA (trans-activating crRNA) for targeting. crRNA forms double-stranded RNA with tracrRNA through base complementary pairing and associates in a complex with the Cas9 protein to target specific DNA sequences. Cas9 proteins recognize protospacer adjacent motif (PAM) sequences and apply endonuclease activity to cut regions of DNA, causing double-strand breaks (DSBs) in DNA (Figure 4)[113]. Cells then activate the DNA repair pathway to repair the damaged DNA strand. During the repair process, DNA is inserted, deleted, or rearranged, leading to modification of the target DNA sequence. Non-homologous end joining (NHEJ) repair frequently leads to frameshift mutations, resulting in gene knockout. Nowadays, crRNA and tracrRNA are combined into a single RNA, often called sgRNA (single guide RNA) when CRISPR tools are used to manipulate DNA molecules. CRISPR/Cas9 is also widely used for single and multiple gene knockouts in cells and animals, as exemplified by the creation of a mouse model of multiple gene knockouts [114]. In applications such as the treatment of Duchenne muscular dystrophy, CRISPR/Cas9 has been used to delete exons from mutated genes and restore a normal reading frame[115].

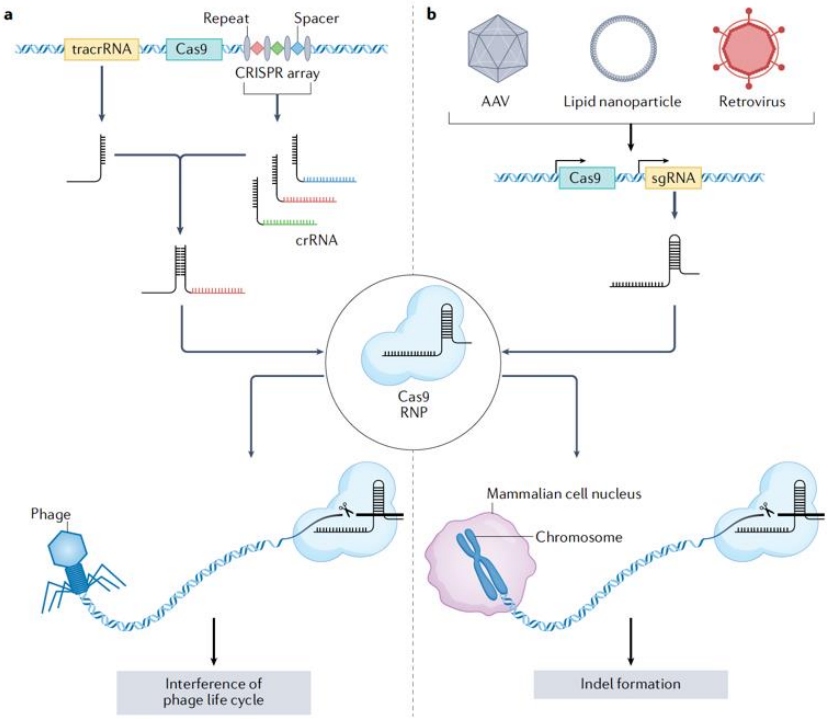

Figure 4. A general outline of CRISPR/Cas9 system. The system includes the Cas9 protein for DNA cutting and crRNA/tracrRNA for targeting specific DNA sequences, as Cas9 protein for cuts DNA and crRNA (CRISPR-derived RNA) and tracrRNA (trans-activating crRNA) for targeting. crRNA forms double-stranded RNA with tracrRNA through base complementary pairing and associates in a complex with the Cas9 protein to target specific DNA sequences[116].

1.6.1Application of CRISPR/Cas9 System into Reproductive Biology

The field of reproductive biology has witnessed significant advancements with the application of CRISPR/Cas9 technology. In the field of reproductive biology, the CRISPR/Cas9 system is used in subjects such as functional analysis of genes in reproduction, gene deletion and correction in model organisms, engineering in mammalian germline, maternal mutant embryo formation, mitochondrial genome editing, and human germline genome editing. Firstly, it is noteworthy that this technology is used to delete specific genes associated with critical reproductive processes. In studies, CRISPR/Cas9 has been used to better understand the functional functions of genes, leading to the creation of homozygous loss-of-function subjects. For example, deletion of a site in the Ast1 gene encoding Ovastacin provided insights into its role in preventing sperm binding during fertilization[117]. In addition, CRISPR/Cas9

technology is also used to eliminate some disorders caused by genetics. Deleting the Crygc gene, which causes cataracts in mice, using CRISPR/Cas9 successfully resolved the disorder[118]. For another example, this method has also been used to correct genetic mutations associated with disorders such as Duchenne muscular dystrophy[119]. Moreover, CRISPR/Cas9 has been effective in studying maternal mutant embryos in zebrafish and addressing mitochondrial diseases through precise editing of mitochondrial DNA[120]. In the field of human reproductive biology, CRISPR/Cas9 has been tested in human germline genome editing, demonstrating its potential to correct mutations in human zygotes and oocytes[121],[122]. Moreover, insights from CRISPR/Cas9 gene editing highlight the important roles of specific conceptus factors, such as IL1B2 and IFNG, in pig development and successful pregnancy establishment, shedding light on the complex biological pathways and consequences of factor loss[123],[124].

1.7 Hypothesis and The Aims of The Current Research

The aims of the current research can be outlined as: *i*. to reveal temporal gene expression profile differentially in endometrial epithelial and endometrial stromal cells throughout the duration of 3D *in vitro* culture systems, *ii*. to identify genes that show a significant expression profile during the culture period, *iii*. to search for the functions of those genes and investigate if they have been related to implantation process previously, *iv*. to edit genome of epithelial and stromal cells separately for altering expression of the determined genes, *v*. to uncover the molecular effects of expression of genes that have not been addressed for implantation previously.

As implantation is a very complex biological phenomenon with so many unknown still to study, we can hypothesize that, some novel genes which have not been linked to implantation process before, can be discovered via use of genome edition.

Chapter 2
MATERIAL AND METHODS

The flow chart designed based on the hypothesis is shown in the fFigure 5.

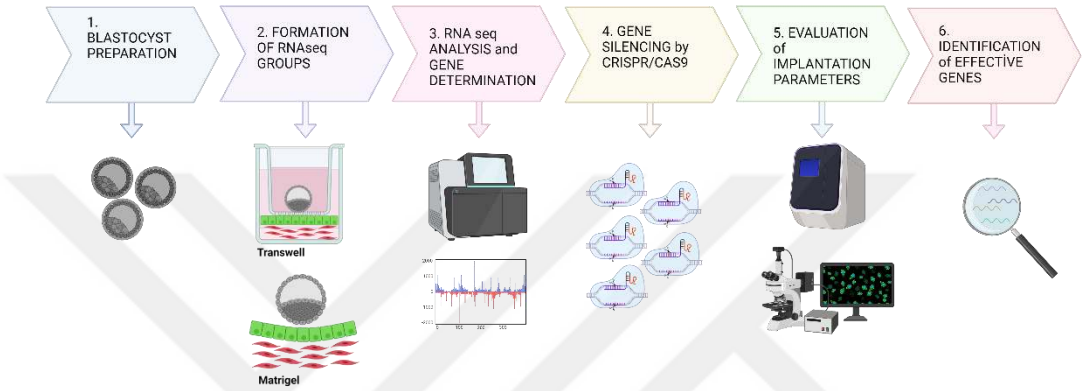

Figure 5. Flow chart of experimental study.

2.1 Experimental Materials and Equipment

2.1.1 Animal Studies

Folligon (MSD, Cat No:186433 R2), Chorulon (MSD, Cat No: 194225 R2), GMOPS (Vitrolife, Cat No: 10130), Bovine Serum Albumin (BSA) (Sigma Aldrich, Cat No: A-3311).

2.1.2 Embryo Isolation and Culture Studies

35 mm culture dish (Nest, Cat No: 706001), hyaluronidase (Sigma Aldrich, Cat No: H1136), NidOil (Nidacon, Cat No: NO-100), The stripper micro pipetter (The STRIPPER, Cat No: MXL-3 STR), denudation tip (Reproline, Cat No:: 447140/20), Hot Plate 062 (Labotect, Cat No: 13854), IVFtech Classica cabinets (IVFtech, Cat No: BE3007), incubator Forma Steri-Cycyle i160 (Thermo Fisher, Cat No: 50163013), Embryo culture medium (Life Global, Ref No: LGGG-100).

2.1.3 Cell Culture Studies

DMEM-F12 Ham's culture media (Multicell, Cat No:319-085-CL), Charcoal-stripped fetal bovine serum (Thermo Fisher, Cat No:12676029), β-Oestradiol (Sigma Aldrich, Cat No: E2758), progesterone (Sigma Aldrich, Cat No: P8783), 12-well plates (Sarstedt, Cat No: 83.3921), 6-well plates (Sarstedt, Cat No:83.3920), 10 cm culture dish (Sarstedt, Cat No: 83.3902), centrifugation device SL-40R (Thermo Fisher, Cat No: 75004527), serological pipettes 5 ml, 10 ml, 25 ml, and 50 ml (Greiner Bio-One, Cat No: 606180, 607180, 760180, 768180), stereo microscope (Zeiss, Cat No: Stemi 508), incubator (New Brunswick, Cat No: Galaxy 170S), Pen/Strep. (Biowest, Cat No: L0022-100), Trypsin-EDTA (MultiCell, Cat No: 325-542-EL), -20°C and -80°C freezers (Arçelik, Cat No:2060MB and Thermo Fisher, Cat No: R207-14), collagenase/dispase (Sigma Aldrich, Cat No:10269638001), DMSO (Sigma Aldrich, Cat No: D2650-100ml), Matrigel® Basement Membrane Matrix (Corning, Cat No: 354234), Live/Dead Viability/Cytotoxicity kit (Thermo Fisher, Cat No: L3224).

2.1.4 Benchwork

Immunofluorescent Staining: Paraformaldehyde powder (Sigma Aldrich, Cat No: 158127- 500g), Triton-X-100 (Sigma Aldrich, Cat No: T9284-100ml), Tween 20 (Sigma Aldrich, Cat No: P1379-500ml), Anti-Mmp9 antibody (Abcam, Cat No: ab38898), Anti-E-Cadherin Antibody (Abcam, Cat No: 76055), Anti-Entactin antibody (Abcam, Cat No: ab14511), Alexa Fluor 488 goat anti-mouse IgG(H+L) (Invitrogen, Cat No: A-11029), Alexa Fluor 488 goat anti-rabbit IgG(H+L) (Invitrogen, Cat No: ab150077), Hoechst 33342 (Thermo Fisher, Cat No: 62249 5ml), Glycerol (Sigma Aldrich, G5516-500ml), Dulbecco's Phosphate-Buffered Saline (DPBS) (Biowest, Cat No: L0615), Zeiss light microscope (Zeiss Primo Star, Germany), STED confocal super-resolution (Leica TCS SP8 STED 3X, Germany).

qRT-PCR: Random Hexamer Primer (Thermo Fisher, Cat No: SO142), dNTP (Invitrogen, Cat No: 28025-013), M-MLV RT enzyme, (Invitrogen, Cat No: 28025-013), 5X First Strand buffer (Invitrogen, Cat No: Y0232), Dithiothreitol (DTT) (Invitrogen, Cat No: D153), Light Cycler® 480 SYBR Green I Master (Roche, Cat No: 0488735200), Quick-RNA Purification Kit (Macharey-Nagel, Cat No: 740955.50), Qiagen Cyber Green Master, 2-mercaptoethanol (Sigma Aldrich, Cat No: M3148),

Nanodrop 2000/2000c Spectrophotometers (Thermo Fisher, Cat No: ND-2000), LightCycler 480 instrument (Roche, LightCycler 480 II).

Western Blot: RIPA Lysis Buffer (EcoTech Biotechnology, Cat No: RIPA-100), Laemli Buffer 2X (Sigma Aldrich, Cat No: S3401), PVDF Membrane (BioRad, Cat No: 1620177), Mini-PROTEAN RGX Stain-Free Gels (BioRad, Cat No:4568085), Blotting-Grade Blocker Non-fat Dry Milk (BioRad, Cat No: 1706404), Odyssey Fc Imaging System Chemiluminescence Sensing System (LI-COR Biosciences).

2.1.5 Molecular Cloning Studies

T4 Ligase Buffer. (New England Biolabs, Cat No: M0202S), T4PNK enzyme. (New England Biolabs, Cat No: M0201S), Nuclease-free water. (Eco Tech biotechnology, Cat No: DW003L), PCR device (Bio-Rad, Cat No: T100), T100 Thermal Cycler (Bio-Rad, Cat No: 1861096), BsmBI (New England Biolabs, Cat No: R0739l), Antarctic Phosphatase (New England Biolabs, Cat No: M0289S), T4 Ligase buffer with ATP (10X) (New England Biolabs, Cat No: M0202S), Lubia Broth (Multicell, Cat No: 800-061-CG), LB Agar (Multicell, Cat No:800-011-CG), Fugene 6 Transfection Reagent (Promega, Cat No: E2692), Puromycin dihydrochloride (Sigma Aldrich, Cat No: P8833-100mg), Digital orbital shakers (WiseShake, Cat No: SHO2D), NucleoSpin Gel and PCR Clean-Up (Macharey-Nagel, Cat No: 740609.50), NucleoSpin Plasmid miniprep kits (Macherey-Nagel, Cat No: 740588.50), SOC Outgrowth Medium (New Englands Biolabs, Cat No: B9020S).

2.2 General Protocols

The protocols repeated at different stages of the study are listed below.

2.2.1Immunofluorescent Staining

Immunofluorescent staining (IF) is a technique that applies antibodies and fluorophores to define certain types of proteins in a cell. The IF protocol consists of a step-by-step procedure to apply. Before beginning the staining, samples should be fixed. The medium of cells seeded onto the class coverslips was removed and washed with DPBS solution. Then, 4% PFA was added to the cells and cells were incubated for 20 minutes at room temperature (RT). After that, the samples were washed two to three times with

DPBS solution to remove the fixative, and they have become ready for IF staining. Initially, cells were passed on a 10-minute incubation at room temperature with 0.1% Triton-X, facilitating cell permeabilization. Subsequently, cells were washed three times with DPBS-T to remove excess Triton-X. Later, a 20-minute incubation with Superblock at room temperature followed, aiming to block nonspecific binding sites and enhance specificity during antibody interactions. The primary antibody incubation step involved either a 90-minute incubation at 37°C or an overnight incubation at 4°C, allowing for the specific binding of primary antibodies to target proteins. Post-incubation, cells underwent a thorough washing process with DPBS-T three times to remove unbound primary antibodies. Afterward, a 90-minute incubation at 37°C with the appropriate secondary antibodies followed, enabling the visualization of the targeted proteins. After another round of three washes with DPBS-T, cells were covered with a mounting medium, which included Hoechst for nucleus staining.

2.2.2 RNA Isolation

RNA isolation was performed according to the Macherey-Nagel NucleoSpin RNA Isolation kit. First of all, the cell pellet was collected in a 1,5 mL Eppendorf tube. Cell lysis was achieved by adding 350 µL Buffer RA1 and 3.5 µL ß-mercaptoethanol to each cell pellet, and vigorous vortexing was applied. The lysate was then filtered through a NucleoSpin filter and centrifuged to remove cell debris. RNA binding was adjusted by adding 350 µL of 70% ethanol to the lysate. The homogenized lysate was transferred onto a NucleoSpin RNA column and centrifuged. To desalt the silica membrane, 350 µL MDB was added and centrifuged to dry the membrane. DNA digestion was carried out by preparing a DNase reaction mixture with rDNase and reaction buffer. After DNase treatment, the silica membrane was washed once with buffer RAW2 and twice with buffer RA3. The final wash allows the membrane to dry completely. The elution step involved adding 25-60 µL of RNase-free H2O to the NucleoSpin RNA Column, followed by centrifugation, and eluted RNA was collected in a 1,5 mL Eppendorf tube. Isolated RNAs were stored at -80°C.

2.2.3 cDNA Synthesis

The cDNA formation process followed a standardized protocol. Initially, RNA samples were retrieved from -80°C storage and placed on ice for handling. The amount of RNA

required for each reaction was calculated, with a recommended range of 200–1000 ng depending on RNA concentration, ensuring consistency in cDNA concentration among comparison samples. The reaction assembly took place in PCR tubes, combining dNTP (2 mM), random hexamer (1 µL), RNA variable (up to 12 µL), and dH2O variable (13 µL) for a total volume of 16.5 µL. Following a thermal cycler program at 65°C for 5 minutes and subsequent transfer to ice, the mix was prepared for each reaction. The RT mix comprised 5X First Strand Buffer (5µL), DTT (0.1M) (2µL), and RNAsin (0.5µL), totaling 7.5 µL. This mix was added to each reaction sample, and the mixture was incubated at room temperature for 10 minutes. Subsequently, 1 µL of the MMLV RT enzyme was added to each reaction. After a brief vortex and centrifugation, the thermal cycler machine was set to 37°C for 1 hour, 70°C for 15 minutes for inactivation, and 4°C indefinitely. Finally, the reaction volume was adjusted to 100 µL by adding 75 µL of DNAse/RNAse-free H2O.

2.2.4 Real-time PCR Analysis

The real-time PCR (qRT-PCR) analysis method is used for cDNA quantification and the determination of specific gene expression in the cells. First, a 96-well plate was taken and designed to accommodate the specific DNA samples and primers for analysis. A master mix was prepared by calculating 10 µL of Sybrgreen, 7 µL of dH2O, and 1 µL of primer mix for each well. Second, each well was loaded with 18 µL of the mix and 2 µL of the respective DNA sample, and the top of the plate was sealed. The prepared plate underwent centrifugation at 1300 rpm for 2 minutes to ensure proper mixing and settling of the contents. The analysis was conducted using a LightCycler480 machine, employing a thermal cycling program. The program included an initial denaturation step at 95°C for 5 minutes, followed by 45 cycles of denaturation at 95°C for 10 seconds, annealing at 60°C for 30 seconds, and extension at 72°C for 30 seconds. The final step involved holding the temperature at 4°C indefinitely.

2.3 Obtaining Mouse Embryos

This step was conducted at Koç University Animal Research Laboratory. The animals were provided by Koç University, KUTTAM, Animal Research Laboratory. A 70 cm^2 area was allocated for each animal, and the daily cycle was arranged as 12 hours of dark and 12 hours of light. Adlibitum nutrition was applied with commercial pellet feed and

automated drinkers. As a result of superovulation, maximum efficiency was obtained with embryo collection. Therefore, 6-8 weeks old, and 20-24 g, CB6F1 female mice were selected to be used in the experiment. The ethical approval number for the animal experiments of this research is 2016.HADYEK.033. A total of 393 female mice were used for experiments.

2.3.1 Superovulation of Female Mice

First, 10 IU of pregnant mare serum gonadotropin (PMSG) was administered intraperitoneally (i.p.) to 6-8 weeks old, 20-24 g CB6F1 female mice. 10 IU of human chorionic gonadotropin (hCG) was applied i.p. 48 hours after injection, and female mice were mated with adult male CB6F1 mice. For the mating strategy, the method of 2 females to a male was applied, and female mice were put into the male cage for the best result. The next morning, mating mice were identified by visualization of the vaginal plug (Figure 6).

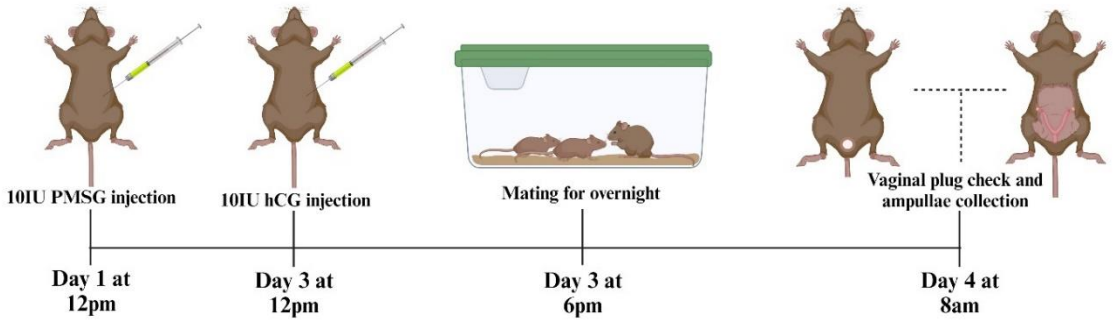

Figure 6. Visual demonstration of superovulation protocol.

2.3.2 Zygote Collection

Vaginal plugs are the clue for fertilization. The morning after mating, females with plugs were separated. After the superovulation, each female mouse carries approximately 20-25 zygotes. Zygotes were collected from the ampullae region of the sacrificed female mice. Cervical dislocation was used for sacrification of the animals. An abdominal incision was performed to reveal the ampullae which were surgically removed and collected into the GMOPS media supplemented with 4 mg/ml Bovine Serum Albumin (GMOPS^{+}) and transported to the lab by maintaining the temperature of 37°C. All dissections and denudations were performed under a stereomicroscope on 37°C pre-heated surfaces in an IVF cabin. Each ampulla was taken separately into

GMOPS$^+$ drops and explored with the help of tweezers at the swollen part, where the zygotes were accumulated. Zygotes scattered into GMOPS$^+$ were collected with a stripper and taken into the fresh GMOPS$^+$ media. The surrounding granulosa cells were removed by washing 3 times in hyaluronidase enzyme and the washing steps were followed in the GMOPS$^+$ media supplemented with 4 mg/ml Bovine Serum Albumin [125]. The figures revealing the details of this process are presented in the "results" section.

2.3.3 In Vitro Culture of the Zygotes

One of the commercial embryo culture mediums (Life Global, USA) was used as an *in vitro* embryo culture medium. 10 µl embryo culture drops were placed on a 35 mm culture plate, and the drops were covered with mineral oil. Good quality zygotes (according to universal embryo grading systems) were transferred to the drops and cultured up to the blastocyst stage at 5% CO_2, 37°C temperature, in a high-humidity incubator. For the zygote selection, the cell size, the distribution, number, and size of the nucleoli precursor bodies (NPB), the location of the polar bodies, and the presence of the cytoplasmic halo were considered[126].

2.3.4 The Selection of the Blastocysts

Good-quality growing blastocysts in the culture medium were used. There is no single blastocyst scoring system used today. For this reason, scoring systems were performed according to the literature for the zygote and blastocyst selection [127]. 4AA/5AA quality blastocysts were selected for the experimental study.

2.4 Isolation of Mice Uterine Epithelial and Stromal Cells

After the uterine horns of the sacrificed mice were removed, they were placed in warm HBSS and dissected under a stereo microscope. Following, tissues were cut into small pieces and for epithelial cell isolation tissues were taken into a mixture of 0.25% trypsin/EDTA and collagenase/dispase solutions. The tissue was first incubated at +4°C for 2 hours then room temperature for 30 minutes and 37°C for 30-45 minutes. After the expiration of the time, a warm medium was added to the sample to inhibit enzymatic activity. Later, the sample was vortexed until the cells were dispersed from the tissue. Subsequently, 70 and 40 µm mesh filters were used respectively to separate the cells

according to their size. The cells residing over 40 µm mesh were obtained by washing this side and used as epithelial cells, as the collected cells were seeded and cultured into the 6-well plate. The cells passing through the 40 µm mesh were suspended in a medium and the sample was centrifuged at 600G for 7 minutes for stromal cell isolation. The resulting pellet was seeded. The culture media was DMEM F-12 Ham's with 10% FBS, 1%PS, 63.5 nmol/L of progesterone, 7.14 nmol/L of estradiol-17b (Repro Medium), and the culture condition was 37°C in 5% CO_2 incubator.

2.4.1 Uterine Cell Characterization Assays

The identity of endometrial epithelial and stromal cells was established by immunofluorescent staining (IF), and real-time PCR (qRT-PCR) analysis (detailed protocols were given in section 2.2). Anti-cytokeratin 18 and anti-vimentin antibodies are used for the characterization of epithelial and stromal cells with IF analysis. For the qRT-PCR analysis, forward and reverse primers were given in Table 1.

Table 1. Primer sequences used for cell characterization. Cytokeratin 18 (CK18), a uterine epithelial marker, and vimentin (Vim), a stroma marker, gene expressions were evaluated using the qRT-PCR method. Gapdh was used as a housekeeping gene for normalization in computational analyses.

	Forward	***Reverse***
CK18	AGATGACACCAACATCACAAGG	TCCAGACCTTGGACTTCCTC
Vim	CGTCCACACGCACCTACAG	GGGGGATGAGGAATAGAGGCT
Gapdh	AGGTCGGTGTGAACGGATTTG	TGTAGACCATGTAGTTGAGGTCA

2.4.2 Decidualization Assay

To check whether the stromal cells were decidualized or not, a decidualization assay was performed. For this, the isolated uterine stromal cells were seeded in a 6-well plate. While half was kept in DMEM F-12, the other half was incubated with REPRO medium for 4 days under the condition of 5% CO_2, 37°C temperature, in a high-humidity incubator.

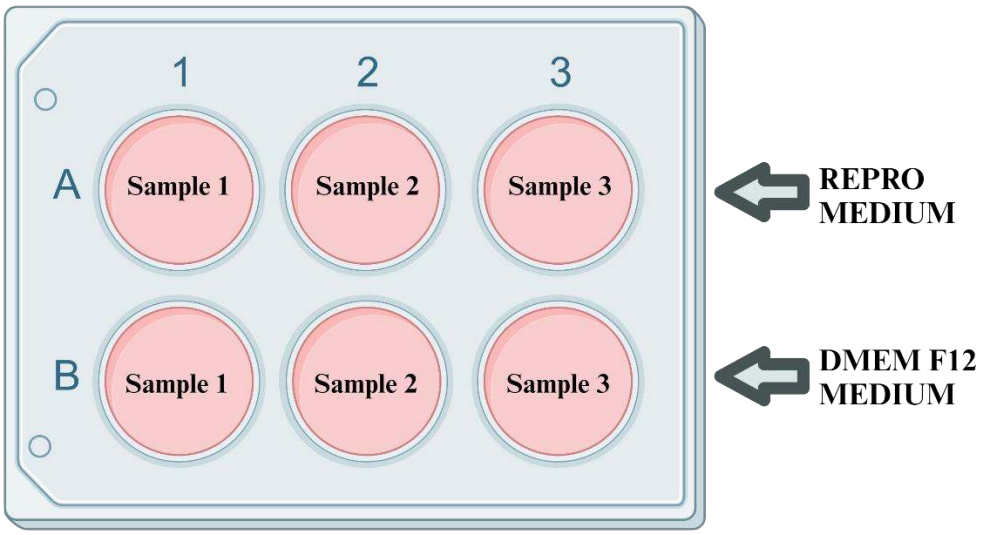

Figure 7. Experimental plate design for decidualization assay. In this assay, three biological replicates were used for each medium. The aim of this study was to show that decidualization takes place efficiently with the REPRO medium that contains estrogen and progesterone.

Following the incubation time, the cells were detached and decidualization markers prolactin (*PRL)* and insulin-like growth factor binding protein 1 (*IGFBP1)* were checked by using qRT-PCR. The experimental plate design is exhibited in Figure 7. The qRT-PCR primer sequence is given in Table 2.

Table 2. Primer sequences are used for decidualization checks. Two decidualization markers (Prl and Igfbp1 gene expression) were checked by qRT-PCR analysis. Gapdh was used for the housekeeping gene.

	Forward	***Reverse***
Prl	GGGACACTCCTCCTGTTGC	CACACGGTCAAACAGCTCTC
Igfbp1	TCGCCGACCTCAAGAAATGG	GACACACCAGCAGAGTCCAG
Gapdh	AGGTCGGTGTGAACGGATTTG	TGTAGACCATGTAGTTGAGGTCA

2.5 Molecular Cloning

Lentiviral vectors are one of the applicable methods to deliver a specific type of sequence to make the cell form cas9-gRNA complex inside the cytoplasm. However, rather than taking each type of viral vector commercially, they can be synthesized in laboratory conditions by using molecular cloning techniques.

2.5.1 sgRNA Design

A carefully designed guide RNA (gRNA) selection process achieved the targeted silencing of specific genes. Target genes were identified, and gRNAs were designed using the ChopChop database (https://chopchop.cbu.uib.no/) and the IDTDNA database (https://www.idtdna.com/pages). The selection criteria encompassed GC percentages within the range of 40-60%, ensuring gRNA efficiency exceeded 50%. Additionally, self-complementary gRNAs with the lowest off-target binding were prioritized. Off-target rates were cross-verified against the IDTDNA database, and gRNAs with off-target rates close to 100% were excluded. Oligo design involved the creation of parent sequences and their complementary counterparts, resulting in three separate oligos for each target gene. To facilitate binding to the target region, a 4-base extension sequence, derived from the BsmbI cutting site, was added to the beginning of the upper sequence using the SnapGene program. Furthermore, the efficiency of polymerase activity was enhanced by adding "G" to the beginning of the designed parent sequence, while a guanine base conjugate, "C," was appended to the end of the complementary sequence. This comprehensive approach aimed to optimize gRNA design for subsequent gene silencing experiments.

2.5.2 sgRNA Annealing

The synthesis of single-guide RNA (sgRNA) involved the strategic design and annealing of forward and reverse oligos to create constructs with appropriate sticky ends for subsequent cloning. The forward oligo, 5’-CACCGNNNNNNNNNNNNNNNNNN-3’, and the reverse oligo, 3’-CNNNNNNNNNNNNNNNNNNCAAA-5’, were ordered to facilitate the generation of cohesive ends upon annealing. For the annealing process, 1 µL of each oligo (100 µM concentration) was combined with 1 µL of 10x T4 Ligation buffer and 7 µL of ddH2O. The annealing reaction was conducted using a thermocycler with the following

program: initial denaturation at 95°C for 5 minutes, followed by annealing at 37°C for 30 minutes, and a final ramp down at 0.1°C/s from 95°C to 25°C. This rigorous procedure aimed to create sgRNA constructs with well-defined sticky ends, ensuring compatibility for subsequent ligation steps in the cloning process.

2.5.3 Plasmid Restriction

The enzyme BsmBI-v2, sourced from an Escherichia coli strain carrying the modified cloned BsmBI gene from Bacillus stearothermophilus B61, was employed in this study. The recognition site of BsmBI-v2 is 5′...CGTCTC(N)$_1$˅...3′ on one strand and 3′...GCAGAG(N)$_5$˅...5′ on the complementary strand. pLentiCRISPR v2 puro backbone was used to insert the sgRNAs prepared for cas9 systems (Figure 8). The enzymatic reactions were conducted under standard conditions provided by the manufacturer's protocol (https://www.addgene.org). A 5 µg vector was cut using 3 µL 1X NEBuffer 3.1, and 3 µL BsmBI enzyme filled up to 30 ul with nuclease-free water, and the incubation temperature was set at 55°C for 16 hours. Following the incubation, heat inactivation of the enzyme was performed at 80°C for 20 minutes to halt the enzymatic activity.

2.5.4 Plasmid Clean Up

DNA purification was conducted using the NucleoSpin Gel and PCR Clean-up Kit. According to the manufacturer's manual, 1 volume of the sample was mixed with 2 volumes of buffer NTI. Following the centrifugation, the DNA was bonded onto a NucleoSpin Gel and PCR Clean-up Column in a collection tube. After discarding the flow-through, the silica membrane was washed with 700 µL Buffer NT3, and another centrifugation step was repeated. After that, to ensure the dryness of the silica membrane, centrifugation for 1 minute at 11,000 x g was performed. 15–30 µL of Buffer NE was added, and after incubation at room temperature for 1 minute, the elution procedure was followed up with centrifugation at 11,000 x g for 1 minute in the new 1,5 mL Eppendorf tube.

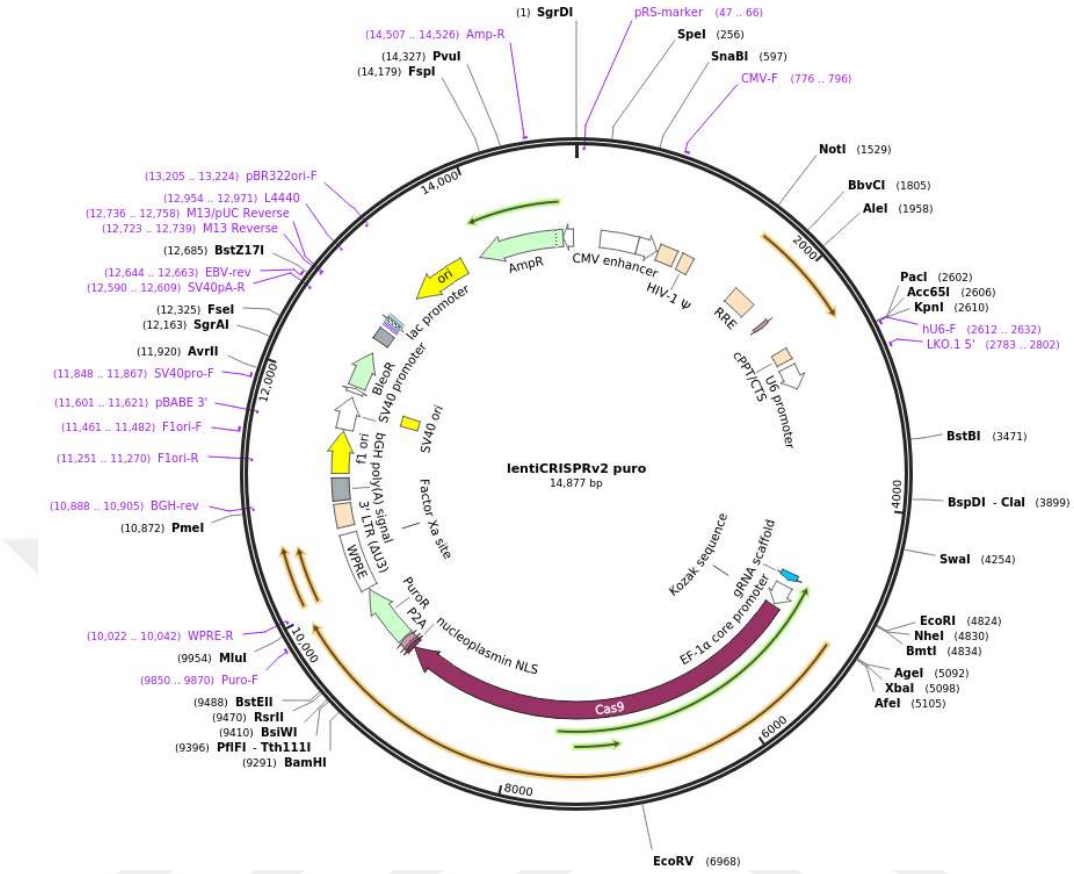

Figure 8. Detailed exhibition of pLentiCRISPR V2 puro backbone. (Addgene Plasmid #98290). pLentiCRISPRv2 is a single viral vector frequently used to deliver CRISPR components: the Cas enzyme, guide RNA, and puromycin antibiotic resistance gene.

2.5.5 sgRNA Ligation

The ligation process is a step to integrate the sgRNA into the previously cut vector, which begins with the dilution of the sgRNA prepared with annealing to a concentration of 1:200 in nuclease-free water. Subsequently, the ligation reaction mixture was prepared by combining 50 ng of the cut vector backbone, 1 µL of the diluted gRNA, 5 µL of T4 Ligase buffer with ATP (10X), and 1 µL of T4 DNA Ligase. The remaining volume is constituted by nuclease-free water to reach a total of 11 µL. The reaction mixture follows up with an incubation period at 16 °C for 16 hours to facilitate the efficient joining of the sgRNA to the cut vector backbone. Afterwards, the ligated sample was preserved at -20 °C.

2.5.6 Bacterial Transformation

Transformation is a critical process for introducing foreign DNA into bacterial cells, and it is performed to incorporate the ligated products into bacteria. The process is done with a heat shock transformation technique. Competent cells were extracted from -80°C storage, thawed on ice, and then mixed with the ligated products. At the same time, agar plates, preloaded with the appropriate antibiotic (1:1000 ampicillin), were taken out of 4°C storage and allowed to reach room temperature. 50 µL of STBL3-competent bacteria and 5 µL of the ligation product were mixed in the same tube. The resulting mixture was cooled for 30 minutes before undergoing a heat shock at 42 °C for 45 seconds. The resulting mixture was cooled for 30 minutes before undergoing a heat shock at 42 °C for 45 seconds. Following this step, 150 µL of SOC medium was added, and the solution was incubated for 1 hour at 37 °C with continuous shaking at 225 rpm. Post-incubation, the mixture was centrifugated at 1500 rpm for 5 minutes, with the subsequent removal of 150 µL of the supernatant. The remaining 50 µL were inoculated on LB agar plates and incubated at 37°C for 16 hours.

2.5.7 Colony Pick-Up and Plasmid Isolation

The detailed process of isolating plasmids began with the selection of a single colony. Single-colony selection ensures the purity of the starting material and thereby reduces the risk of contamination with other sequences. The initial steps involved cultivating bacterial samples and subsequently picking colonies from agar plates. Following overnight incubation, colonies were examined the next morning, and agar plates were wrapped with parafilm to prevent desiccation before storage in a 4°C cold room until needed. Mini cultures were prepared the day before plasmid isolation. In this step, 3-5 ml of LB broth with antibiotic was aliquoted into round-bottom tubes. A single bacterial colony was carefully selected using either an inoculation loop (by touching the colony) or the tip, stabbing the agar while ensuring contact with only one colony. The inoculation loop, or tip, was then shaken inside the LB broth to detach the colony. Subsequently, the tubes were placed in a 37 °C shaker for overnight incubation. On the following day, the tubes were removed from the shaker. The NucleoSpin plasmid isolation kit (Macherey Nagel) was employed for plasmid isolation, following the manufacturer's manual datasheet. The purified plasmids were stored at -20 °C, ensuring their stability for subsequent molecular analyses. The verification of the process is done

with the Sanger sequencing. For sample preparation, 1 µl of hU6 primer was mixed with at least 500 ng of obtained plasmids and the amount was completed up to 10 µl with the nuclease-free water. Sequencing was conducted by a commercial company (Macrogen, https://dna.macrogen.com).

2.5.8 Viral Transfection and Viral Concentration

Before transfection, 293T cells were seeded as 2.5 x 10^6 cells on a 10 cm plate and allowed to reach 60–70% confluency on day 0. On the evening of day 1, transfection mixtures were prepared for a 10 cm culture plate per plasmid vector transfection. One contains 20 µL FuGene and 180 µL DMEM with PS and without FBS (+/-), and the other contains the DNA mixture consisting of 250 ng VSVG, 2250 ng PsPax2, 2500 ng vector (Figure 9) in DMEM (+/-). The final volume was 200 µL. After thorough mixing and a 30-minute incubation at room temperature, the resulting mixture was introduced to the 293T cells dropwise, which were then placed in a CO_2 incubator. 18–20 hours later, the medium was replaced with fresh, complete DMEM containing 10 % FBS, and 1 % Pen/Strep. The next day, the medium was refreshed, and the first collection of the medium, which contains lentiviral particles, was taken into a 50 mL Falcon tube and stored at +4 °C. This process was repeated the next day, and the two-day collected mediums were combined and passed through a 45 µm filter to remove debris and cells. Subsequently, 1/4 PEG was added to the medium and incubated at +4 ºC overnight. After that, the virus-PEG samples were centrifugated at 2700 rpm and 1200 rpm respectively. The pellet volume was completed to 160 µL for 100x concentrated virus. 40 µL aliquots were prepared for further usage. The aliquoted viruses were stored at -80 ºC.

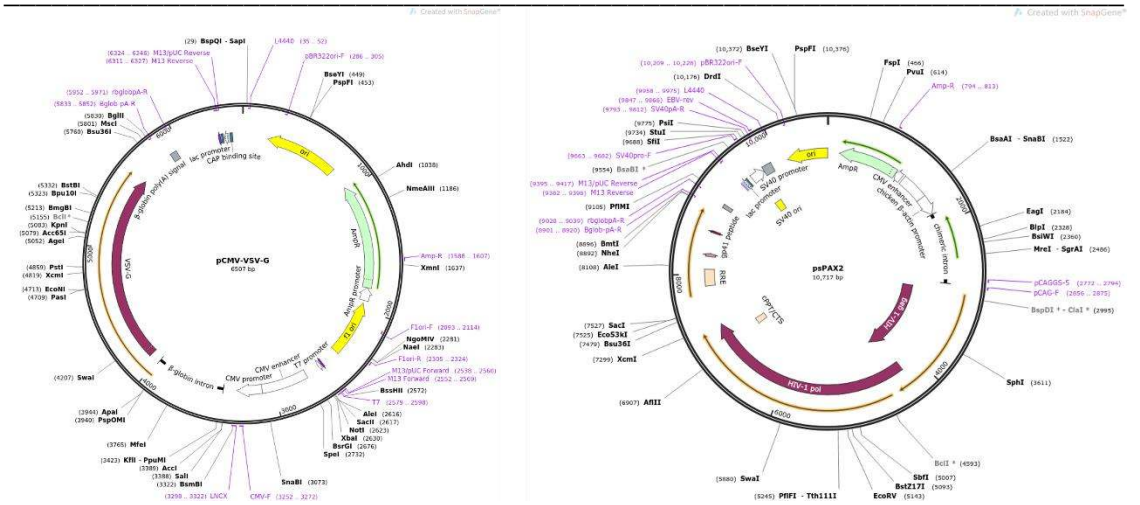

Figure 9. Illustration of pCMV-VSV-G (#8485) and psPAX2 (#12260) plasmids. These are the two plasmids that are the widely used for virus production. The VSV-G protein is the most frequently used protein for pseudotyping lentiviral vector envelope proteins. On the other hand, the psPAX2 is a packaging plasmid containing the Gag and Pol genes, which carry the structural and enzymatic proteins of the virus.

2.6 Sample Preparation for RNA sequencing

As it has been aimed to detect the genes expressed during the implantation process, samples ought to be prepared for RNA sequencing.

2.6.1 Multiplicity of Infection (MOI) Calculation

The multiplicity of infection (MOI) number defines the number of viral particles utilized per well. The experimental setup (Figure 10) involved seeding uterine epithelial and stromal cells in separate 12-well culture plates 18–24 hours before transduction and incubating overnight with 5% CO_2 at 37°C. The time of transduction is decided when the confluency reaches between 60% and 70%. For transduction, six different doses of prepared GFP or FMC lentivirus concentrations (1 µL, 2 µL, 5 µL, 10 µL, 15 µL, and 20 µL) were used, each with two different concentrations of protamine sulfate (PS) as 8 mg/mL and 16 mg/mL. The medium was replaced with the fresh medium, 16 hours post-transduction, and 48 hours later, fluorescent expression was assessed using a fluorescent microscope. An MOI was selected for inducible vectors to achieve high induction (bright fluorescent expression in the induced set) and low leakiness (no or faint fluorescent expression in the non-induced set). The detected MOI value was subsequently applied for the forthcoming experiments.

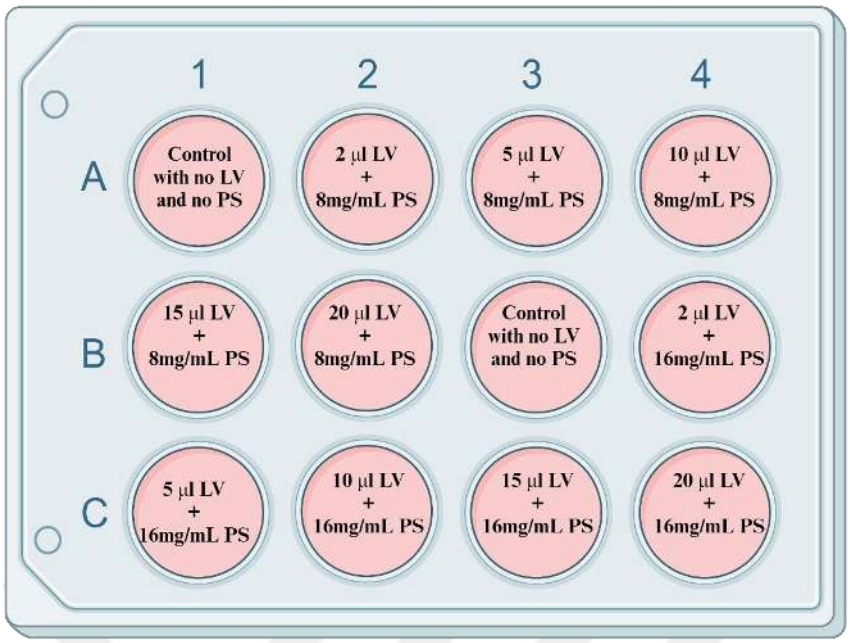

Figure 10. Plate design for the MOI calculation. Different viral concentrations and two different concentrations of protamine sulfate were used to detect the optimum amount for transduction.

2.6.2 Antibiotic Titration Assay

The pLentiCrispr V2 plasmid backbone utilized in this study incorporates a puromycin (PURO) resistance sequence. The integration of this resistance sequence allows for the selection of successfully transduced cells, as they are expected to exhibit resistance to puromycin. This is a crucial step to eliminate cells that did not undergo successful viral transduction. To determine the optimal concentration of puromycin for selection, following the calculation of the multiplicity of infection (MOI) as outlined in section 2.6.1, various antibiotic concentrations (1, 0.5, 0.3, 0.2 µg/mL) were administered to the cells (Figure 11). This step aimed to identify the concentration that effectively selects transduced cells while minimizing potential cytotoxic effects.

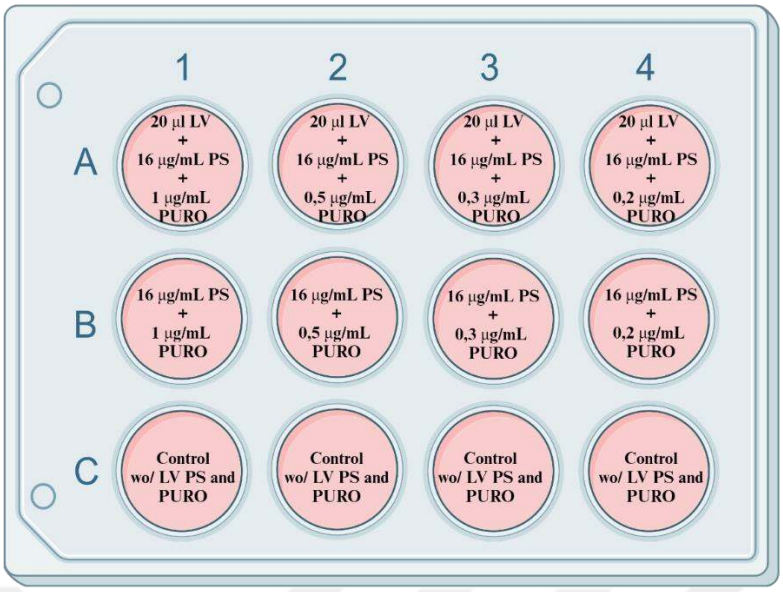

Figure 11. Plate design for antibiotic titration assay. Different puromycin concentrations were used to detect the optimum amount for selection.

2.6.3 GFP and FMC Labelling of Uterine Cells

In order to sort the cells for RNA sequencing and other purposes epithelial and stromal cells needed to be labeled by different fluoroproteins. Seeded uterine cells were infected by viruses prepared including related sequences to produce the green fluorescent protein (GFP) or fluorescent mCherry (FMC) protein. For the epithelial cells GFP, and the stromal cells, FMC sequence carrying viruses were used. To get rid of the cells that have not taken the viruses, elimination by puromycin antibiotic selection was accomplished. Transduction and selection concentrations were administrated according to methods mentioned in sections 2.6.1 and 2.6.2.

2.6.4 3D Culture Environment Construction to Mimic Implantation Area

To construct a 3D culture environment, BD Matrigel® (an extracellular matrix) was used. First, BD Matrigel® was dissolved in cold only DMEM F-12 (without PS and FBS addition) at a ratio of 3:1, according to the manufacturer's recommendations. Stroma cells were added to this media and incubated at 37 °C for 30-45 minutes, so that the Matrigel® polymerizes, and the stroma cells become embedded in the extracellular matrix. Epithelial cells were left on the formed structure, and after some time of incubation, the cells formed a reticulated interaction with each other. When the co-culture construct was accomplished, the blastocysts prepared were placed onto the co-

culture directly or a transwell has been used to separate blastocysts from the co-culture, as depicted in Figure 11. For each culture well two to three blastocysts have been used. The aim of using two different culture systems is to reveal the genes differentially as the ones originating from the co-culture of epithelial and stromal cells and the blastocysts, vs. the genes arising from the co-culture of epithelial and stromal cells.

2.6.5 Formation of the Experimental Groups for RNA Sequencing

Sample preparation for RNA sequencing was completed after 24 or 72 hours of culture incubation (Figure 12). To be able to understand the source of the RNA seq data, each cell group was tagged by viral transduction; GFP for endometrial epithelial cells; FMC for endometrial stroma cells; and non-targeting for blastocysts. Twenty to thirty blastocysts were used per group and samples were sequenced into three replicates. Experimental groups are indicated in the following figure. After the incubation of the co-cultures, cells were detached by using trypsin/EDTA solution and they were sorted by fluorescence-activated cell sorting (FACS) system.

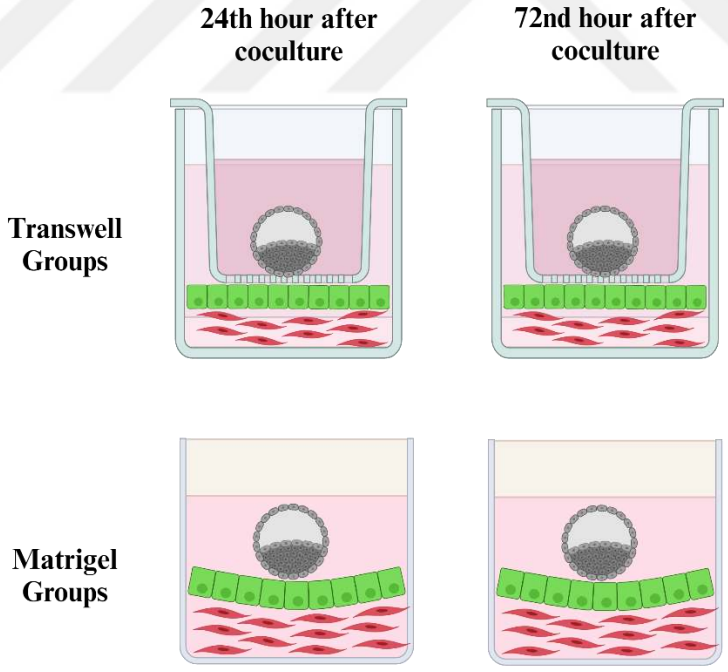

Figure 12. Co-culture groups designed for RNA sequencing. Two different *in vitro* culture systems were constructed. The transwell systems (up) are needed for the paracrine effects of the blastocysts on endometrial cells and vice versa. As the blastocysts do not touch the endometrial cells directly the profile of active genes may be

different than the directly interacting systems (down). The RNA seq data was expected to show the common genes in both systems.

2.6.6 Fluorescence Activated Cell Sorting (FACS)

GFP (+), FMC (+), and non-targeted cells were sorted using the FACS Aria III Cell Sorter and FACS Diva software (BD Biosciences, USA). The sorting process was conducted with a 100-micron nozzle under a pressure of 20 psi. Cell passage during sorting was maintained at a speed of 500-1500 events/second, and purity was targeted at <95% using the purity option. To minimize the impact of electromagnetic fields on cells during sorting, the sample chamber temperature was maintained at +4 °C. Following the identification of cells on the FSC x SSC plot, single cells were gated using the FSC-A x FSC-H plot. In the GFP x FMC plot, GFP(+) epithelial cells and FMC(+) stromal cells were identified and sorted into separate tubes. A minimum of 3 x 10^5 cells were sorted to obtain enough starting material for RNA isolation, cDNA synthesis, and sequencing. Flow cytometry analyses were performed using FlowJo v10.8.1. The gating strategy for sorting and a representative graph illustrating post-sort sample purity is presented in Figure 13.

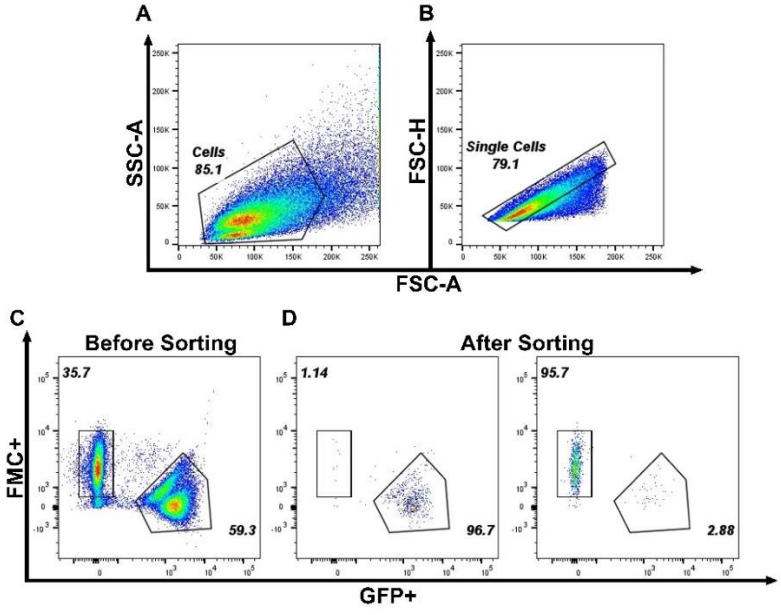

Figure 13. Representative gating strategy for sorting GFP(+) and FMC(+) Cells.

A) Cells were gated on the FSC x SSC gate, B) Single cells were selected on FSC-A x FSC-H plot, C) GFP **(+)** and FMC **(+)** cells before sorting, D) Cell purity after sorting.

2.6.7 RNA Isolation

For a healthy transcriptome analysis, the RNA amount must be more than 50 ng/µl and the RNA integrity number (RIN) must be at least 8. RNA isolation was performed for each sample according to the manufacturer's instructions that is briefly explained in section 2.2.2, and the RNA quantity was measured with Qubit Assay.

2.6.8 Qubit Assay

RNA was quantified using the Qubit™ RNA HS (High Sensitivity) Assay Kits. The procedure involved setting up Qubit™ tubes for standards and samples. The Qubit™ working solution was prepared by diluting the Qubit™ RNA HS reagent at 1:200 in the Qubit™ RNA HS buffer. Subsequently, 200 µL of the QubitTM working solution was added to each tube, followed by 10 µL of each Qubit™ standard and 1–20 µL of user samples to the appropriate tubes. Vigorous vortexing for 3–5 seconds was performed. The tubes were incubated at room temperature for 2 minutes, and readings were performed with the standards and samples using the Qubit™ 4 fluorometer.

2.7 Transcriptome Analysis

Transcriptome analysis was performed by the relevant company, Genoks Lifescience, Research and Application Center (*https://www.genoks.com.tr).* The outline of the analysis methods is as follows:

2.7.1 RNA Sequencing

Construction of the RNA sequencing library and next-generation sequencing was undertaken by the same lab for RNA sequencing. Illumina Hi-Seq4000 was used for sequencing, and at least 20 million 50 base pairs of paired-end reads were obtained for each sample. Because RNA sequencing is a highly reproducible technology, independent biological repeats were used for each experimental group rather than a technical replicate.

2.7.2 Bioinformatic Analysis and Gene Determination

RNA-seq analysis involves first aligning the raw sequencing reads to a reference genome and then establishing a relationship between the raw sequencing reads and the

transcript. It then includes evaluating the level of expression of genes or transcripts relative to sequencing reads aligned to the reference genome. Normalization and differential expression (DE) analyses were required to identify intergroup differentially expressed genes (DEGs). An expression matrix was created using normalization methods to evaluate gene expression based on calculations. The algorithms of DESeq2, edgeR and Limma were all used for determination of DEGs.

2.7.3 RNA Seq Validation

The genes determined as the result of the bioinformatic analysis were analyzed and expressions were validated by the qRT-PCR analysis. The primer sequences for each gene are listed in Table 3. Commonly expressed DEGs were given at the "results" section and an outline has been added to the "appendix" section.

Table 3. qRT-PCR Primers used in sgRNA validation.

Gene	Forward	Reverse
mHmga2	TCGCGGGTGGGCTGAGT	TCAGCCCAGGGACAACCT
mPcmtd1	AAAGAAGCTCAGTACATCCGAAC	TTGTAAGCATTGTCTCGGTAGC
mUxs1	CCAGAAATACCCGCCTGTAAAG	CCAGAAATACCCGCCTGTAAAG
mGm15452	GATCCCGCTTACTCTTCTGC	CCAAGTCTCCTCCACTCCTC
mTmem158	AACATCAGCGTGCAACGACA	AGCCCCAGATGCTCGATGA

2.8 Crispr/Cas9 Gene Edition Experiments

According to the genes determined in section 2.7.2, gene editing experiments were conducted.

2.8.1 sgRNA Design for Gene Edition

For the *Hmga2* and *Gm15452* genes selected for epithelial cells and the *Uxs1* and *Gm15452* genes selected for stroma cells, 3 different sgRNA were designed for each gene using the method specified in section 2.5.1. Designed sgRNAs are exhibited in Table 4. The design of each sgRNA comprised a 20-base sequence essential for target specificity. To facilitate downstream molecular manipulations, a strategic modification was implemented based on the BsmbI cutting region. Specifically, the addition of the sequence "CACC" at the 5' terminus of the forward primers served as a requisite for

subsequent cloning procedures. Additionally, the incorporation of "G" at this juncture aimed to enhance the efficiency of polymerase activity during amplification. Similarly, the reverse primers underwent customization with the addition of "AAAC" at the 5' terminus and "C" at the 3' terminus.

Table 4. Designed sgRNA sequences for CRISPR/Cas9 experiments.

Gene	**Sequence 5'-3'**
gRNA1-Hmga2-F	CACC G ATCCCTACAAACCTTCTCAA
gRNA1-Hmga2-R	AAAC TTGAGAAGGTTTGTAGGGAT C
gRNA2-Hmga2-F	CACC G CATTTCATGTTGGTCGTGTG
gRNA2-Hmga2-R	AAAC CACACGACCAACATGAAATG C
gRNA3-Hmga2-F	CACC G CAGCCGTCCACATCAGCCCA
gRNA3-Hmga2-R	AAAC TGGGCTGATGTGGACGGCTG C
gRNA1-Gm15452-F	CACC G TCGATGAGCACTACGAGTAC
gRNA1-Gm15452-R	AAAC GTACTCGTAGTGCTCATCGA C
gRNA2-Gm15452-F	CACC G CTTGGTGTCCAACAGAGTCT
gRNA2-Gm15452-R	AAAC AGACTCTGTTGGACACCAAG C
gRNA3-Gm15452-F	CACC G GTGTCCAACAGAGTCTAGGA
gRNA3-Gm15452-R	AAAC TCCTAGACTCTGTTGGACAC C
gRNA1-Uxs1-F	CACC G TCCCGGGCATGGTGAGCAAG
gRNA1-Uxs1-R	AAAC CTTGCTCACCATGCCCGGGA C
gRNA2-Uxs1-F	CACC G TCTCTTCAGTCAACCGCAGG
gRNA2-Uxs1-R	AAAC CCTGCGGTTGACTGAAGAGA C
gRNA3-Uxs1-F	CACC G TTCCCGGGCATGGTGAGCAA
gRNA3-Uxs1-R	AAAC TTGCTCACCATGCCCGGGAA C

2.8.2 Molecular Cloning for Crispr/Cas9 Experiments

All the designed sgRNAs were integrated into the pLentiCrispr V2 restricted backbone by following the instructions mentioned in section 2.5. After the validation of the guide integration via Sanger sequencing, lentiviral transfections were performed.

2.8.3 sgRNA Selection

To select the most effective sgRNA, 3 different sgRNAs produced for each gene and prepared by the molecular cloning method were transduced into cells in predetermined amounts (the amount and method are described in sections 2.6.1 and 2.6.2). The experimental setup is exhibited in Figure 14. RNA was isolated from the cells resulting from antibiotic selection and the expression of each gene was determined by the qRT-PCR method. The sgRNA that caused the greatest decrease in mRNA expression was selected to be used in CRISPR experiments.

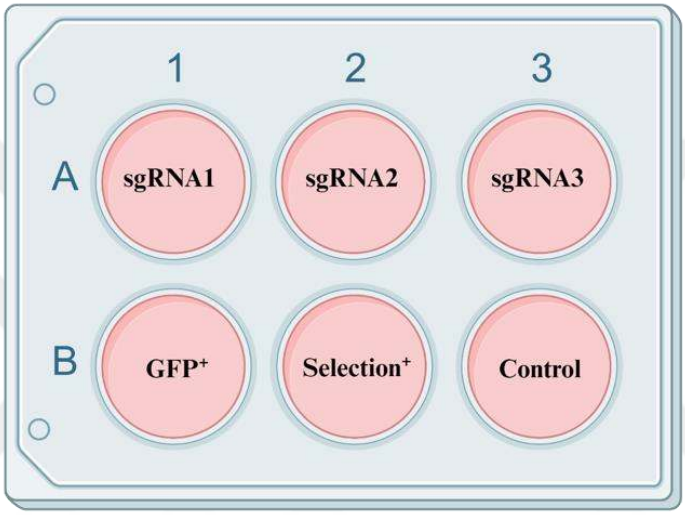

Figure 14. Experimental setup for sgRNA Selection. The figure consists of a 6-well plate design. The first row (A1, A2, and A3) wells show the wells in which sgRNA was administered to the cells. The bottom row, well B1, shows the GFP virus group introduced to check whether the cells were taking up the viruses correctly. The B2 well was created for the accurate follow-up of antibiotic selection. It was the well where no virus was administered but antibiotic selection was made. In the well B3, there was a control group in which no action was taken.

2.8.4 CRISPR/Cas9 Experimental Group Design

The most effective sgRNAs of the genes were transduced to the relevant cells and mutant epithelium and stroma were produced. CRISPR/Cas9 experimental groups created with these cells are in two time points 24 and 72hr according to the previous 3D Matrigel® culture conditions (section 2.6.4).

Gene editing for epithelial cells;

Group 1 Wild blastocyst + wild epithelium + wild stroma (control group)

Group 2 Wild blastocyst + non-targeted epithelium + wild stroma (NT-Epithelial Group)

Group 3 Wild blastocyst + mutant epithelium + wild stroma (KO (*knock-out*)-Epithelial Group)

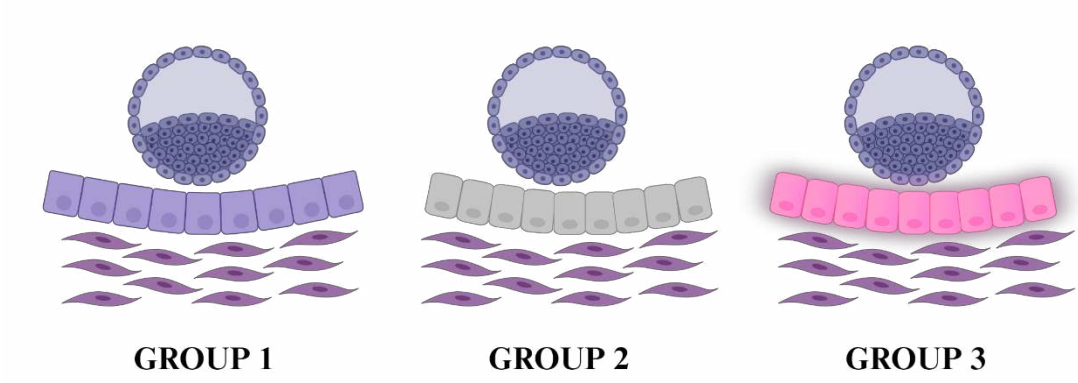

Figure 15. Gene editing groups for endometrial epithelial cells. The glowing pink color in group 3 represents that the genome of the epithelial cells in this group have been edited.

Gene editing for stromal cells;

Group 1 Wild blastocyst + wild epithelium + wild stroma (control group)

Group 2 Wild blastocyst + wild epithelium + non-targeted stroma

Group 3 Wild blastocyst + wild epithelium + mutant stroma (KO (*knock-out*)-Stromal Group)

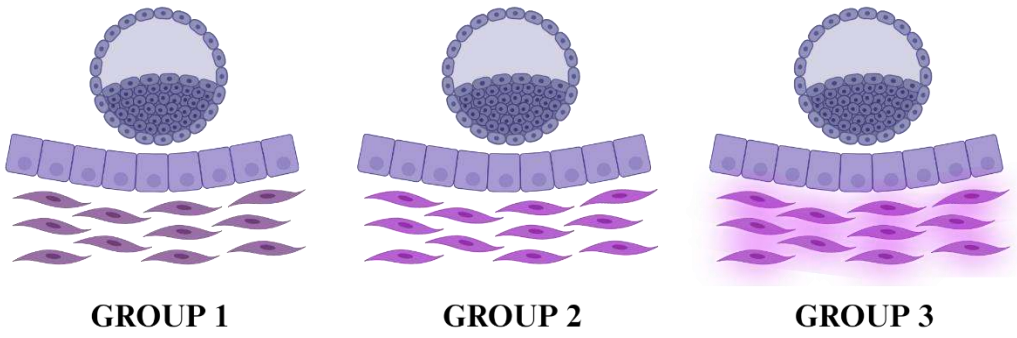

Figure 16. Gene editing groups for endometrial stroma cells. The glowing pink color in group 3 represents that the genome of the epithelial cells in this group have been edited.

2.9 Evaluation of Implantation Parameters

There exist several methods to evaluate implantation parameters. The evaluation setup is demonstrated in Figure 17.

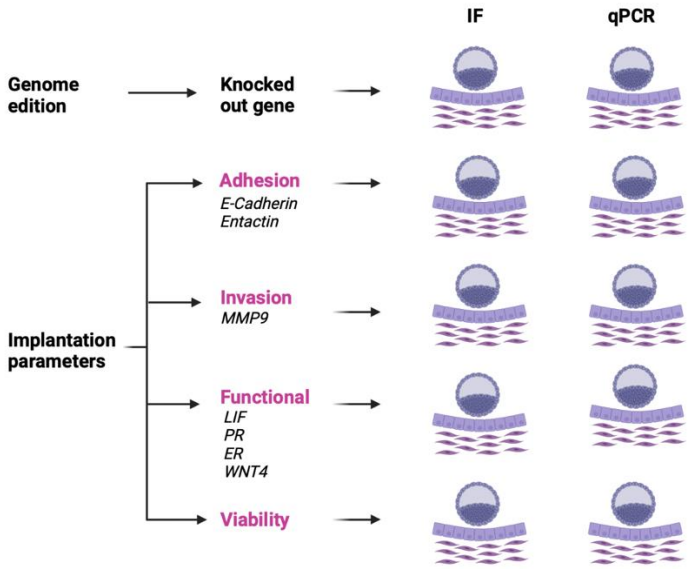

Figure 17. A brief scheme for evaluation of implantation parameters. An evaluation gene and protein expression profiles along with viability assays was performed.

2.9.1 qRT-PCR Analysis

Expressions of adhesion, invasion, and functional marker genes were determined by the real-time quantitative polymerase chain reaction method which was expressed in detail in section 2.2.4. A list of primer sequences is exhibited in Table 5.

Table 5. Primers that were used for implantation parameter evaluation.

Gene	Forward	Reverse
E-Cadherin	TCGGAAGACTCCCGATTCAAA	CGGACGAGGAAACTGGTCTC
Entactin	CCCAGCTTCGGCTCAGTAG	AACGGGGATAAGTCTTCTCGAT
Fibronectin	GATGTCCGAACAGCTATTTACCA	CCTTGCGACTTCAGCCACT
MMP9	TCCCCAAAGACCTGAAAACC	CTGCTTCTCTCCCATCATCTG
Lif	AAACGGCCTGCATCTAAGG	AGCAGCAGTAAGGGCACAAT
Esr1	TCCAGCAGTAACGAGAAAGGA	AGCCAGAGGCATAGTCATTGC
Pr	GCCAGCCAGAGCCCACAATA	TGTGCTGCCCTTCCATTGCC
Wnt4	AGACGTGCGAGAAACTCAAAG	GGAACTGGTATTGGCACTCCT

Hoxa10	GGCAGTTCCAAAGGCGAAAAT	GTCTGGTGCTTCGTGTAAGGG
Gapdh	AGGTCGGTGTGAACGGATTTG	TGTAGACCATGTAGTTGAGGTCA

2.9.2 IF Staining and Imaging

For the evaluation of adherence and invasion Anti- E cadherin, anti-MMP9 and anti-Entactin immunofluorescent stainings were performed according to protocols mentioned in the section 2.2.1. The 3D cultures grown on cover slips were visualized directly without mounting to avoid pressure over the blastocysts and then samples were mounted for long term storage. The images were obtained under a Leica dmi8/SP8 confocal microscope equipped with 405, 488 and 552 semi-solid laser lines as 1024x1024 scanning mode, with z-stacks when needed.

2.9.3 Live/Dead Cell Assay

Cell viability was checked via a live/dead cell assay, which was conducted with the LIVE/DEAD® Viability/Cytotoxicity Kit. According to the manufacturer's manual, first, the LIVE/DEAD® reagent stock solutions were thawed to room temperature. Then, a working solution was prepared by combining 20 µL of the 2 mM EthD-1 stock solution with 10 mL of sterile DPBS. The resultant solution was further enhanced by adding 5 µL of the 4 mM calcein AM stock solution. This final working solution was directly applied to the cells seeded onto the 12mm glass coverslips, ensuring comprehensive coverage. Following the 30- to 45-minute incubation process at room temperature, live (green) and dead (red) cells were observed under the fluorescence microscope. Calcein and ethidium-stained cells in the images taken from 5 different areas were counted and averaged for statistical analysis.

2.9.4 Data Analysis

Gene levels were calculated according to the housekeeping gene *Gapdh* normalization via ΔCT and ΔΔCT analysis. The GraphPad Prism program was used for statistical analysis. Semi-quantitative and quantitative differences between the groups in terms of implantation parameters were evaluated statistically and the effect of the genome edition on implantation was observed. The difference between independent groups was calculated using one-way ANOVA, and the significance between both groups was calculated using Sidak post-hoc test.

Chapter 3
RESULTS

3.1 Superovulation of Female Mice and Isolation of the Zygotes

Zygotes were successfully obtained from female mice as a result of superovulation. 10iu hCG was administrated 48 hours later after 10IU PMSG i.p. injection, and female mice mated with males at night. The next morning females that show vaginal plugs were sacrificed and the ampulla part of the uterus is collected for the zygote collection (Figure 18).

Figure 18. Uterus acquisition after the ovulation of mice. Female mice that have vaginal plaques (A, arrow) were used. After sacrification, the uterus (B, black arrow) and ampullae were quickly dissected. At the same time, the uterus (C, black arrow) is obtained for the isolation of endometrial epithelial and stroma cells. The red arrow indicates the transparent and swollen ampullae region attached to the ovary. The uterus of mouse has a didelphys form, different than the human uterus.

To show which part of the uterus is taken and to exhibit the location of the zygotes, one horn of an animal with its neighboring ovary has been prepared for histological examination and imaged under a bright field microscope (Figure 19).

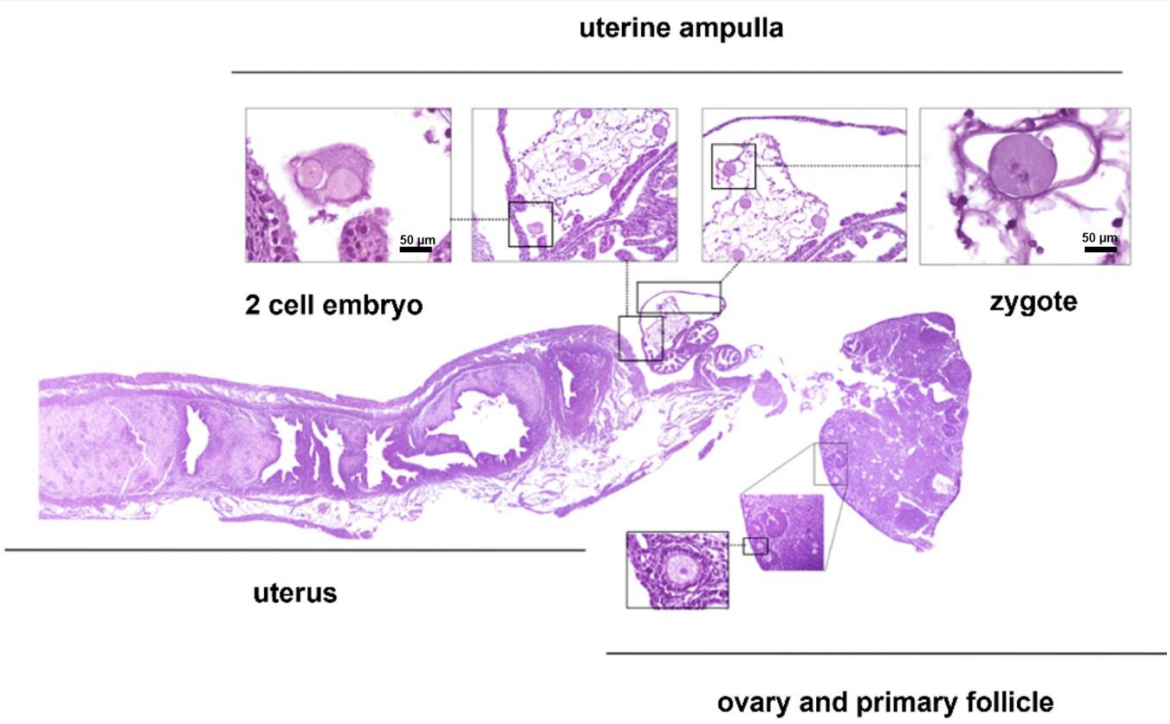

Figure 19. Histological examination of uterus, uterine tubes and ovary after fertilization of the oocytes. A longitudinal section of the uterus can be followed. The part of the uterus facing the ovary has been depicted. Two rectangular areas have been marked on the tortuous ampullary region of the uterine tube. Fertilization and zygote formation take place in this region and a newly formed 2-cell cleavage embryo along with a zygote with two pronuclei can be discriminated at the ampullary region. The status of the ovary shows some primary follicles. Staining: Hematoxylin & eosin.

Also, a part of the uterus, ampulla region, and an ovary were received a thorough histological evaluation to observe changes of the structures following ovulation induction and mating (Figure 20). Uterine endometrial cells have shown intense glycogen storage, as depicted by PAS staining. The ampulla was found to be accumulated with spermatozoa and the zygotes as well. Some growing follicles were still observed in the ovaries as left after superovulation.

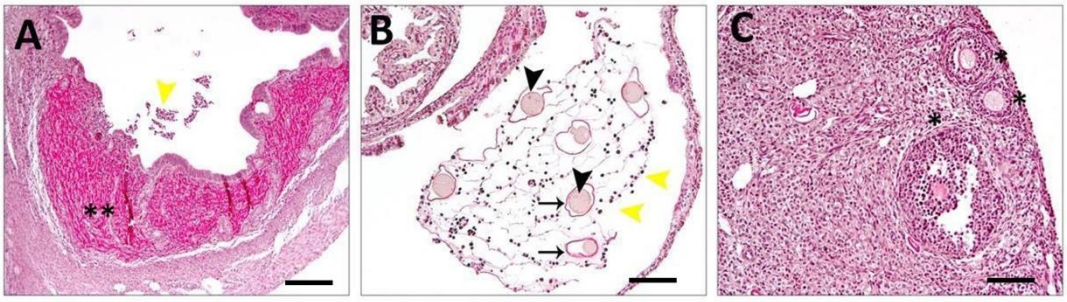

Figure 20. Histological examination of the uterus and ovary before obtaining endometrial cells and zygotes. Glycogen-rich stroma is seen in the uterine endometrial cells (A, double asterisk). Aggregations of cells are observed in the uterine lumen (A, yellow arrowhead). Zygotes (B, black arrowheads) and spermatozoa (yellow arrowheads) located in the ampulla part of the uterine tube are observed. The zona pellucida surrounding the zygotes is visible due to its glycoprotein structure (B, black arrows). Some growing follicles at different developmental stages are still observed after ovulation (C, asterisks). Staining: PAS. Scale bars: *A=200* ***µm; B, C=100 µm.***

3.2 In Vitro Embryo Cultures and Embryo Selection

The ampullae were disintegrated in GMOPS solution with BSA added, which was previously heated, and then they were taken into 80 IU/ml hyase solution resulting in the emergence of zygotes and shedding of cumulus. The resulting zygotes were quickly placed on 35 mm culture plates in single-stage embryo medium drops of 10 µl (Figure 21) and kept in a CO_2 (6-6.5 %) incubator for pH of the medium adjusted to 7.34-7.35.

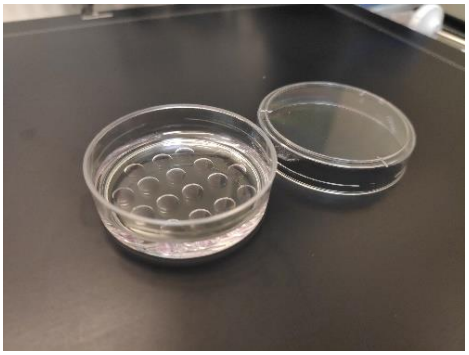

Figure 21. Embryo culture plate. 10 µl embryo culture drops were placed on the 35 mm culture place surface and mineral oil was overlaid on the culture drops o inhibit evaporation and contamination.

The collected zygotes were cultured in the single-step medium for 5 days, up to reaching the blastocyst stage. The daily development of embryos over 5 days is exhibited in Figure 22.

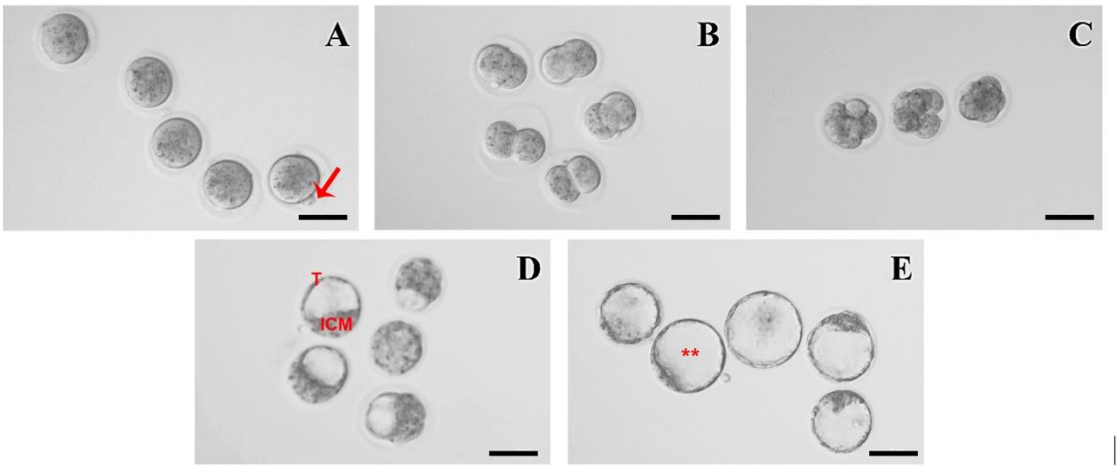

Figure 22. Temporal development of the zygotes. The development of the zygotes is observed daily by using a live cell microscope. On the first day, the zygotes (A) are seen surrounded by zona pellucida and polar bodies in the perivitelline space (A, red arrow). On early second day, 2-cell embryos that have already formed (B). On day 3, embryos with 6 or more blastomeres are observed (C). On the fourth day, early blastocysts were seen with the blastocoel, also trophoblast (T) and inner cell mass (ICM) can be distinguished easily (D). On the fifth day, the blastocoel is filled with fluid, and it is observed that the structure expands, the zona is stretched, and hatching begins in some blastocysts (E, asteriks). *Scale bars= 60 µm.*

Good quality blastocysts (grade 5AA and 4AA) were selected according to Gardner's scoring criteria. For this purpose, an enlarged blastocoel, i.e., score 4, or 5 if hatching has already begun; a tightly and compactly packed inner cell mass containing many cells, i.e., score A; and trophectoderm cells containing many cells and a cohesive epithelial structure, i.e., score A, were preferred for good-quality blastocyst selection (Figure 23).

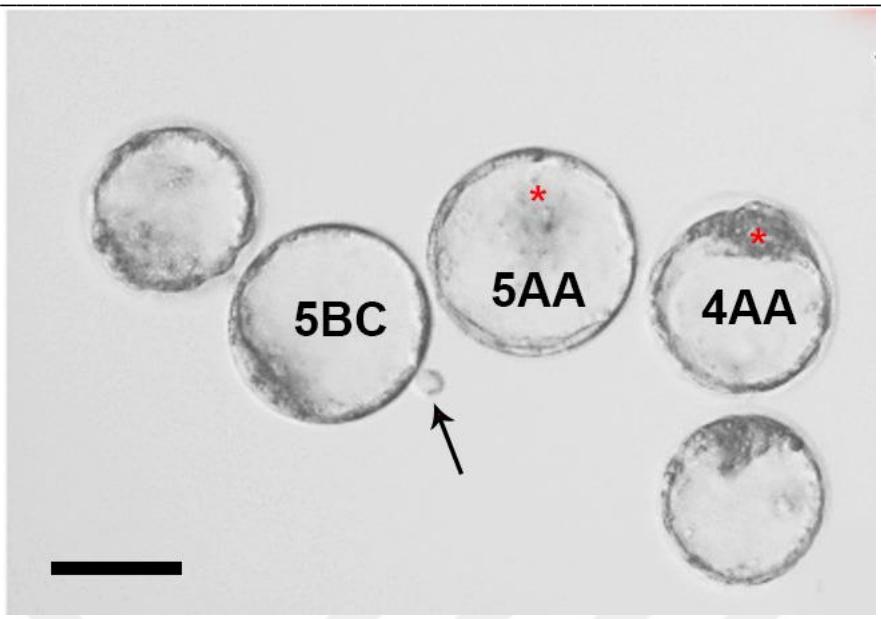

Figure 23. Selection of *in vitro* cultured blastocysts. In the single-stage culture medium, 80% of the zygotes formed blastocysts. 4AA and 5AA quality blastocysts are usually selected for the experiments. Occasionally blastocysts of moderate quality have also been used. The black arrow indicates the hatching site on a moderate quality blastocyst. Inner cell mass areas of high quality blastocysts (4AA, 5AA) have been marked by red asterisk. *Scale bars = 60 µm.*

3.3 Isolation and Characterization of Uterine Epithelial and Stromal Cells

The uterus was removed immediately after the resection of the ampullary regions and placed in HBSS to be brought to the IVF cabin for further manipulation. The lumens were exposed by cutting the uterine horns longitudinally with the help of a sterile scalpel. Tissue was minced and treated with trypsin-EDTA and collagenase/dispase enzymes to isolate epithelium (both lining and glandular) and stroma components. HBSS or medium supplemented with serum was added to end the enzymatic activation of the obtained lysate. For cell isolation, the lysate was passed through a 70 µm and 40 µm meshes, respectively. For epithelial cell isolation, cells above the 40 µm mesh were collected, while for stroma cell isolation, cells below the 40 µm mesh were collected. The pellet obtained by centrifugation was seeded in 6 well plates (Figure 24).

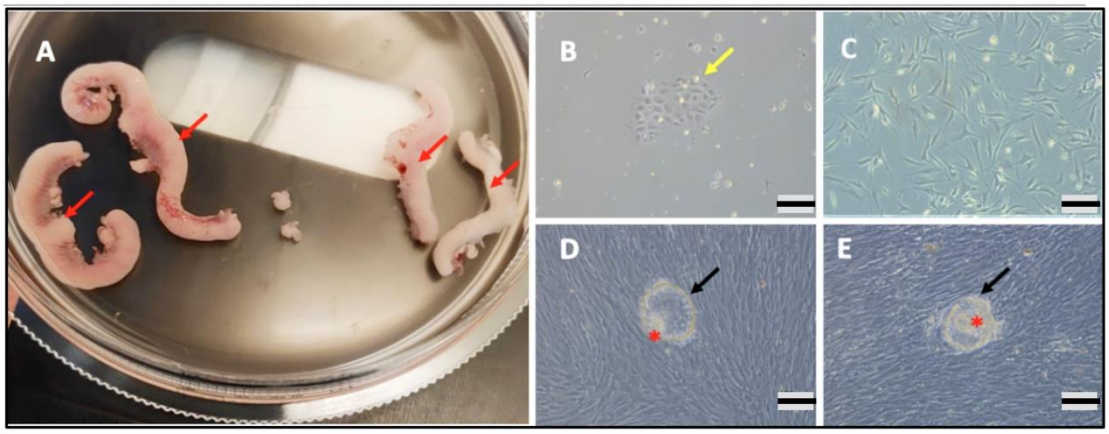

Figure 24. Isolation and culture of endometrial cells. Dissected uteruses (A, red arrows) were cut into small pieces and taken into enzymatic solution. Epithelial cell clusters were identified by typical cobble-stone appearance (B, yellow arrow), and stromal cells (C) have shown fusiform phenotype at the 48hr of isolation. Blastocysts (D, E; black arrows) with the visible inner cell mass structure (D, E; red asterisks), were cocultured with the epithelial and stromal cells. It is observed that the blastocysts have been attached to the culture just below the asterisk (E). *Scale bars=100 µm.*

The characterization of epithelial and stromal cells was demonstrated by qRT-PCR and IF stainings (Figure 25).

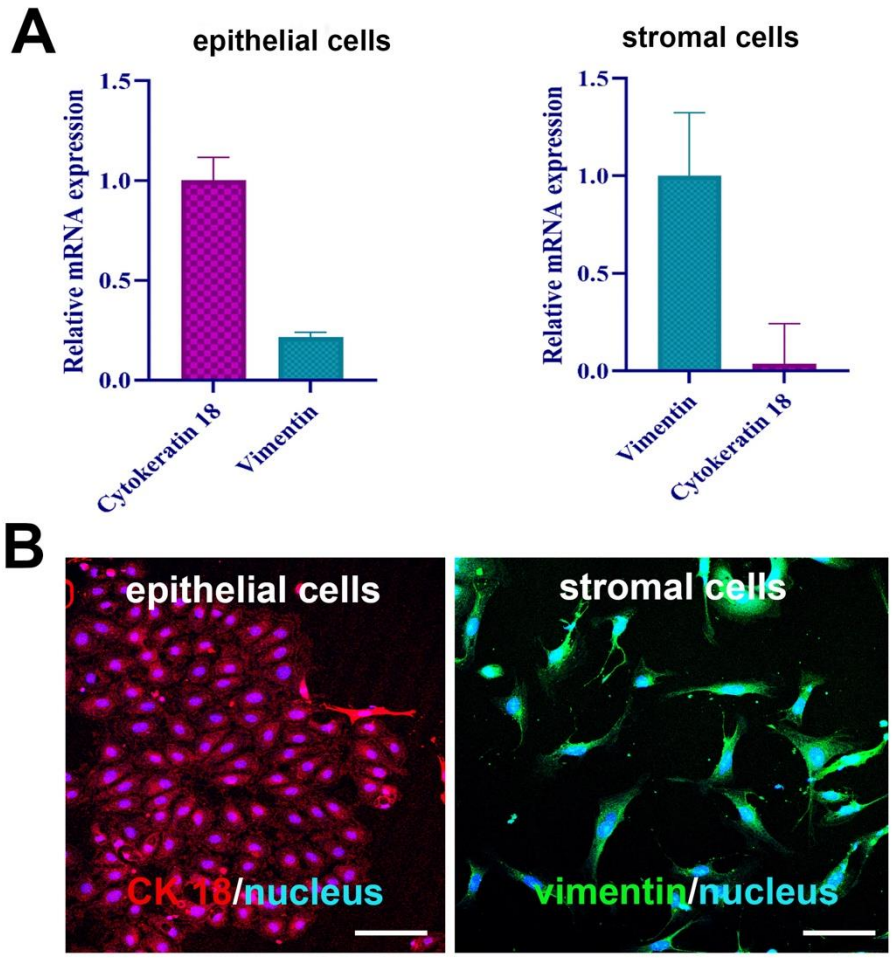

Figure 25. Characterization of epithelial and stromal cells. Cultured cells were sampled for characterization during the second passage for epithelial cells and third passage for stroma cells. Gene expression analysis has revealed strong expression of cytokeratin in epithelial cells and vimentin for stroma cells (A). A similar expression profile has been obtained at protein level, as polygonal epithelial cells were positive for CK-18, whereas stromal cells were vimentin-positive, depicted by IF staining. *Scale bars =50 µm.*

3.3.1 Decidualization Assay Results

Decidualization markers (*PRL* and *IGFBP1*) were checked by qRT-PCR (Figure 26). As a result of the ΔΔCT analysis, it was shown that *PRL* and *IGFBP1* gene expressions were significantly increased in the REPRO group, where the E2 and P4 hormone-added medium was used.

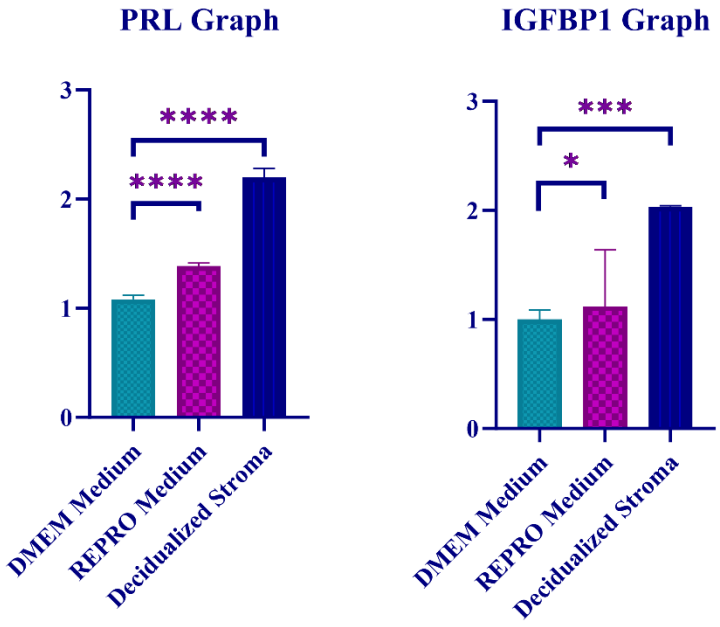

Figure 26. The expression of decidualization markers PRL and IGFBP1. The purple asterisk represents the statistical significance between the groups, $p<0.05$. It is shown that in samples using repro medium for 4 days, higher amounts of prolactin and insulin-like growth factor-binding protein 1 expression are observed compared to normal DMEM medium. At the same time, an already decidualized and isolated stroma sample (from a superovulated mouse uterus) was used as a positive control.

3.4 Preparation of GFP and FMC Lentiviruses

Labeling of the cells was done by lentiviral transduction. For this reason, virus production was carried out as specified in the relevant section.

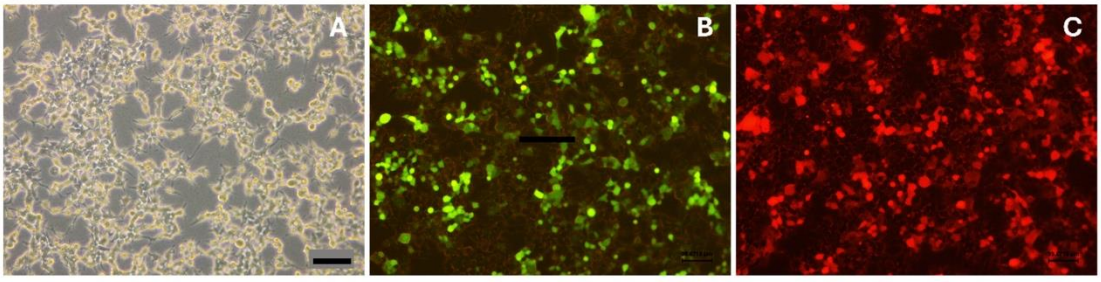

Figure 27. Transfection: LV Production. Bright field appearance of 293T cells (A), LV-GFP producing cells (B), and LV-FMC producing cells (C). *Scale bars =100 μm.*

3.4.1 MOI Calculation and Antibiotic Titration Results

MOI calculation was done according to the protocol given in Chapter 2 section 2.1.5.

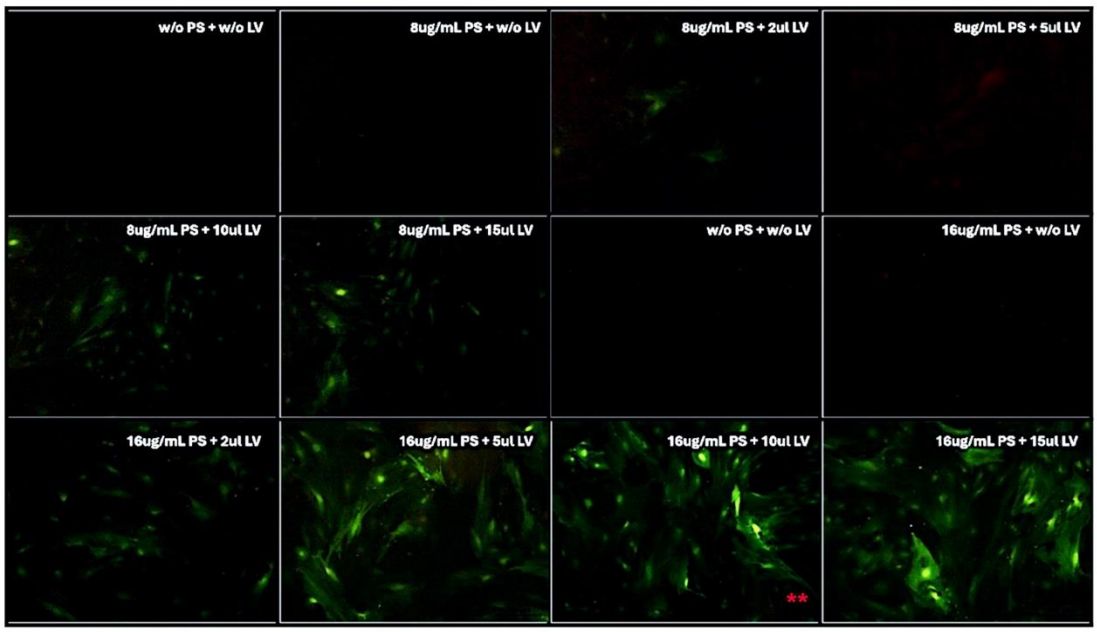

Figure 28. MOI Calculation for LV-GFP induction. At this stage, where different protamine-sulfate and lentivirus concentrations were used, the brightness of GFP was similar with of 16 µg/mL PS and 5, 10 and 15 µl virus at a rate of around 50-60 % of glowing. Of all, a mixture of 16µg/ mL PS and 10 µl virus (double red asterisk) was used for LV-GFP induction.

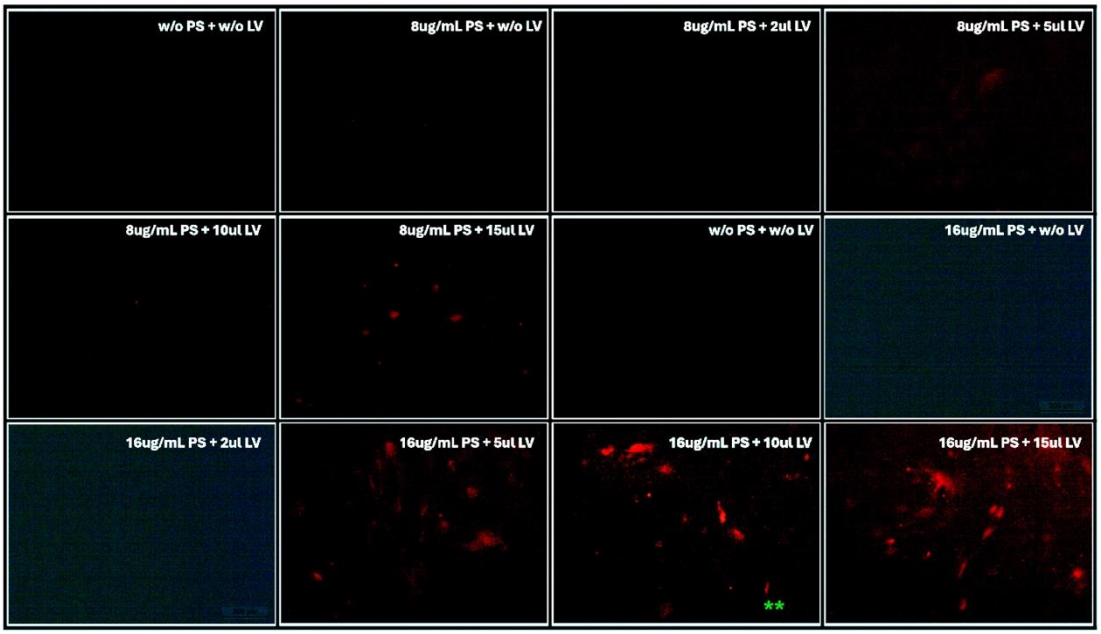

Figure 29. MOI Calculation for FMC induction. The best dose was determined by using different protamine-sulfate and lentivirus concentrations for FMC transduction to be applied to the cells. At this stage, a mixture of 16ug/mL PS and 5-10 µl virus with 50-60 % of glowing (double green asterisk) was determined to be used in the forthcoming experiments.

3.5 Labelling Cells with a Fluorescent Protein by Transduction Method

Epithelial cells were labeled with GFP, and stromal cells were labeled using FMC lentiviruses.

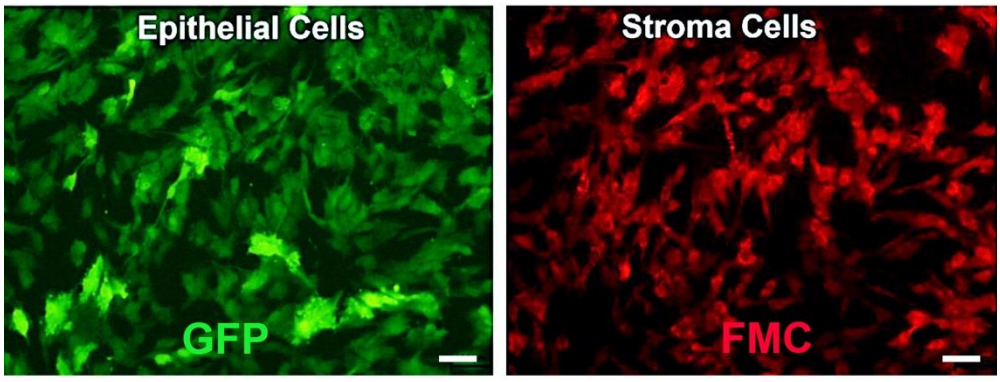

Figure 30. Preparation of the uterine cells. The transduction process was performed in 6-well plates. For this reason, the LV and PS amount determined in 12-well plates arranged according to the surface area and increased 2 folds, which means both cells were transduced with 20 µl LV and 32 µg/mL PS solution. *Scale bars =100µm.*

3.6 Construction of 3D Culture Environment

Matrigel® diluted in serum-free medium was placed in a 12-well culture dish at 200 µl per well, and gel formation was completed after waiting for half an hour at 37 °C. After gel formation, epithelial and stromal cells were seeded in Matrigel® as separate suspensions, and seeded in Repro Medium (1:1) for 3-dimensional culture formation. A transwell was placed on the wells with Matrigel® to create the transwell groups.

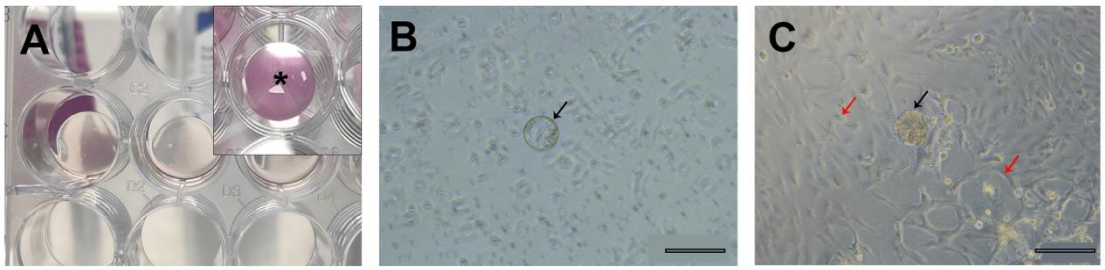

Figure 31. Construction of three-dimensional endometrial co-culture. Matrigel® (A, black asterisk), a semi-solid gel extracellular matrix, allows cells to be seeded in a stratified state. In this 3D endometrial co-culture, cultured cells can be observed at different focus at z-axis (B,C; red arrows). Black arrows show the position of blastocysts at the beginning (B) and towards the end (C) of the culture. *Scale bars =200 µm.*

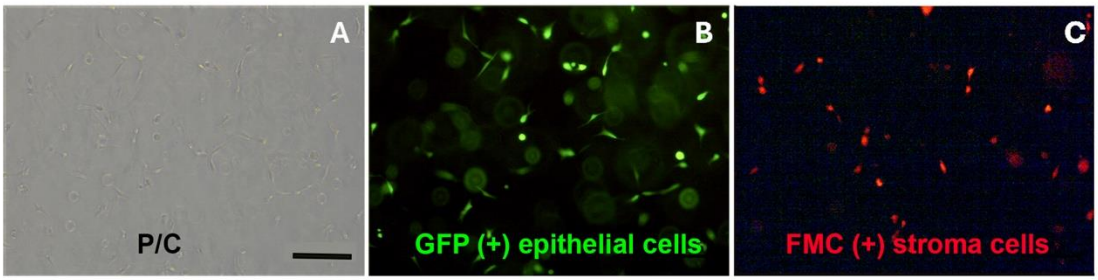

Figure 32. Endometrial co-culture of cells marked with fluoroproteins. Phase contrast (P/C) image shows endometrial epithelial and stroma cells embedded in the extracellular matrix and displaying a reticular appearance (A). GFP positive epithelium (B) and FMC positive glowing stromal cells (C) are also observable in the same culture by fluorescence imaging. *Scale bar =200 µm.*

3.7 FACS Results and RNA Seq Sample Preparation

To determine the gene expressions of the cells in the implantation area differentially, the cells in the co-culture were sorted by FACS. Cell distribution is given for each group in the following figures (Figure 33Figure 34Figure 35Figure 36).

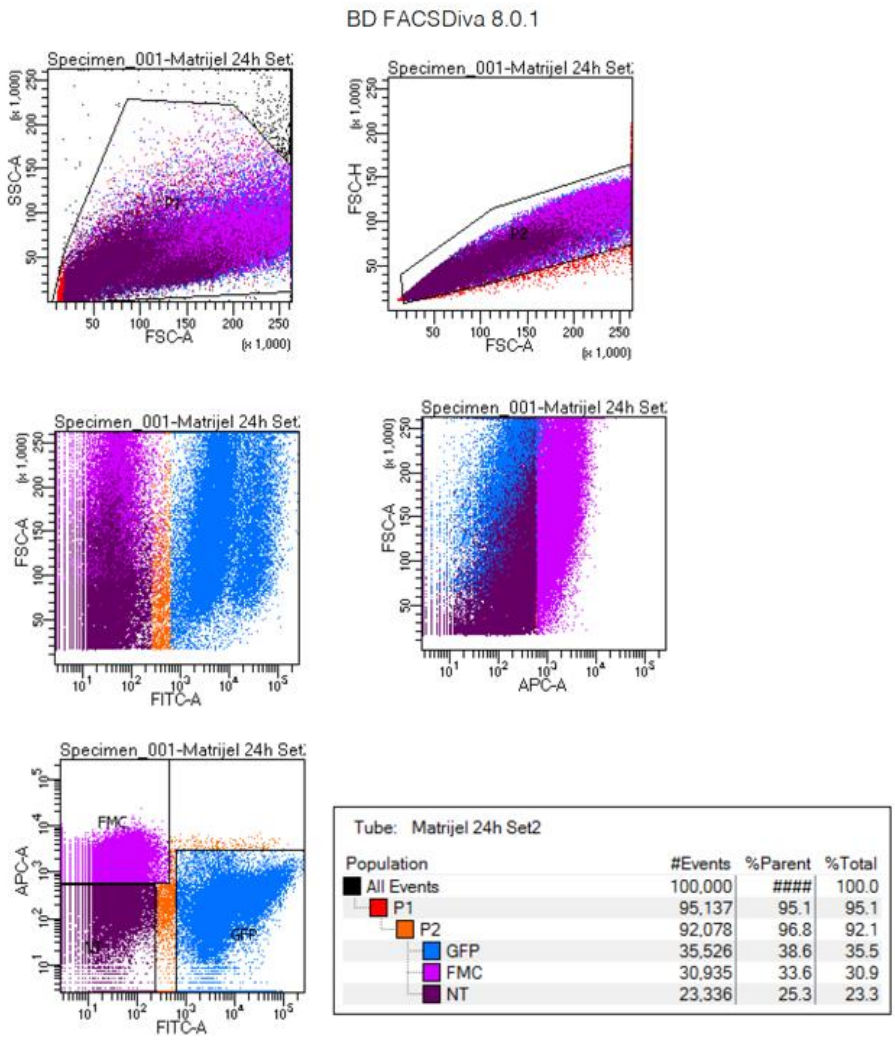

Figure 33. Sorting results of 24-hour co-culture Matrigel® group. Approximately 35000 GFP positive (epithelial), 30000 FMC positive (stroma), and 23000 non-targeted cells were obtained.

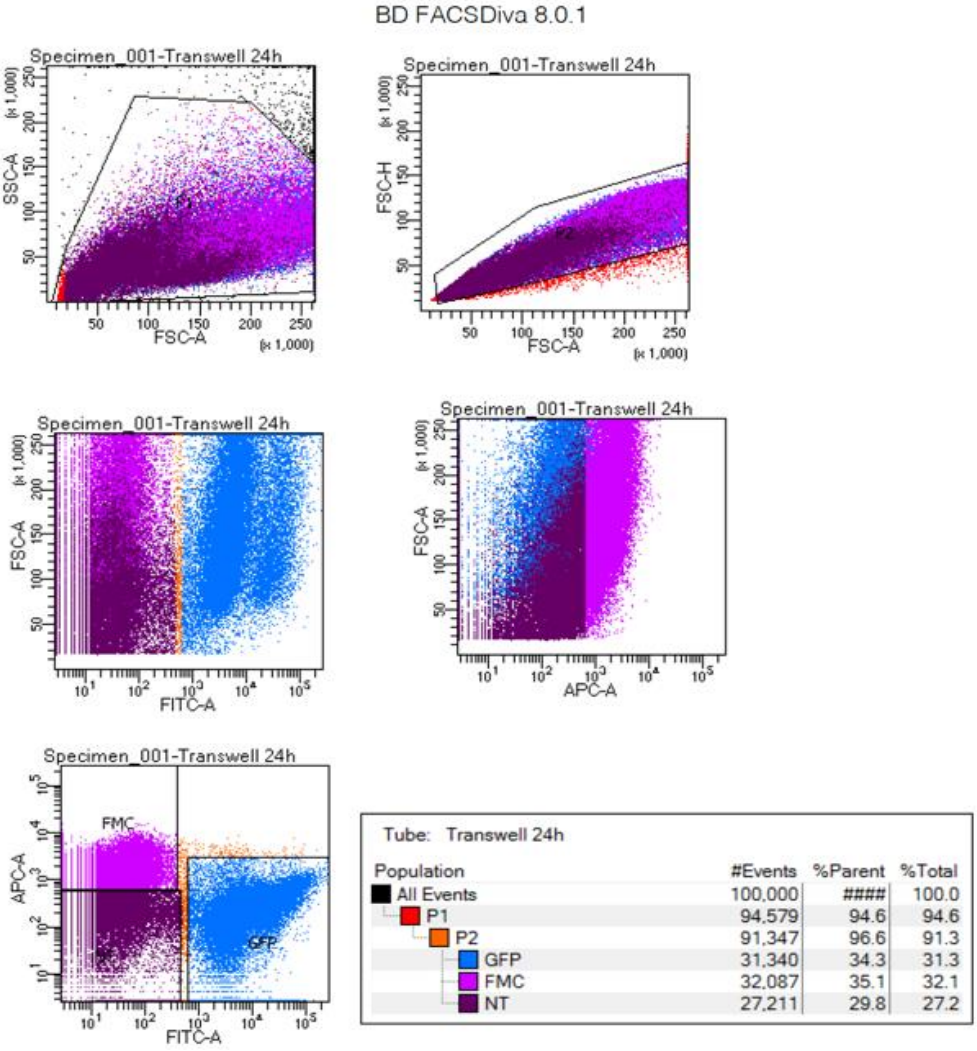

Figure 34. Sorting results of 24-hour co-culture transwell group. Approximately 30.000 GFP-positive (epithelial), 30.000 FMC-positive (stroma) and 27.000 non-targeted cells were obtained.

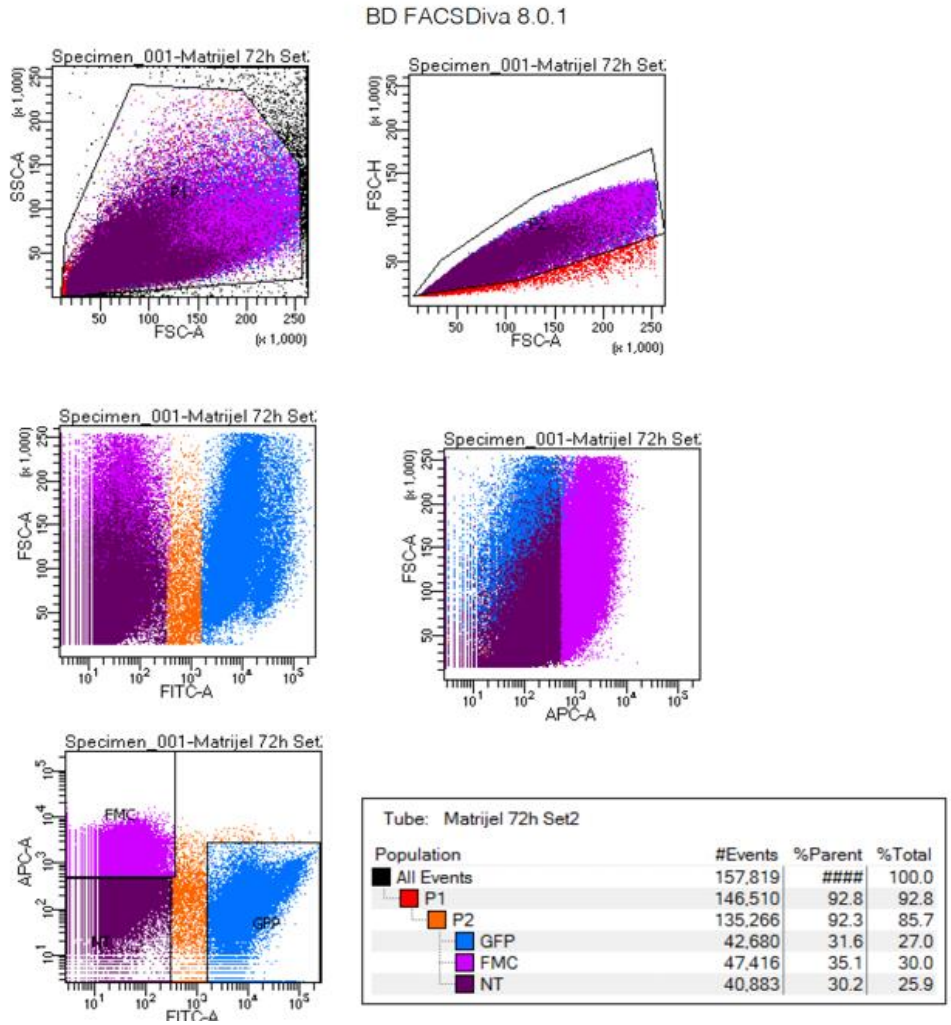

Figure 35. Sorting results of 72-hour co-culture Matrigel® group. Approximately 40.000 GFP positive (epithelium), 47.000 FMC positive (stroma), and 40.000 non-targeted cells were sorted.

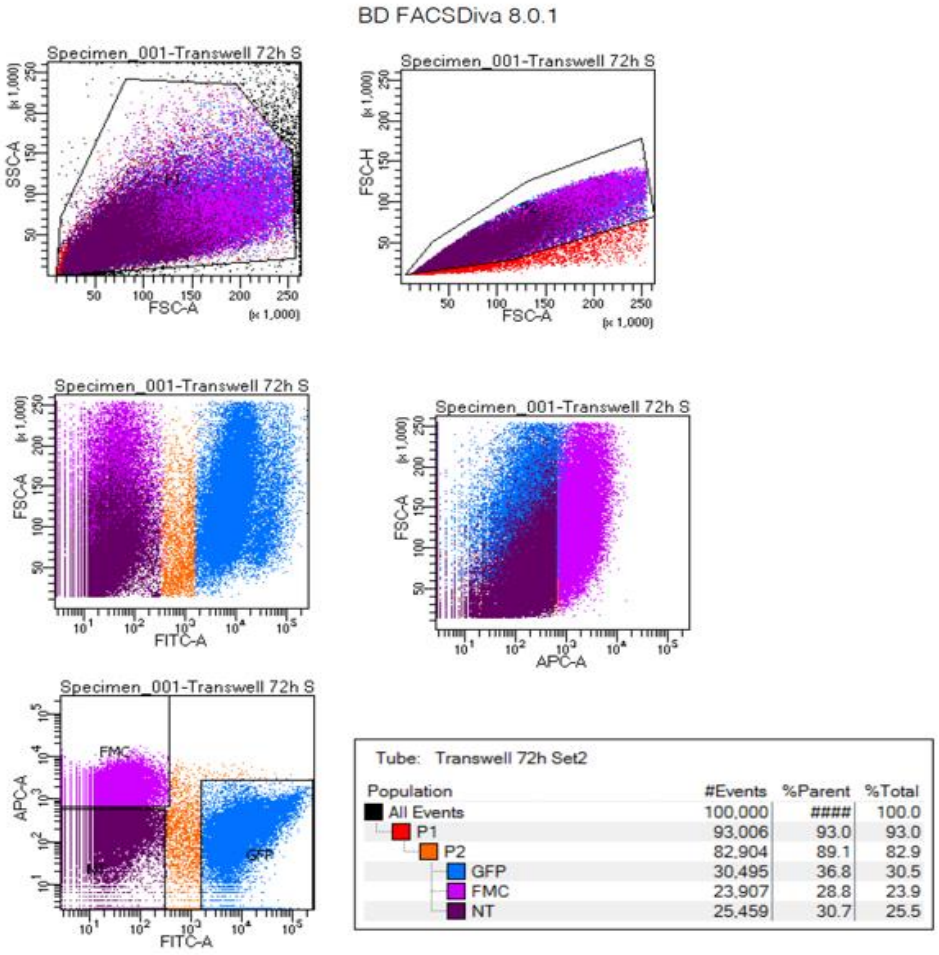

Figure 36. Sorting results of 72-hour co-culture transwell group. Approximately 30.000 GFP positive (epithelium), 23.000 FMC positive (stroma), and 25.000 non-targeted cells were sorted.

For RNA sequencing, 3 samples were prepared from each epithelial and stromal group for two times. Blastocysts (that make up the major portion of the non-targeted groups) could not be studied because they did not reach 50ng/µl. While the amount of RNA required for analysis was >50 µg/ml, the preferred RIN >9, the desired amount of RNA could not be obtained in some of the samples and all of the blastocysts. Approximately 60 unlabeled blastocysts were used in each group, but with the normal degradation of RNA during transfer after cell sorting, it was calculated that approximately 1500 blastocysts should be placed in each group to obtain the desired level of RNA from blastocysts. The calculation is as follows: 10 picograms of total RNA are obtained from 1 cell, 1 nanogram from 100 cells, and 5000 cells are required for 50 ng (Huang et al.,

2018). The amount required for RNA sequencing analysis is 50 ng/ul, and the elution amount is at least 30 µl, that is, 1500 ng of RNA should be obtained. There are an average of 90 (80-100) cells in one mouse blastocyst. This corresponds to approximately 1 ng of RNA. In this case, less than 1500 blastocysts in each group are needed for blastocyst sequence analysis, even if there is no RNA degradation. Obtaining this amount exceeds the number of mice that can be used beyond ethical limits, so the blastocysts were not included in the RNAseq analysis.

O.N.	Sample Name	Tube Number	Sample Type	Buffer Solution	Volume (µl)(>50ul)	RNA HS Qubit Result
1	Matrigel® Epithelium 24hr	1	RNA	Nuclease Free Water	25	144
2	Matrigel® Epithelium 24hr	2	RNA	Nuclease Free Water	25	82
3	Matrigel® Epithelium 24hr	3	RNA	Nuclease Free Water	25	77
4	Matrigel® Stroma 24hr	4	RNA	Nuclease Free Water	25	100
5	Matrigel® Stroma 24hr	5	RNA	Nuclease Free Water	25	86
6	Matrigel® Stroma 24hr	6	RNA	Nuclease Free Water	25	69
7	Transwell Epithelium 24hr	7	RNA	Nuclease Free Water	25	190
8	Transwell Epithelium 24hr	8	RNA	Nuclease Free Water	25	96
9	Transwell Epithelium 24hr	9	RNA	Nuclease Free Water	25	88
10	Transwell Stroma 24hr	10	RNA	Nuclease Free Water	25	168
11	Transwell Stroma 24hr	11	RNA	Nuclease Free Water	25	86
12	Transwell Stroma 24hr	12	RNA	Nuclease Free Water	25	85
13	Matrigel® Epithelium 72hr	13	RNA	Nuclease Free Water	25	61
14	Matrigel® Epithelium 72hr	14	RNA	Nuclease Free Water	25	66
15	Matrigel® Epithelium 72hr	15	RNA	Nuclease Free Water	25	64
16	Matrigel® Stroma 72hr	16	RNA	Nuclease Free Water	25	62
17	Matrigel® Stroma 72hr	17	RNA	Nuclease Free Water	25	88
18	Matrigel® Stroma 72hr	18	RNA	Nuclease Free Water	25	77
19	Transwell Epithelium 72hr	19	RNA	Nuclease Free Water	25	97
20	Transwell Epithelium 72hr	20	RNA	Nuclease Free Water	25	85
21	Transwell Epithelium 72hr	21	RNA	Nuclease Free Water	25	63
22	Transwell Stroma 72hr	22	RNA	Nuclease Free Water	25	145
23	Transwell Stroma 72hr	23	RNA	Nuclease Free Water	25	75
24	Transwell Stroma 72hr	24	RNA	Nuclease Free Water	25	70

Figure 37. Illustration of samples prepared for RNA sequence analysis. Each sample set was designed to include three biological replicates.

3.8 RNA Seq Results and Gene Determination

As a result of the sequence analysis, evaluation was performed according to the edgeR and DESeq2 analysis packages (as Limma did not reveal any results), and the |log2FC|>1 threshold was used to identify differentially expressed genes (DEGs) (an example of whole transcriptome analysis results are presented in the "Appendix" section). For each group; the significantly expressed genes that have not been studied before were prioritized and the significancy of expression of genes was determined according to the fold change of gene expressions (FoldChange). Genes co-expressed in

epithelial cells in Matrigel® and transwell, groups and genes co-expressed significantly in stroma cells were used for further studies. Since these genes are coding genes, qRT-PCR was performed to confirm the expression of genes in cells in the experimental groups after gene selection.

In terms of endometrial epithelial cells, no significant genes were detected in the transwell group. Therefore, no gene has been obtained from the common group and five genes with the highest significance in the Matrigel® group; **H19, Hmga2, Pcmtd1, Uxs1, and Gm15452,** were evaluated. Since H19 is a non-coding gene, it was eliminated.

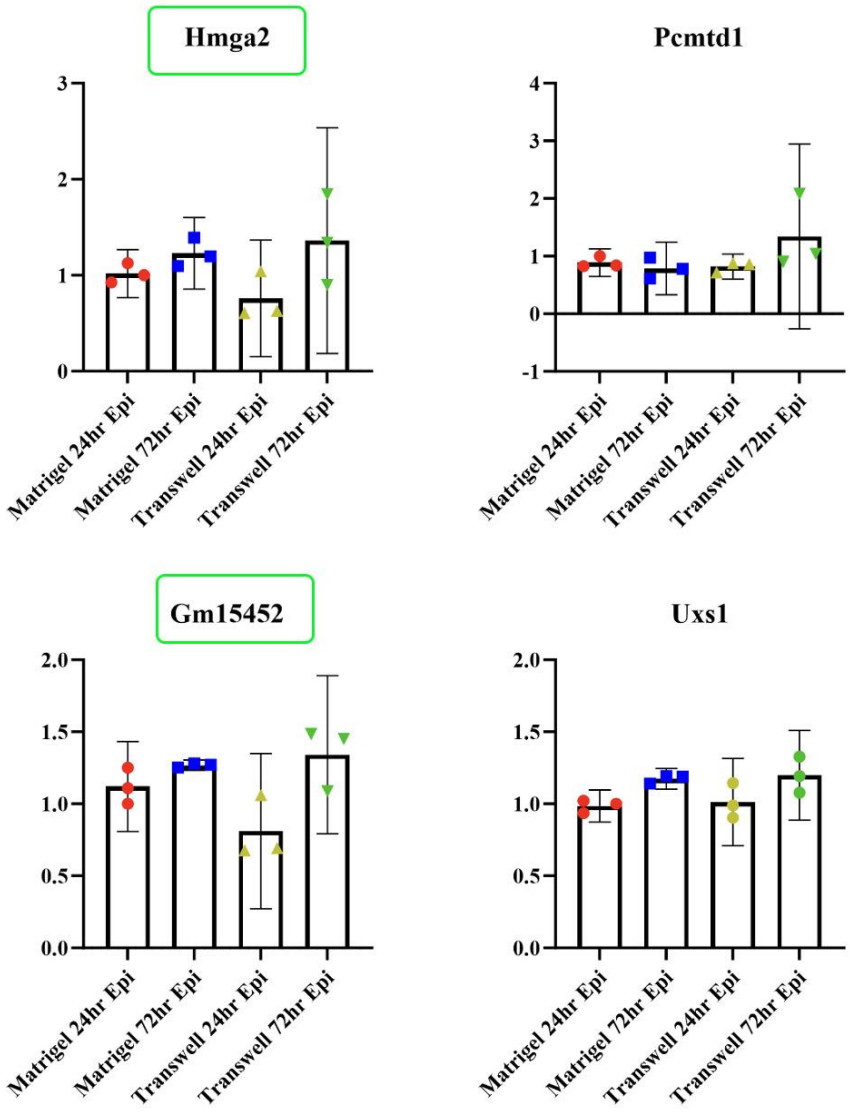

Figure 38. Confirmation of epithelial cell genes identified as a result of transcriptome analysis by qRT-PCR analysis. In the Matrigel® groups, there is an increase in all genes (Hmga2, Gm15452, and Uxs1) at hour 72, except for the Pcmtd1

gene. In Transwell groups, an increase in all gene expressions is observed between 24-72 hours. However, out of 4 genes, Hmga2, Gm15452, and Uxs1 entered at CT value 30 and earlier in qRT-PCR. Hmga2 and Gm15452 were selected. Gm15452 was prioritized over Uxs1, as it has been listed as a "predicted gene" and can lead to some novel relation with implantation process. The selected genes are marked with green rectangles.

For stroma cells, five candidate genes with the highest level of significance from the two analyses were selected. These genes are **Tmem158, Pcmdt1, Gm9826, Uxs1, and Gm15452**. First of all, to prove the expression of these genes in the relevant cells, qRT-PCR was performed, and the experiment was continued with the genes (Uxs1 and Gm15452) that have shown CT value of below 30.

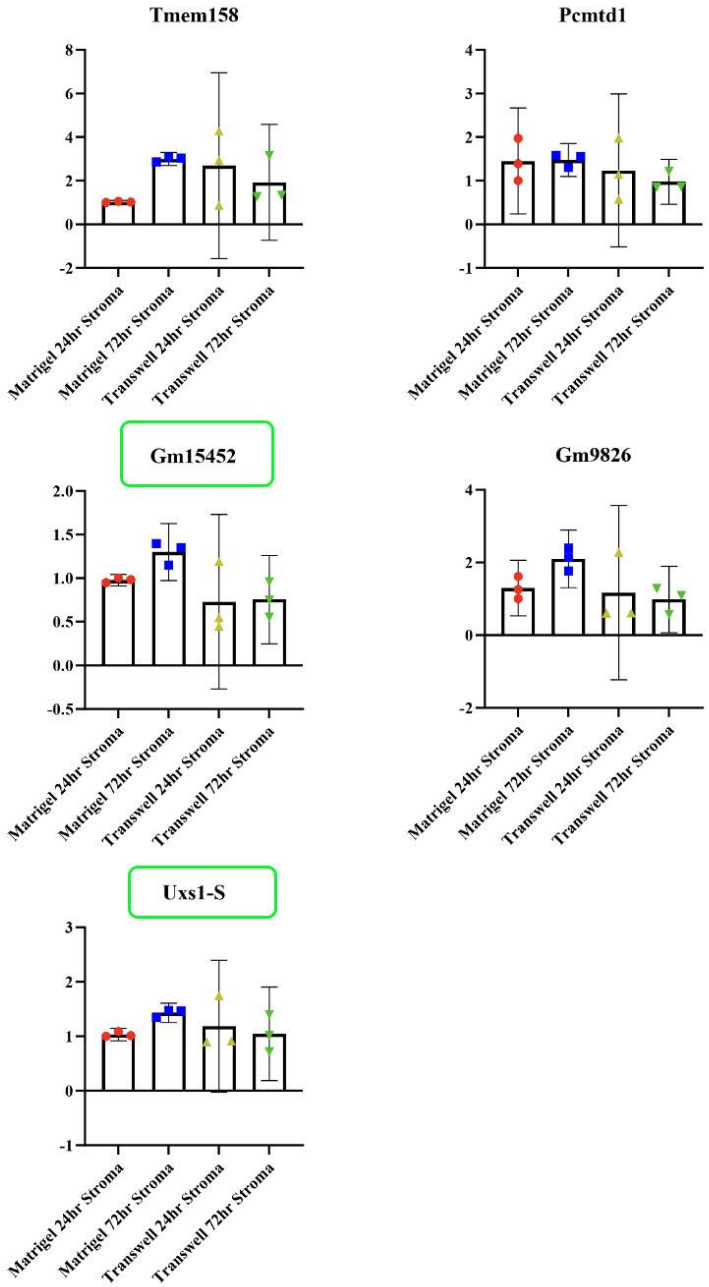

Figure 39. Confirmation of gene expression identified as a result of transcriptome analysis by qRT-PCR analysis in stromal cells. As a result of sequencing, five most expressed genes between the groups were validated using the qRT-PCR. Accordingly, it was observed that all 5 genes increased from the 24th hour to the 72nd hour in the Matrigel® groups, by the sequence results. However, out of 5 genes, Gm15452 and Uxs1 entered at CT value earlier than 30 in qRT-PCR, and they were selected. The selected genes are marked with green rectangles.

3.9 CRISPR/Cas9 Mediated Gene Editing on Uterine Epithelial and Stromal Cells

According to the RNA Seq results and qRT-PCR validation, Hmga2 for epithelial cells, Uxs1 for stroma cells, and Gm15452 for both cell types were selected to be used in CRISPR experiments.

3.9.1 sgRNA Preparation and Cloning

For each gene, 3 different sgRNAs were designed to target the exon1 region. Relevant sequences are shown in the table. While designing the guide RNAs, CACC and then G was added to the 5' region of the forward sequence by the BsmbI cutting site of the plenticrisprV2 plasmid; AAAC was added to the 5' region of the reverse sequence, and a cytosine base was added to the 3' region to match the guanine added in the forward sequence.

Table 6. sgRNAs to be used in CRISPR experiments.

Genes	*Forward*	*Reverse*
Hmga2 sgRNA1	CACC G ATCCCTACAAACCTTCTCAA	AAAC TTGAGAAGGTTTGTAGGGAT C
Hmga2 sgRNA2	CACC G CATTTCATGTTGGTCGTGTG	AAAC CACACGACCAACATGAAATG C
Hmga2 sgRNA3	CACC G CAGCCGTCCACATCAGCCCA	AAAC TGGGCTGATGTGGACGGCTG C
Gm15452 sgRNA1	CACC G TCGATGAGCACTACGAGTAC	AAAC GTACTCGTAGTGCTCATCGA C
Gm15452 sgRNA2	CACC G CTTGGTGTCCAACAGAGTCT	AAAC AGACTCTGTTGGACACCAAG C
Gm15452 sgRNA3	CACC G GTGTCCAACAGAGTCTAGGA	AAAC TCCTAGACTCTGTTGGACAC C
Uxs1 sgRNA1	CACC G TCCCGGGCATGGTGAGCAAG	AAAC CTTGCTCACCATGCCCGGGA C
Uxs1 sgRNA2	CACC G TCTCTTCAGTCAACCGCAGG	AAAC CCTGCGGTTGACTGAAGAGA C
Uxs1 sgRNA3	CACC G TTCCCGGGCATGGTGAGCAA	AAAC TTGCTCACCATGCCCGGGAA C

pLentiCrispr V2 plasmid was restricted successfully with the digestion enzyme BsmbI as shown in Figure 40.

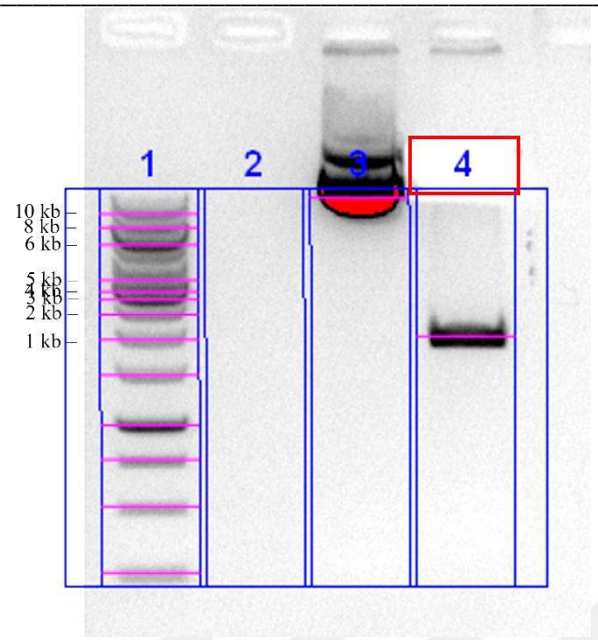

Figure 40. BsmbI restriction after electrophoresis. pLentiCRISPR V2 is a plasmid with a 14877-base pair, and the BsmbI enzyme cuts the plasmid from two different regions and divides it into two parts, one with 1885 bp and the other with 12992 bp. For this reason, both parts must be visible in gel electrophoresis imaging (row 4). The fragment to be used in the continuation of the experiment is obtained by isolating DNA from the gel (row 4, red square). The DNA ladder is shown in the 1st row, and the uncut plasmid is seen as the control in the 3rd row. The 2nd row was left empty.

sgRNA ligation was also performed successfully and the results were validated with the Sanger sequencing (Figure 41Figure 42, andFigure 43).

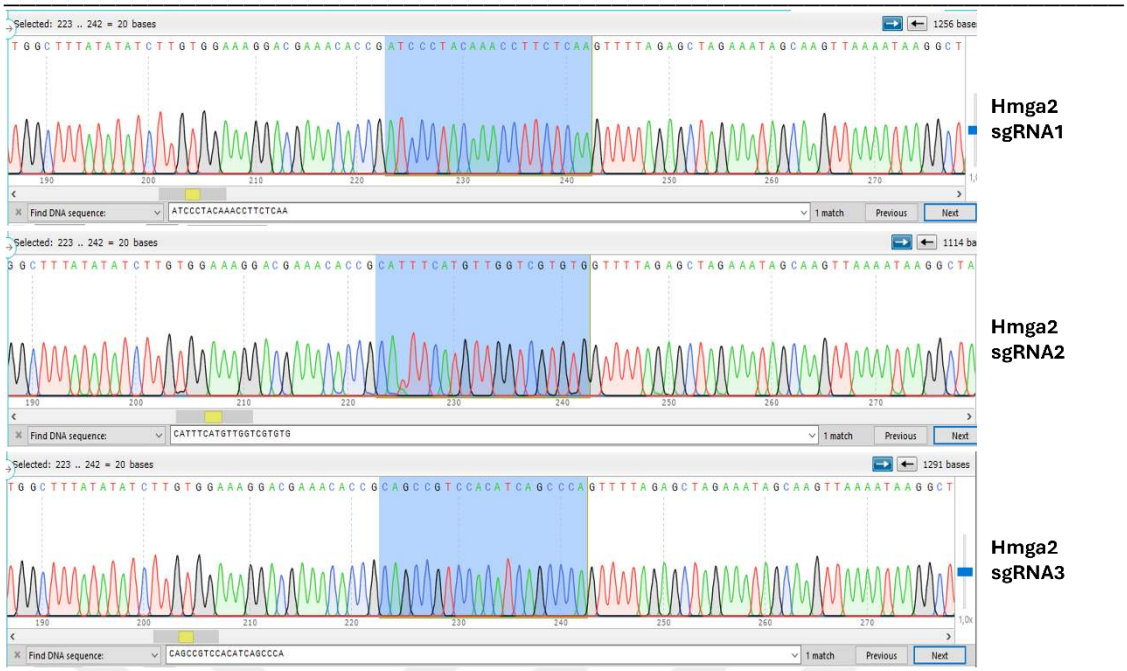

Figure 41. Demonstration of the accuracy of ligation of the *Hmga2* sgRNAs sequence into the pLentiCRISPR V2 plasmid by the Sanger sequencing method. All 3 designed guide sequences were ligated successfully.

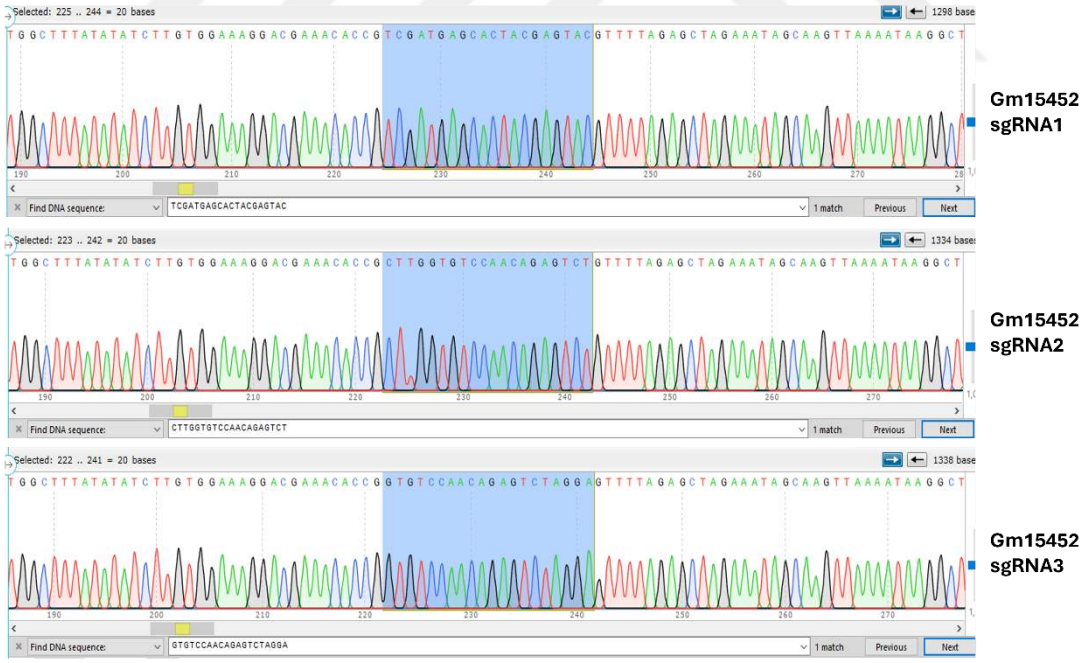

Figure 42. Demonstration of the accuracy of ligation of the *Gm15452* sgRNAs sequence into the pLentiCRISPR V2 plasmid by the Sanger sequencing method. All 3 designed guide sequences were ligated successfully.

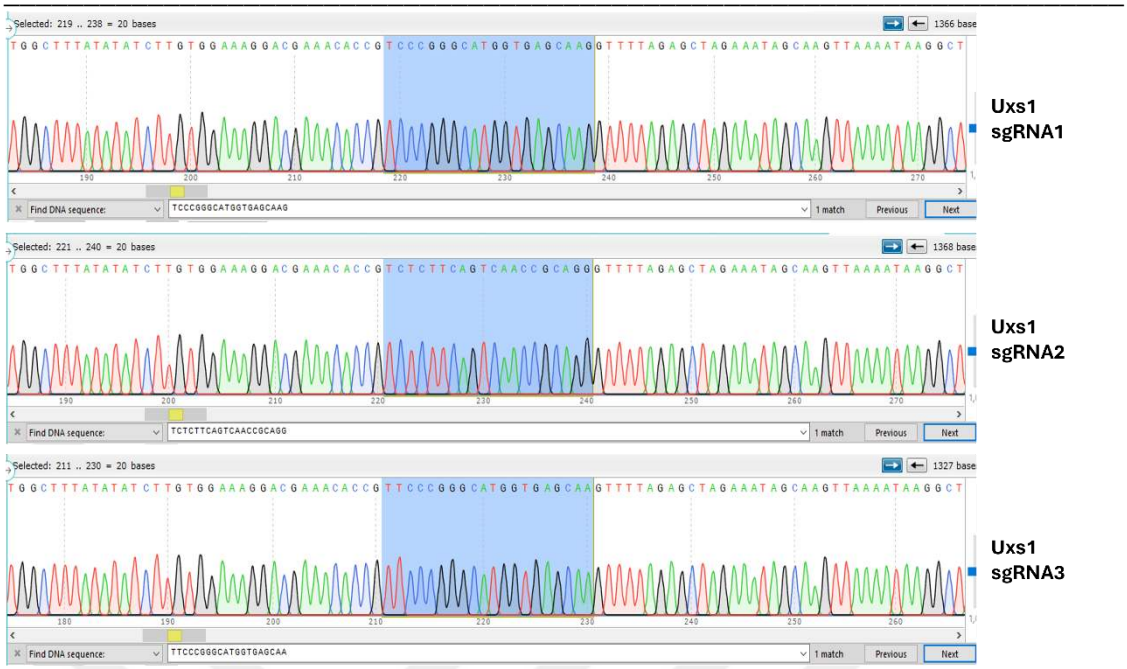

Figure 43. Demonstration of the accuracy of ligation of the *Uxs1* sgRNAs sequence into the pLentiCRISPR V2 plasmid by the Sanger sequencing method. All 3 designed guide sequences were ligated successfully.

3.9.2 Selection of Suitable sgRNA

According to the sgRNA tested, epithelial or stromal cells were seeded onto 6-well plates and transduced with 20µl of prepared sgRNA-carrying lentiviruses. To eliminate the cells that did not get the viruses, puromycin antibiotic selection was applied (Figure 44). At the end of the selection, remaining cells (cells that have not been inhibited to grow by puromycin) were collected, and qRT-PCR analysis was performed to check the sgRNA efficiency after the RNA isolation (Figure 45). Figure 43 shows an example of selection procedure for GM15452 for stromal cells.

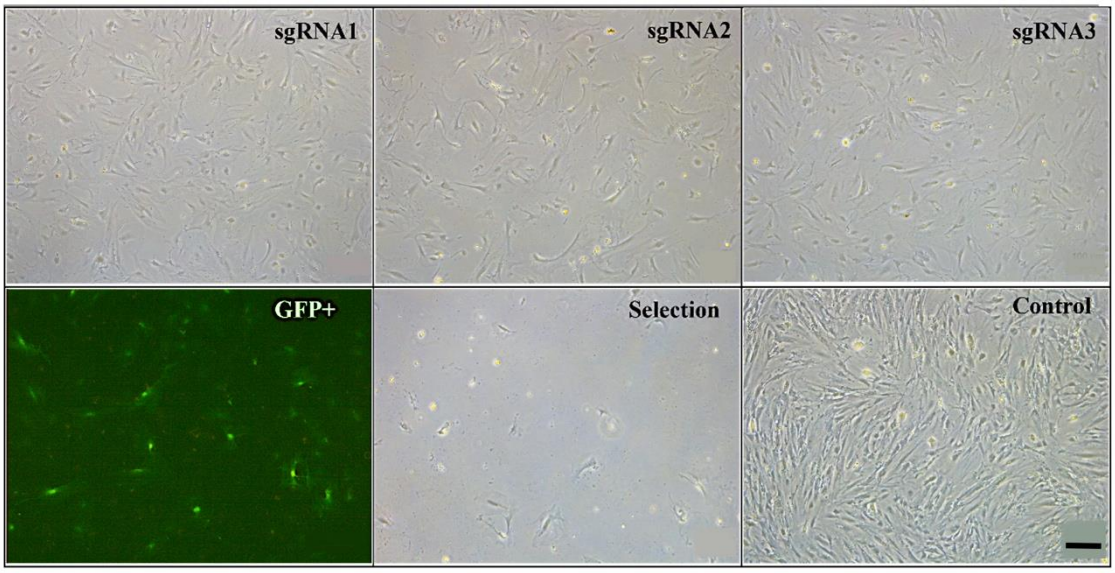

Figure 44. Selection of suitable sgRNA. Viruses capable of silencing appropriately for epithelial and stromal cells were selected for the continuation of the experiment, and gene modifications were made in the relevant genes by incubating them with the cells for up to 18 hours in the condition of 37°C and 5% CO_2. Cells that did not take up the virus were removed by puromycin selection, as cells that take up virus should be resistant to puromycin. For selection follow-up, there was a control group in which LV was not given but selection was applied. At the same time, to show that the cells were transduced, a control group was created with GFP carrier LVs produced together with the sgRNA carrier LV. Scale bar for all figures is shown in the control group and it represents 200 µm.

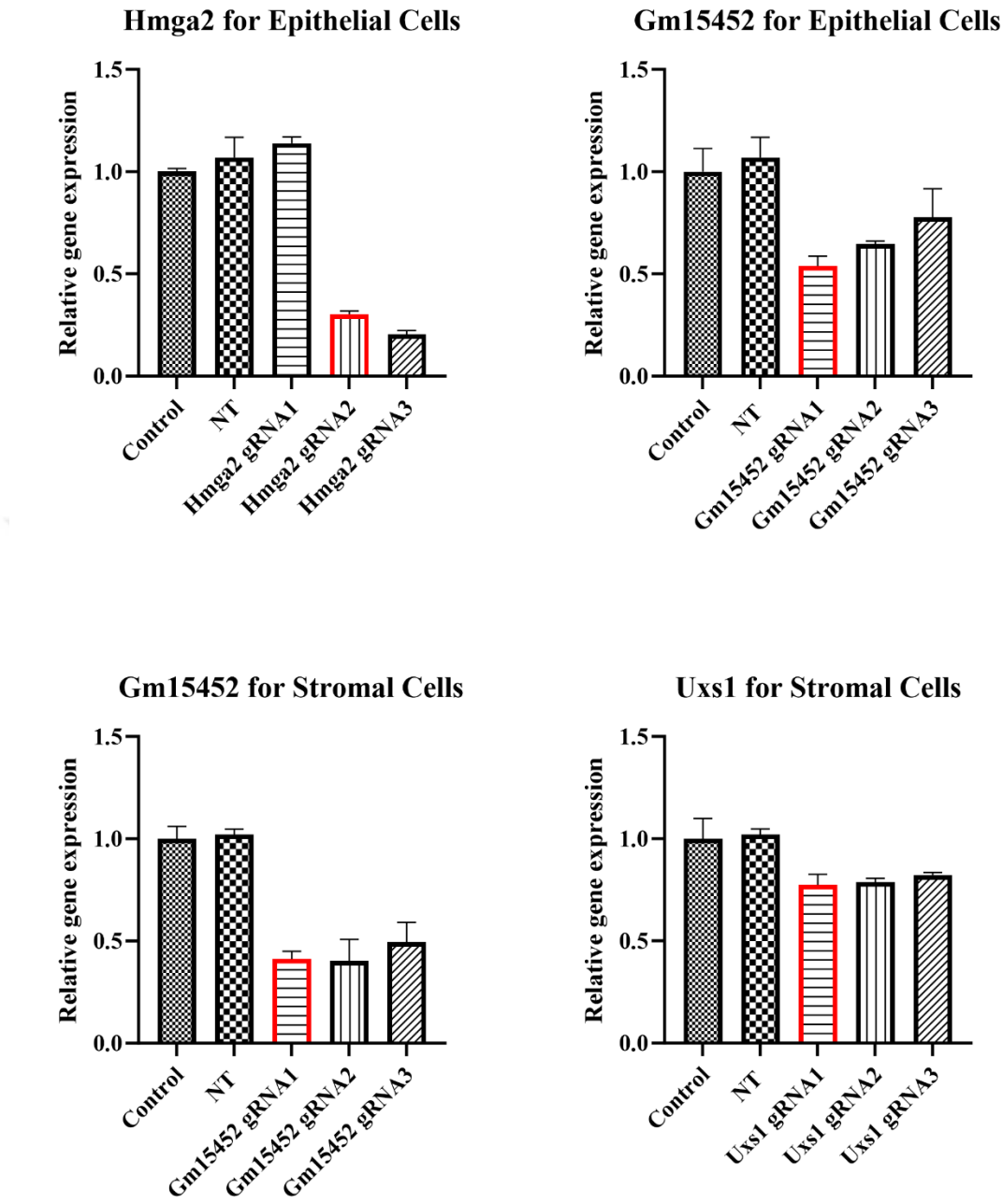

Figure 45. sgRNA effect validation on epithelial and stromal cells by using qPCR analysis. To silence the Hmga2 gene in epithelial cells, sgRNA 2, which can be silencing more than 50%, was chosen. For the Gm15452 gene, sgRNA 2, which can downregulate up to 50%, was used for both epithelial and stroma cells. Uxs1 sgRNA 3 was picked, although it worked with low efficiency as a single gene in the stromal cells. The red color indicates the selected sgRNAs for the further of the experiment. NT stands fort he non-targeted groups, where has only Cas9 without any sgRNA.

3.10 Evaluation of Implantation Parameters for Endometrial Co-Cultures

Expression distributions of implantation parameters in the created 3D endometrial co-cultures were determined by the qRT-PCR method. These implantation markers were examined in 3 different groups in terms of attachment, invasion, and functional markers (Figure 46). As a result of the analysis, it was determined that *E-cad* showed a significant decrease in its expression amount at hour 72 of incubation when compared with the 24th hour of incubation. Although it was not significant in entactin and fibronectin expressions, it was determined that there was a slight decrease in entactin and a more visible fall in fibronectin at hour 72.

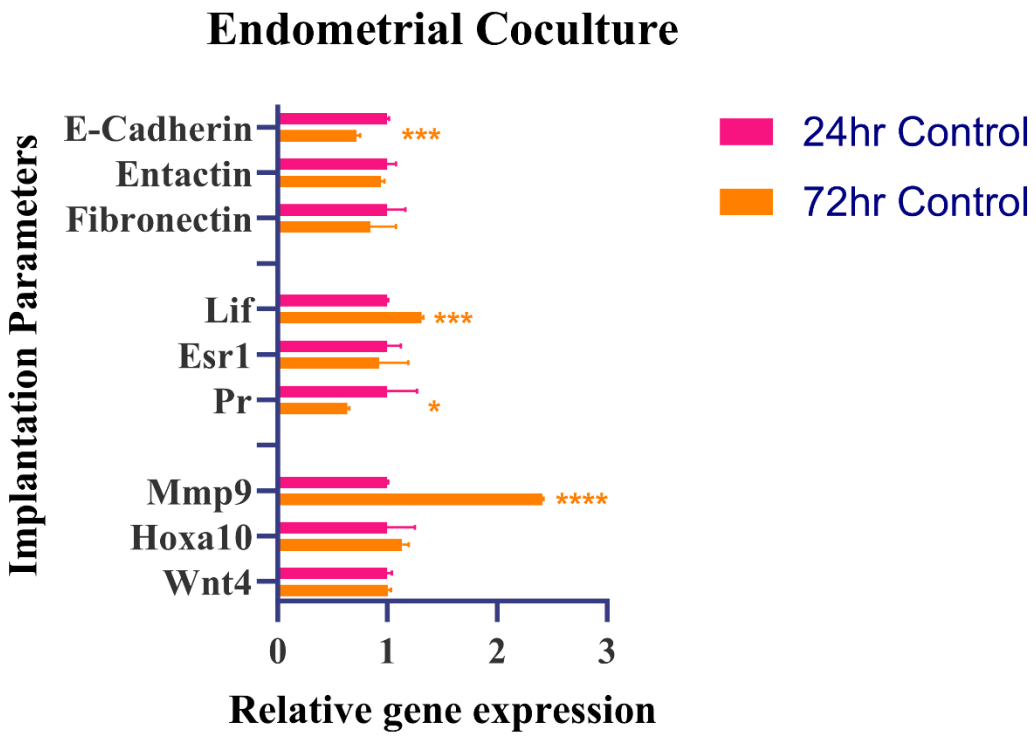

Figure 46. Expression distributions of implantation parameters in the *in vitro* created 3D endometrial co-culture. Significance; (*) p<0.05, (**) p<0.001, (***) p<0.0001, (****) p<0.00001

As functional genes, *Lif, Esr* and *Pr* expression was evaluated. As a result of the qRT-PCR analysis, it was observed that there was a significant increase in *Lif* expression in endometrial co-cultures created *in vitro* at the 72nd hour compared to 24 hours of incubation. A non-significant decrease was observed in the expression of *Esr1*, which is

an estrogen receptor marker, at the 72nd hour, and a significant decline was observed in the expression of *Pr*, which is a progesterone marker. As an invasion marker, gene expression of *Mmp9* was examined It was determined that the expression of the invasion marker *Mmp9* increased statistically significantly at the 72nd hour compared to the 24-hour of endometrial cocultures. To reveal the developmental status *Hoxa10* and *Wnt4* expression was examined *in vitro* by qRT-PCR analysis. A slight, although not significant, increase in *Hoxa10* expression was observed at the 72nd hour, and there was no difference in *Wnt4* expression. Immunofluorescent staining was performed for e-cadherin, entactin and MMP9 to examine the adherence and invasion status. The results have been outlined in Figure 47.

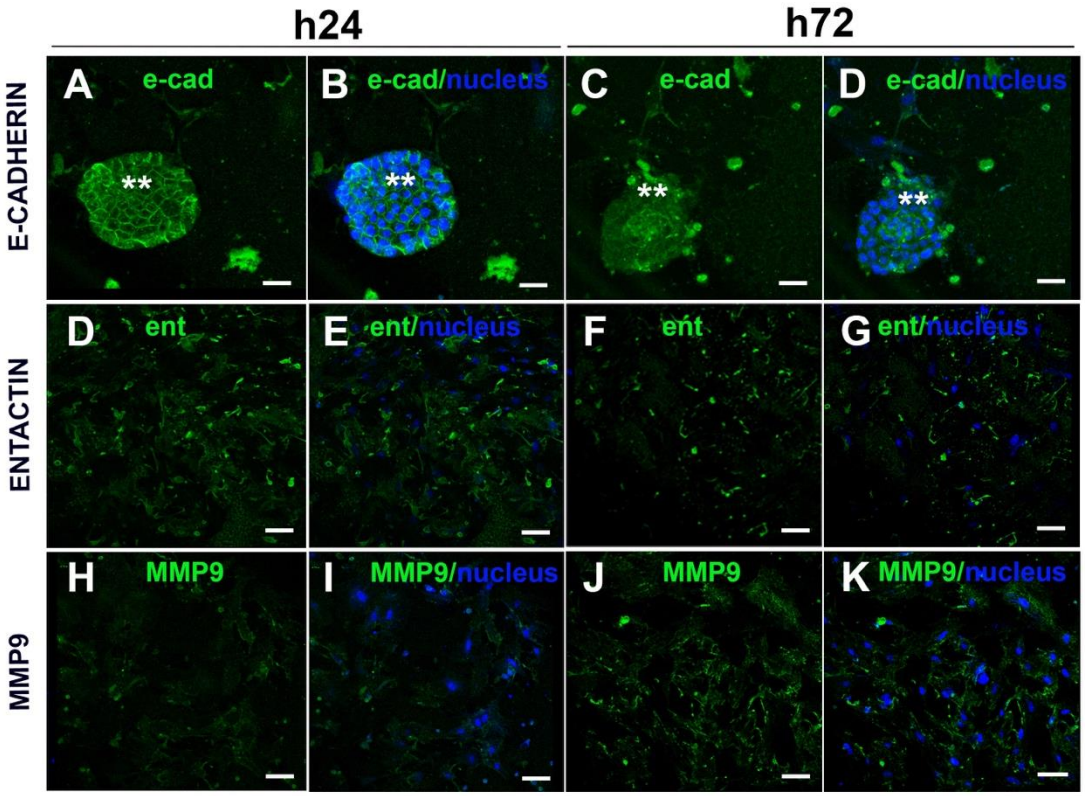

Figure 47. Temporal expression of some implantation related proteins through 24 to 72 hours of culture. In correlation with gene expression, a decline in e-cadherin has been observed (A-D), especially in the trophoblastic cells of the blastocyst (double asterisk, A-D), as well slight decrease of expression in the implantation area. MMP9, supportively has incrased steeply (H-K). Entactin has shown slight differences, as the gene expression itself (D-G). *Scale bars= 50 µm*.

3.11 Evaluation of Implantation Parameters in Endometrial Co-cultures with Gene Edited Epithelial Cells

3.11.1 Hmga2 Overall Analysis

3D endometrial coculture experimental groups were established with epithelial cells in which the Hmga2 gene was knocked out, and qRT-PCR was performed to evaluate implantation parameters by isolating RNA from the samples collected after 24 and 72 hours. The results obtained from qRT-PCR analyzes are outlined below. Significance rates are given below the graphics in Figure 48Figure 49, and Figure 50. As will be discussed later, the expression results show different rates of significance as they are normalized to whether control or NT groups and the results of NT groups were detailed in the related graphics. (*NT groups although showed similar expression as the control groups in gRNA validation experiments (figure 44), showed various expression patterns in long term cultures, probably due to effect of Cas9 and the virus they contain. Due to this situation comparative analysis was conveyed between control and KO groups, however, still the expressions in NT groups and temporal changes (which were non-significant in most cases) were shown in the following graphics).*

In terms of **adhesion markers** (Figure 48), as cells have elapsed 24 hours in co-cultures, compared to control group, a significant decrease in ***e-cadherin*** expression was observed in KO groups. In the 72-hour culture groups, there is a significant decrease in the KO group compared to both the control groups. The results indicate that, although expressed less than control groups, e-cadherin expression decreased significantly between 24 and 72 hours. As ***entactin*** expression is examined, it is observed that the expression in the KO groups decreased significantly compared to the control group in both 24- and 72-hour groups. When the culture continuity is examined in general terms, a significant decrease is observed in the KO groups in the 72-hour culture environment compared to the 24-hour culture environment. In the examination of ***fibronectin*** expression, while the expression levels in the control group and the KO group remained similar in the 24-hour culture, there was a decrease at the 72nd hour. When the temporal comparison of the KO groups was examined, a significant decrease was detected at the 72nd hour.

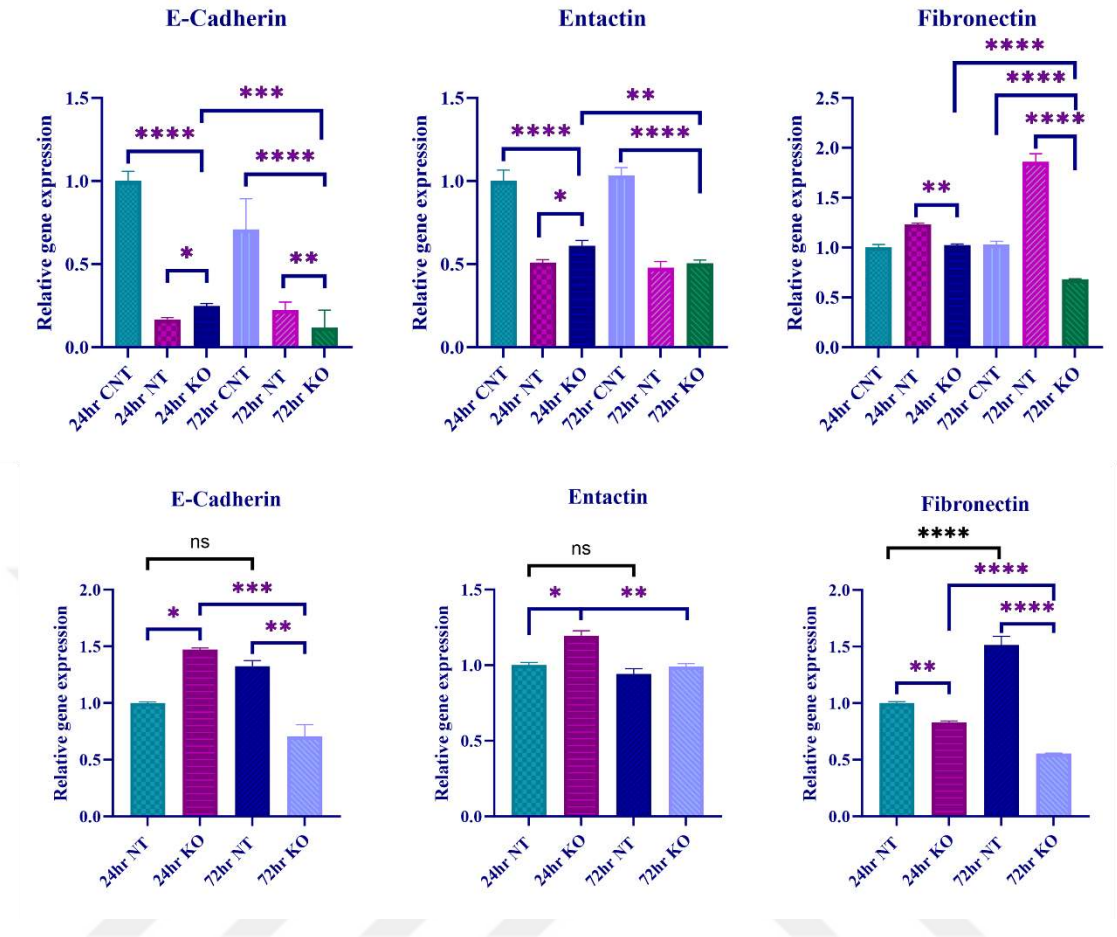

Figure 48. Expression of adhesion marker genes in co-culture groups after Hmga2 Knockout. Significant alterations were detected especially in e-cadherin and entactin expression. NT groups show some non-significant variations temporally. CNT: Control; NT: Non-targeted; KO: Knock out. Significance; (*) p<0.05, (**) p<0.001, (***) p<0.0001, (****) p<0.00001

When the **functional markers** (Figure 49) of implantation were examined, it was determined that the KO group showed a significant increase in ***LIF*** expression in the culture groups at hour 24 compared to control groups. When the KO groups were examined temporally, it was observed that LIF expression decreased at the 72nd hour, unlike control groups that have showed significant increase, as depicted in Figure 46. When ***Esr1*** gene expression was examined, a significant decrease was observed both in the KO groups as it goes from 24 to 72, and in the KO groups when compared to the control groups. When ***PR*** was examined in terms of gene expression, a significant decrease was detected in the KO groups compared to the control group in both 24- and

72-hour culture environments. In the analysis between the KO groups, a significant decrease in PR expression is observed towards the 72nd hour, unlike the control group.

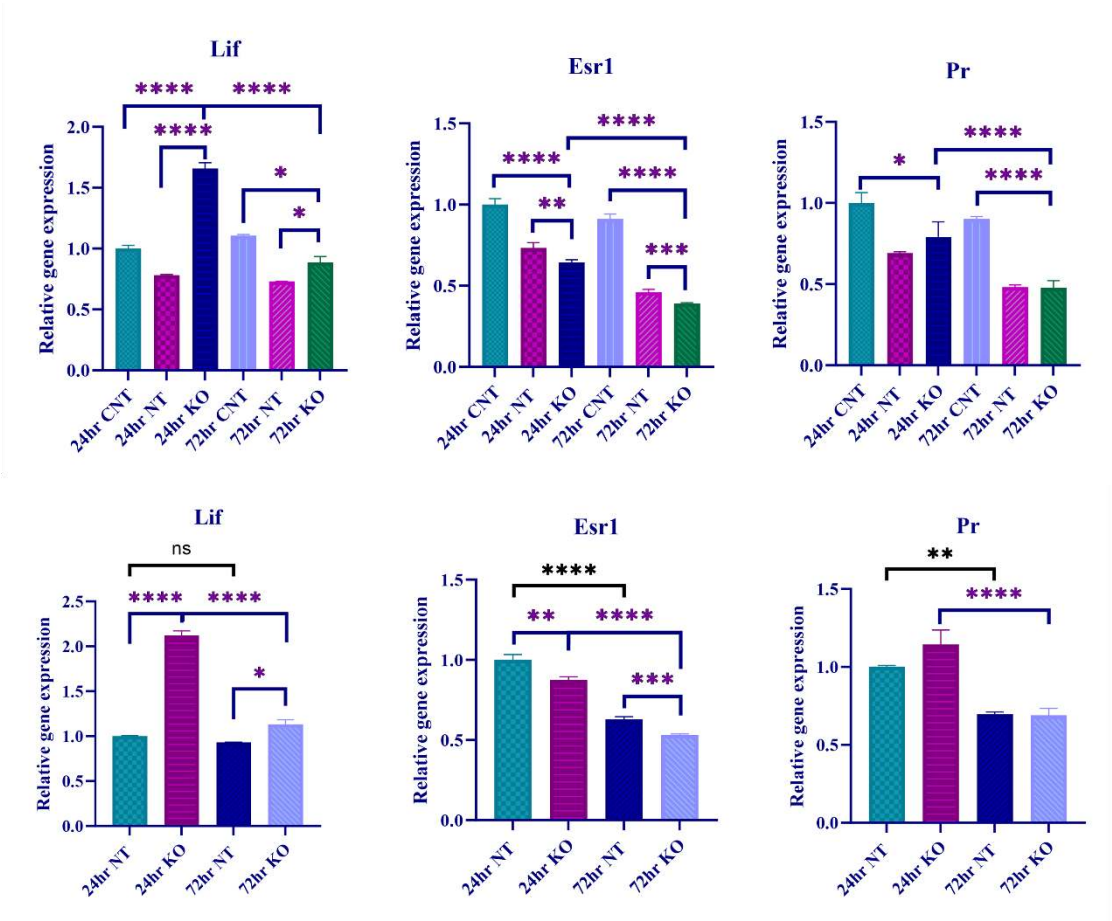

Figure 49. Expression of genes, that play a functional role during implantation, in coculture groups after Hmga2 Knockout. LIF was affected differentially and significantly between control and KO groups. NT groups show some non-significant variations temporally at LIF. CNT: Control; NT: Non-targeted; KO: Knock out. Significance; (*) p<0.05, (**) p<0.001, (***) p<0.0001, (****) p<0.00001

Implantation was also examined in terms of genes related to **invasion and developmental** (Figure 50). ***MMP9*** showed some significant changes. This gene, which plays an important role for invasion significantly increases in normal groups while it declines steeply from 24 to 72 hours in KO groups. Although we did not see any significant difference from 24 to 72 hours in control groups, both WNT4 and Hoxa10 temporally decreased significantly in KO groups. It should also be noted that these the expression of these decreased in KO groups compared to corresponding KO groups.

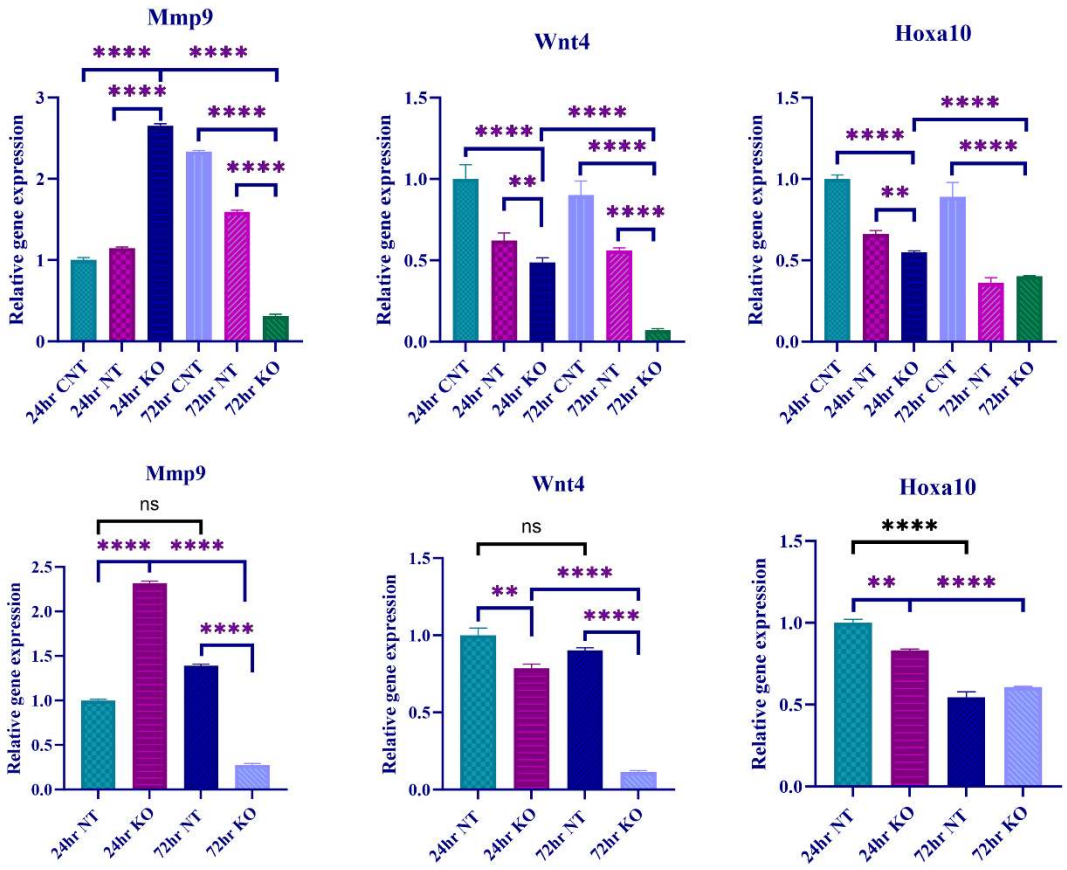

Figure 50. Expression of invasion and development marker genes in coculture groups after Hmga2 Knockout. MMP9 showed a sharp decline which can interfere with a healthy, expected invasion process. Significant decrease in expression of developmental genes also should be noted. CNT: Control; NT: Non-targeted; KO: Knock out. Significance; (*) $p<0.05$, (**) $p<0.001$, (***) $p<0.0001$, (****) $p<0.00001$

The expression profil was also supported by IF staining for some parameters, as shown in Figure 51. As outlined in the figure labels, gene expression findings were especially supported for e-cadherin and entactin expression profile for proteins, through 24 to 72 hours.

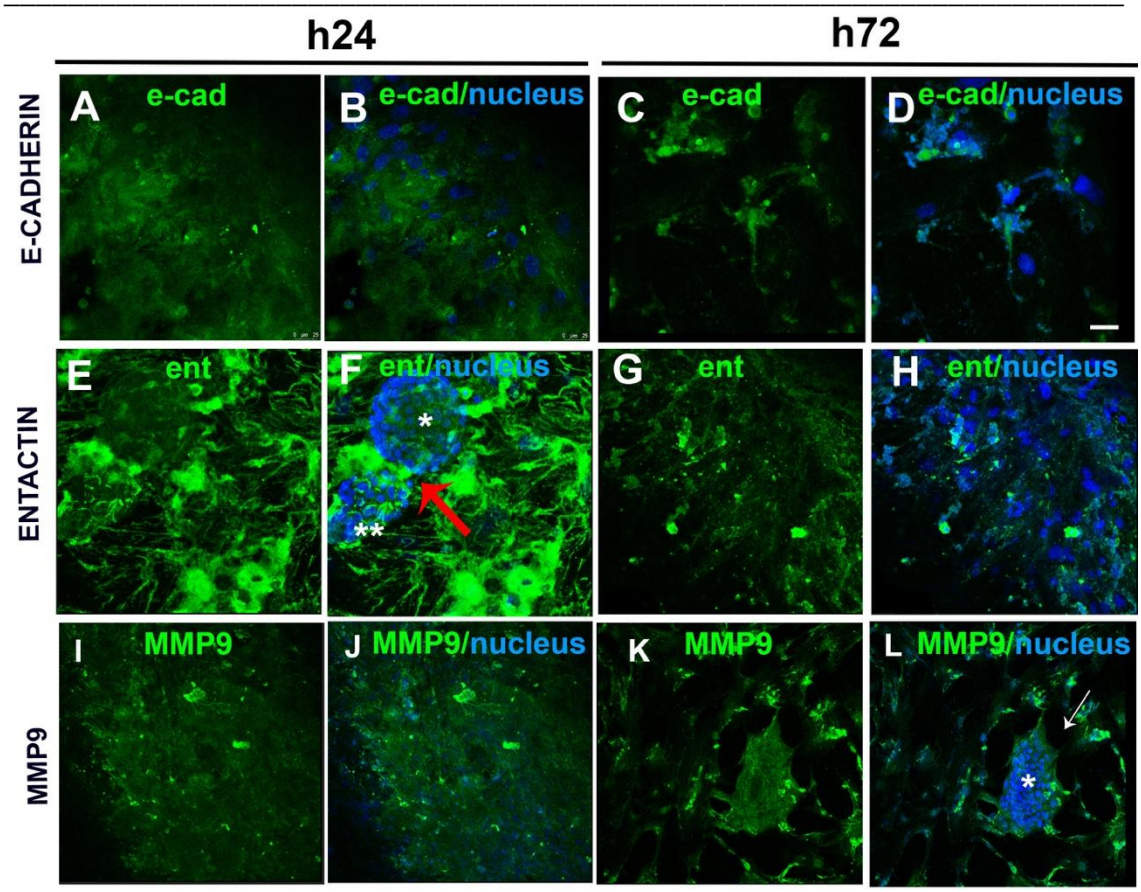

Figure 51. IF staining of Hmga2 KO group. Some implantation markers that showed significant difference in expression have also been stained for protein expression. The temporal difference of expression was seen especially in e-cadherin and entactin, showing a decline from 24 to 72 hours. MMP9 showed slight decrease. Asterisk: blastocysts (F, L), red arrow (F): hatching area, double asterisk (F): invasion area, white arrow (L): acellular area around the blastocyst due to activity of MMP9. Scale bar for all images has been represented in D and it is 50 µm. The images are constructed as maximum projection of 10 z-stacks.

3.11.2 Gm15452 Overall Analysis

As a result of Gm15452 knockout in epithelial cells, co-culture groups were created and implantation markers were examined in terms of adhesion (Figure 52), invasion (Figure 54) and functional gene expression (Figure 53).

In terms of **adhesion** markers, ***E-Cad*** showed a significant decrease in the KO groups compared to the control groups. In time-dependent examination, there was a significant increase in the 72nd hour compared to the 24th hour in the KO groups. While a significant decrease was observed in ***entactin*** expressions in the KO groups compared

to the control group. There was an increase in ***fibronectin*** expressions in both the 24th and 72nd hours in the KO groups compared to the control group. A significant increase was detected when temporal expression was examined between control and KO groups at hour 72.

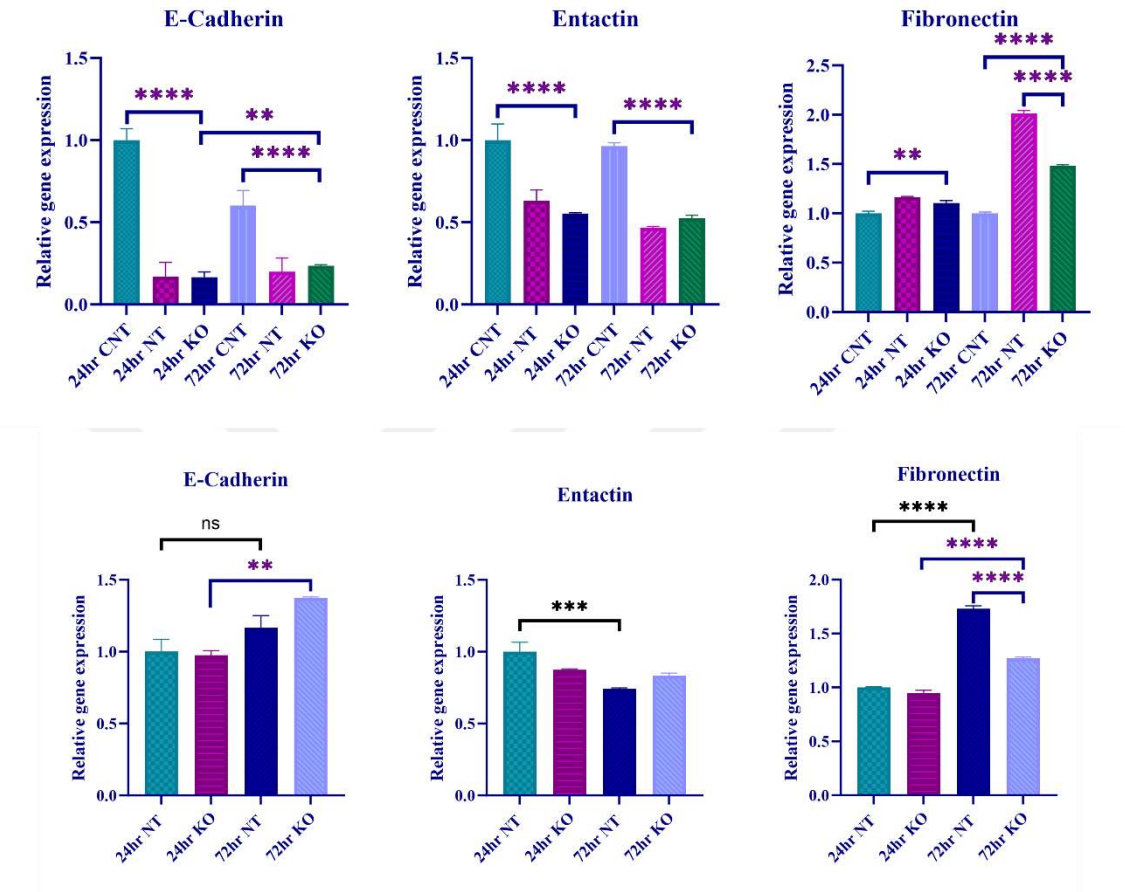

Figure 52. Expression of adhesion marker genes in coculture groups after Gm15452 Knockout. CNT: Control; NT: Non-targeted; KO: Knock out. Significance; (*) p<0.05, (**) p<0.001, (***) p<0.0001, (****) p<0.00001

LIF, one of the functional genes of implantation, showed a significant decrease only at the 24th hour in the KO group compared to the control group. There was no significance between the two groups at the 72nd hour. At the same time, when looked at among KO groups, there is an increase in the 72nd hour compared to the 24th hour. At the results in terms of ***Esr1*** and ***PR*** expression, the distribution of the two genes between groups appears to be similarly reflected. While a significant decrease in expression was observed for both genes when compared to the KO groups, no

significance was observed when compared to control groups. Additionally, KO groups showed a significant decrease from 24 to 72.

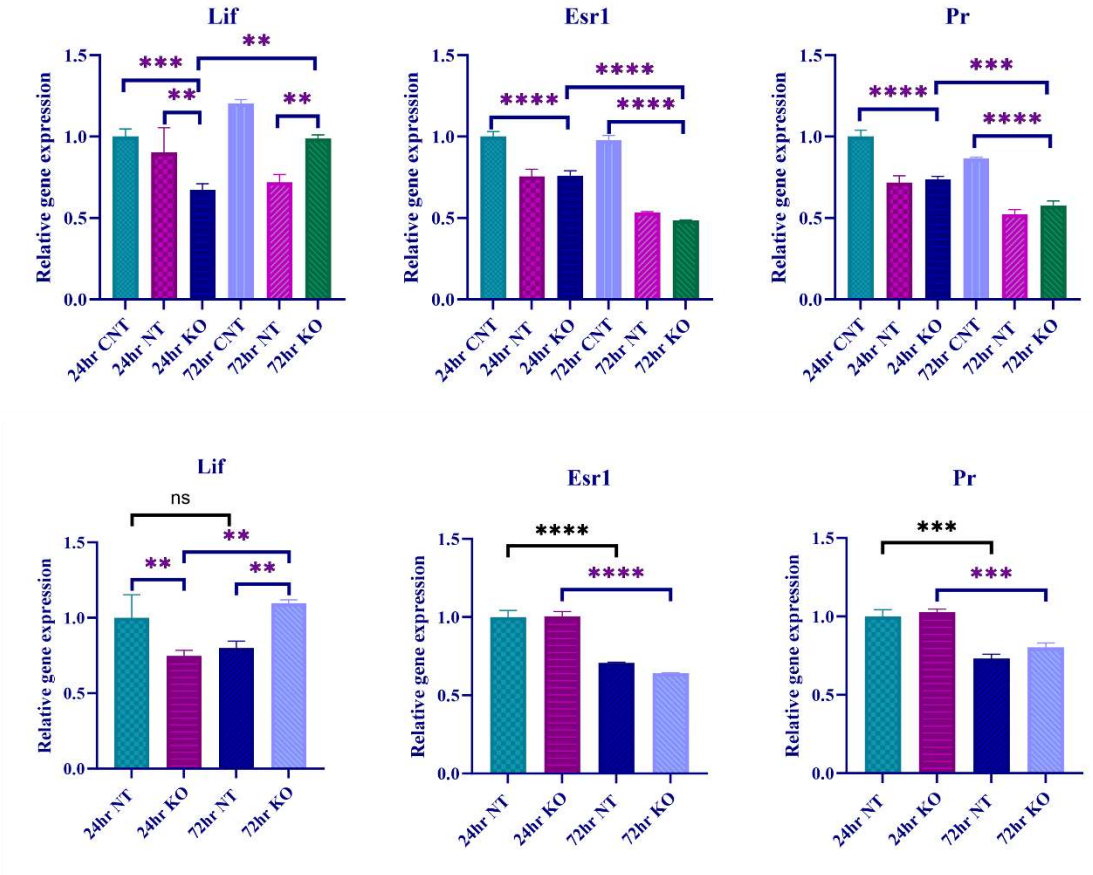

Figure 53. Expression of genes, that play a functional role during implantation, in coculture groups after Gm15452 Knockout. CNT: Control; NT: Non-targeted; KO: Knock out. Significance; (*) p<0.05, (**) p<0.001, (***) p<0.0001, (****) p<0.00001

As a result of ***Mmp9*** expression, which is an indicator of invasion, a significant decrease was observed in the KO group at both the 24th and 72nd hours compared to the control group. A significant expression was detected in the KO groups from 24 to 72. A significant decrease was observed in the KO groups when compared to the control group. A significant decrease was noted in the time-dependent KO groups from 24 to 72. There was also a significant decrease in ***Hoxa10*** and ***Wnt4*** expression between the control groups and the KO groups. Depending on time, a significant decrease was detected in the KO groups towards the 72nd hour.

IF staining mostly supported these findings, as depicted and explained in Figure 55.

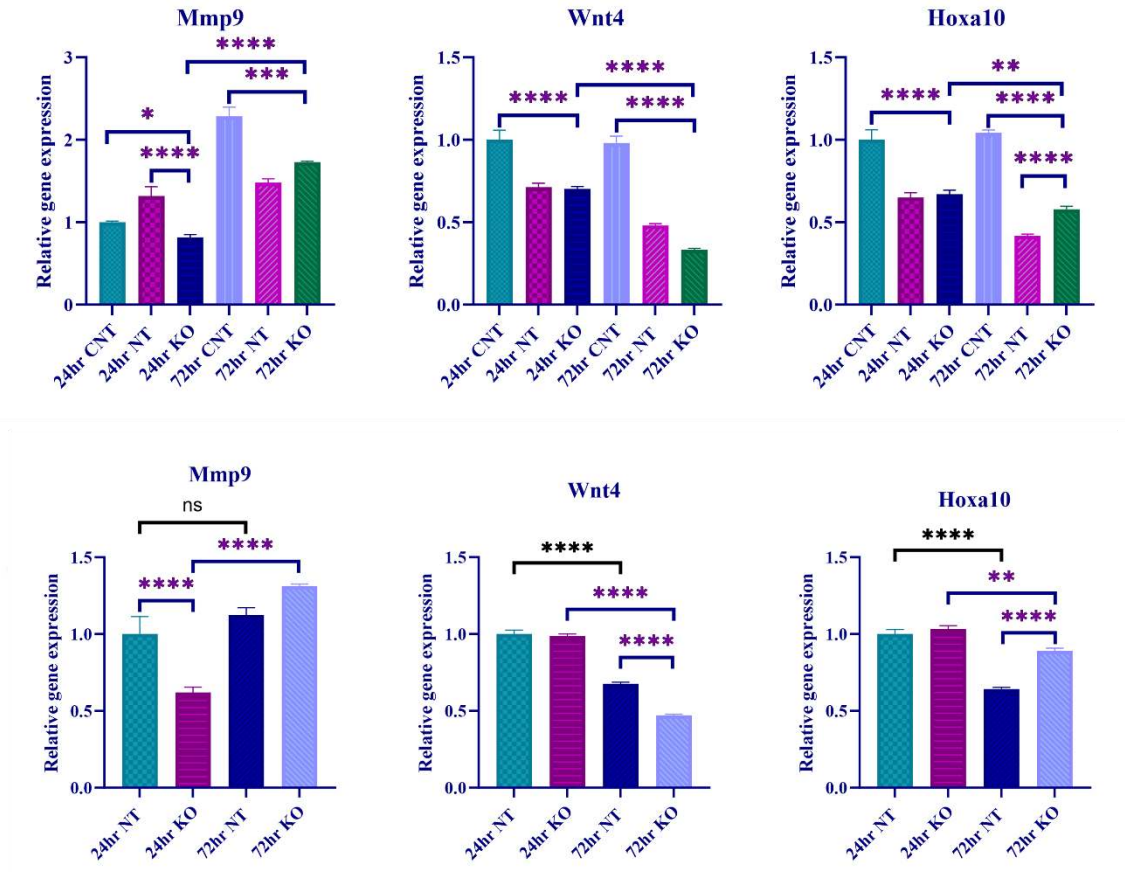

Figure 54. Expression of invasion and development marker genes in coculture groups after Gm15452 Knockout. CNT: Control; NT: Non-targeted; KO: Knock out. Significance; (*) p<0.05, (**) p<0.001, (***) p<0.0001, (****) p<0.00001

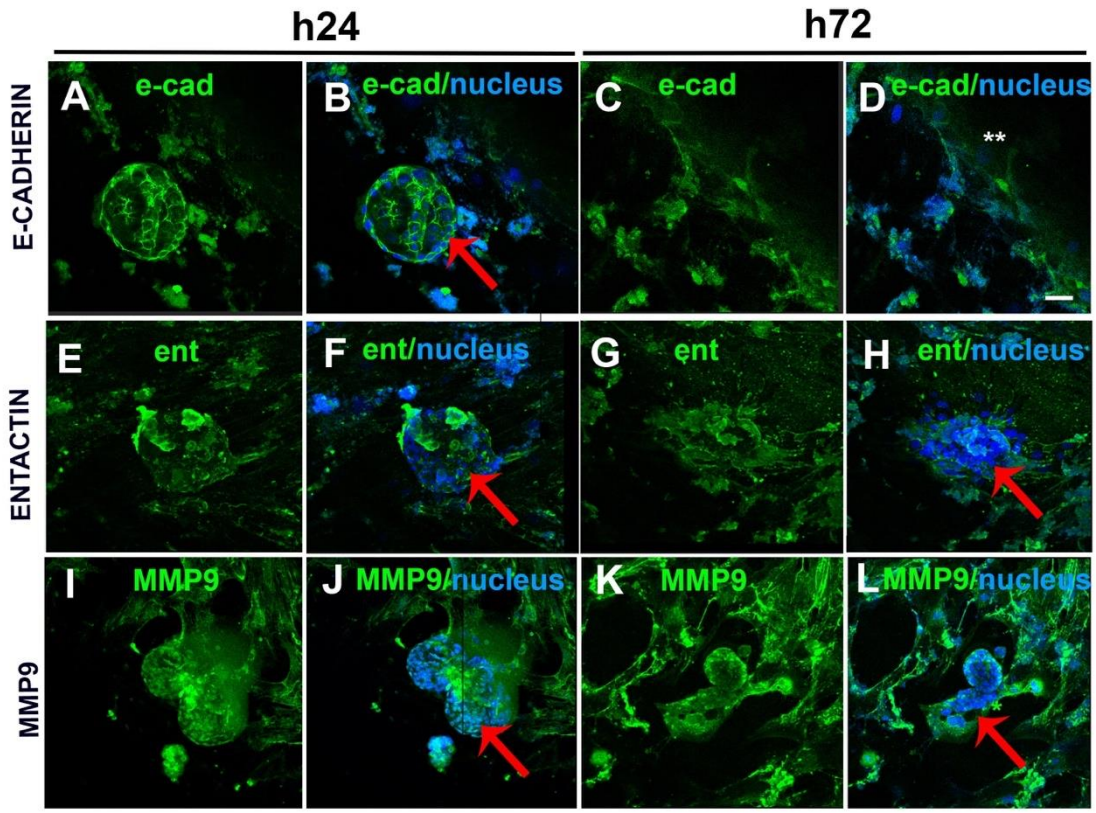

Figure 55. IF staining of GM15452 in KO epithelial cell group. Some implantation markers that showed significant difference in expression have also been stained for protein expression. The temporal difference of expression was seen especially in e-cadherin and MMP9, showing an increase from 24 to 72 hours. Entactin showed similar expression. Red arrows: blastocysts, asterisk: increased expression of MMP9 in the implantation area, double asterisk (D): increased expression of e-cadherin in the implantation area. Scale bar for all images has been represented in D and it is 50 µm. The images are constructed as maximum projection of 10 z-stacks.

3.12 Evaluation of Implantation Parameters for Endometrial Co-cultures Carrying Gene Edited Stroma Cells

3.12.1 Uxs1 Overall Analysis

Implantation parameters, adhesion (Figure 56), invasion, development (Figure 57) and functional (Figure 58) gene expressions were examined in coculture samples created with endometrial stroma cells in which the Uxs1 gene was knocked out.

First of all, ***E-cad***, one of the adhesion genes, showed a significant increase in the KO group compared to the control groups in the 24-hour culture environment. On the

contrary, a decrease was detected at the 72nd hour. When looking at the change over time, a significant decrease was detected at the 72nd hour in the KO groups. When ***Entactin*** expression was considered, a significant decrease was noted in the KO groups compared to the control groups. No significant change in KO groups over time was detected. A significant increase in ***fibronectin*** expressions was detected in the KO groups compared to both the control and NT groups. At the same time, a significant increase was recorded over time.

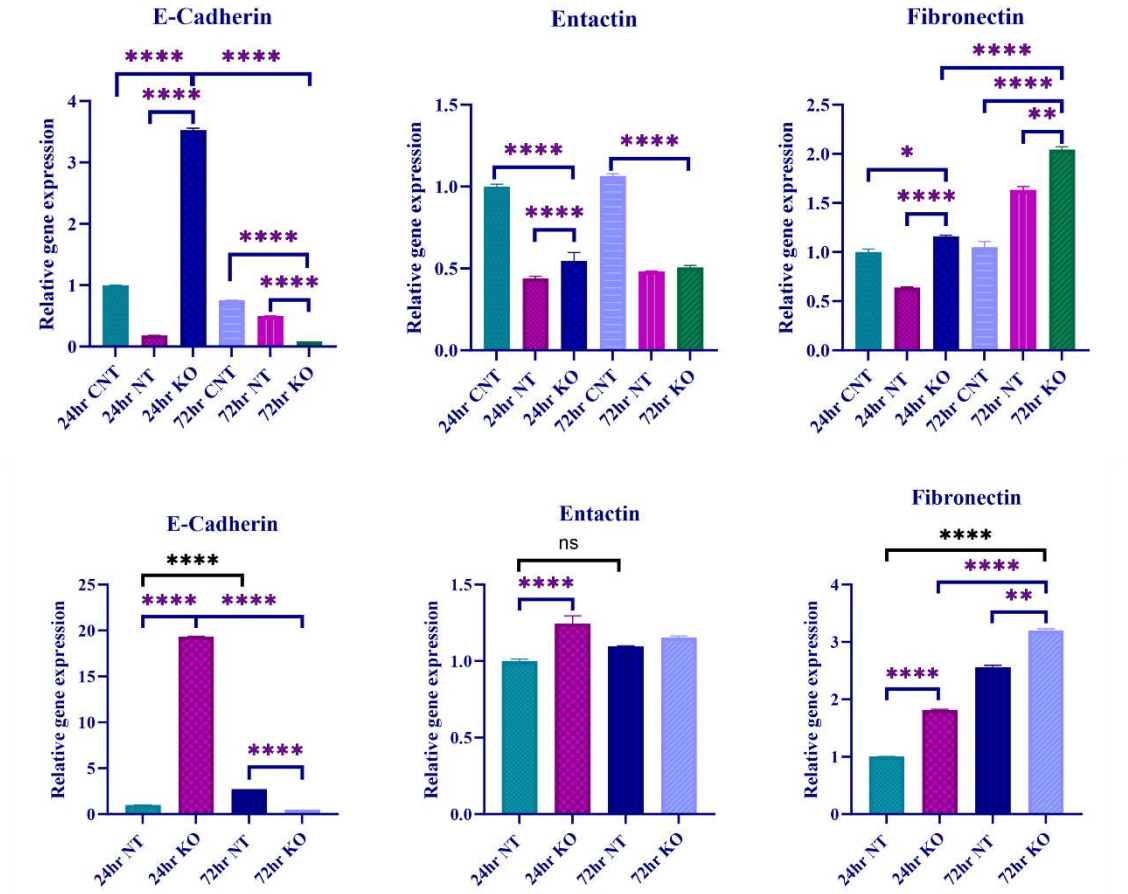

Figure 56. Expression of adhesion marker genes in coculture groups after Uxs1 Knockout. CNT: Control; NT: Non-targeted; KO: Knock out. Significance; (*) p<0.05, (**) p<0.001, (***) p<0.0001, (****) p<0.00001

Compared to the control group, ***LIF*** expression was found to be higher in the KO groups at the 24th hour. No difference was observed at the 72nd hour. A significant decrease was noted in the KO groups depending on time. In the study, ***Esr1 and PR*** gene expressions showed similar changes. A significant decrease was noted in the KO

groups compared to the control groups at both the 24th and 72nd hours. When looking at the time-dependent expression of the KO groups, a significant decrease was observed at the 72nd hour compared to the 24th hour.

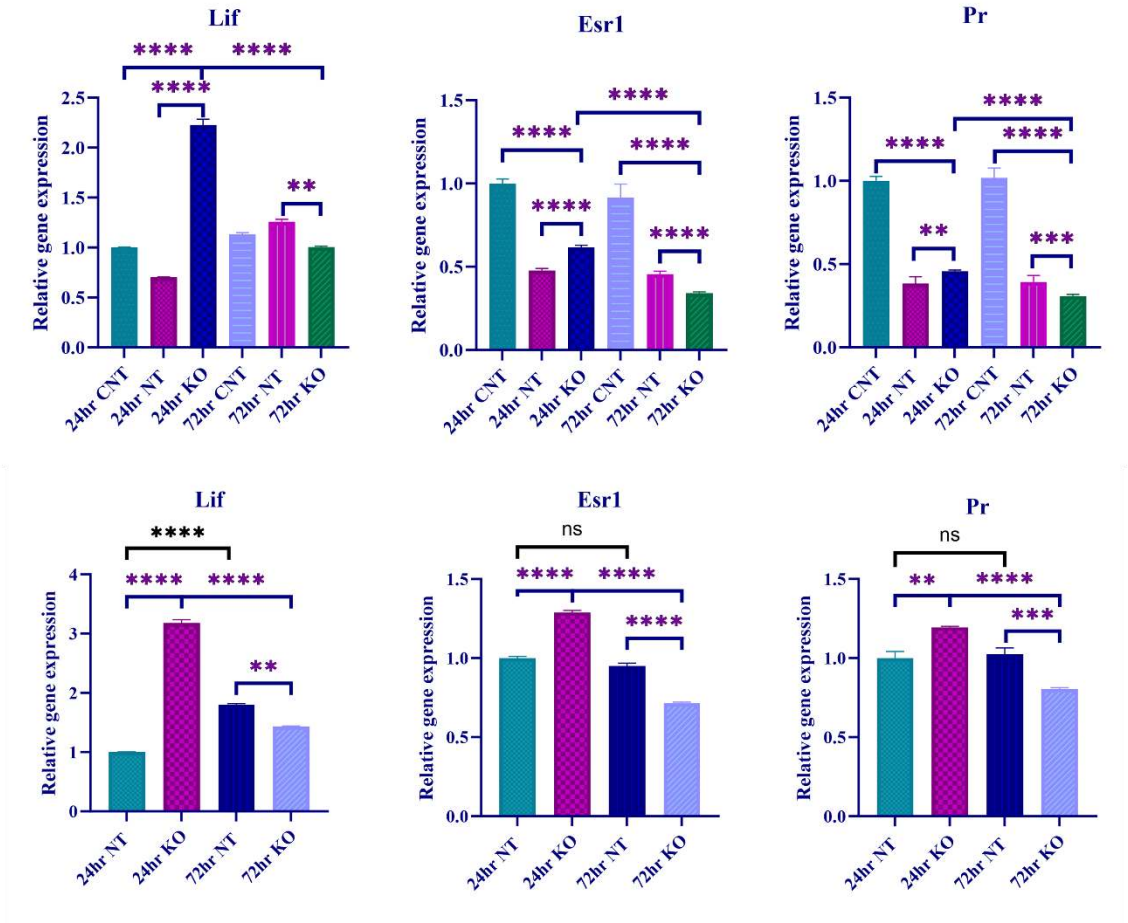

Figure 57. Expression of genes, that play a functional role during implantation, in coculture groups after Uxs1 Knockout. CNT: Control; NT: Non-targeted; KO: Knock out. Significance; (*) p<0.05, (**) p<0.001, (***) p<0.0001, (****) p<0.00001

The increase in ***Mmp9*** expression in the KO group at 24 hours and decrease at 72 hours compared to both the control and NT groups is significant. A significant decrease was also noted among the KO groups, from 24 to 72. The decrease in ***Wnt4*** expression in the KO group compared to both the control and NT groups at two times was significant. No significant change over time was detected between KO groups. A significant decrease in ***Hoxa10*** expression was noted in the KO groups compared to the control groups.

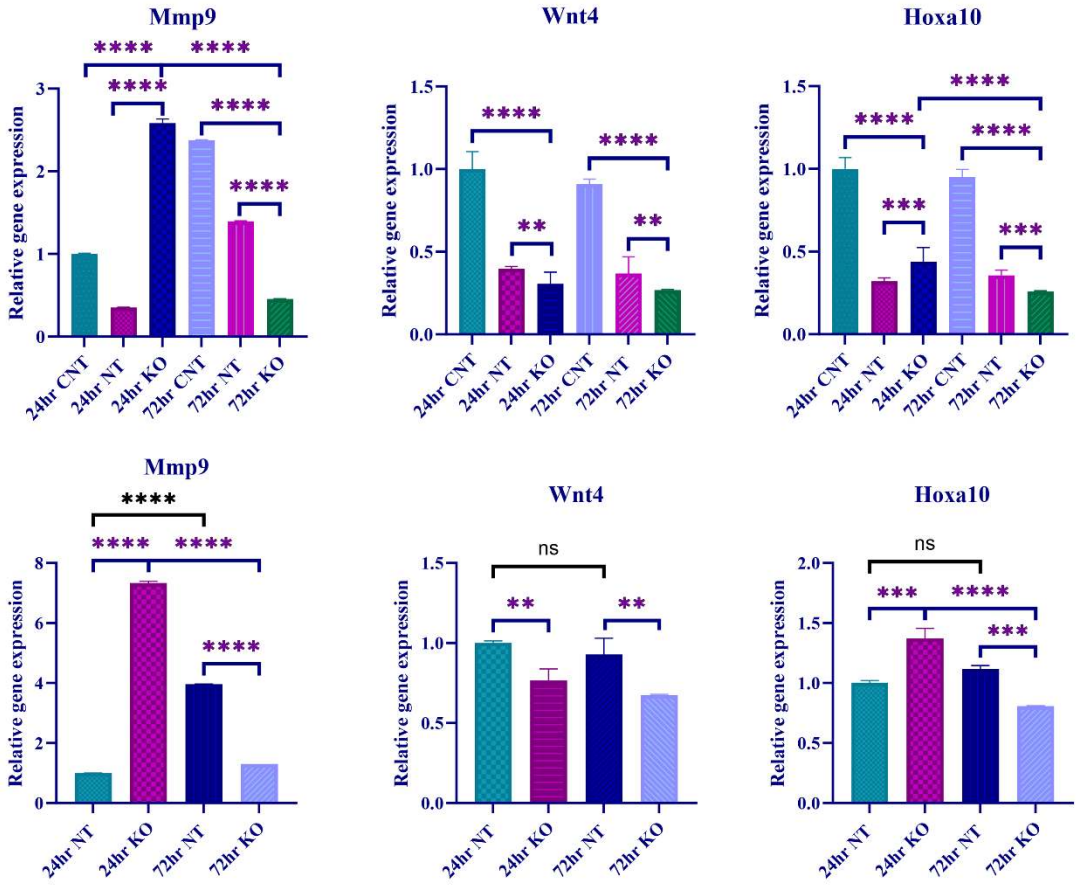

Figure 58. Expression of invasion and development marker genes in coculture groups after Uxs1 Knockout. CNT: Control; NT: Non-targeted; KO: Knock out. Significance; (*) p<0.05, (**) p<0.001, (***) p<0.0001, (****) p<0.00001

IF staining showed various results as shown in Figure 59. Entactin shows no changes as expected, however the expected decreased expression of e-cadherin and MMP9 was not seen, on the contrary a certain increase has been noted in MMP9, which can be related to effect of sample variance on immunofluorescent stainings.

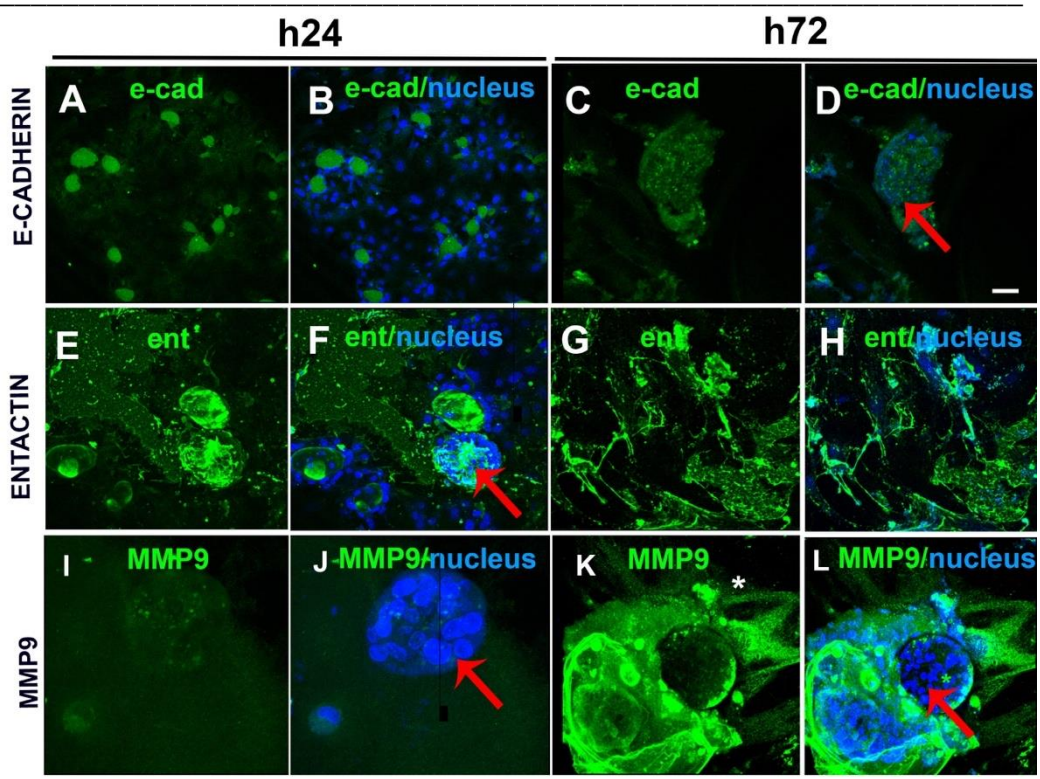

Figure 59. IF staining of Uxs1 in KO groups. Some implantation markers that showed significant difference in expression have also been stained for protein expression. The temporal difference towards decrease of expression was not seen in e-cadherin and MMP9. Entactin showed similar expression. Red arrows: blastocysts. Scale bar for all images has been represented in D and it is 50 μm., except for I-J, at which it represents 25 μm. The images are constructed as maximum projection of 10 z-stacks.

3.12.2 Gm15452 Stroma KO Overall Analysis

Implantation parameters in endometrial cocultures created with stroma cells in which the Gm15452 gene was knocked out were analyzed in terms of adhesion (Figure 60), development, invasion (Figure 61) and functional (Figure 62) gene expression.

In terms of ***E-Cad***, a decrease was observed in the KO groups compared to the control groups at the 24th hour, while no significant change was observed at the 72nd hour. There is a significant increase in KO groups when compared to NT groups. However, no change was observed between KO groups over time. When examined in terms of ***entactin***, it was determined that the KO groups showed a significant decrease compared to the control groups at two different times. The relation between 24 and 72 hours in the

KO groups showed less expression was observed at the 72nd hour in the KO groups. No significance was observed between groups in ***fibronectin*** expression.

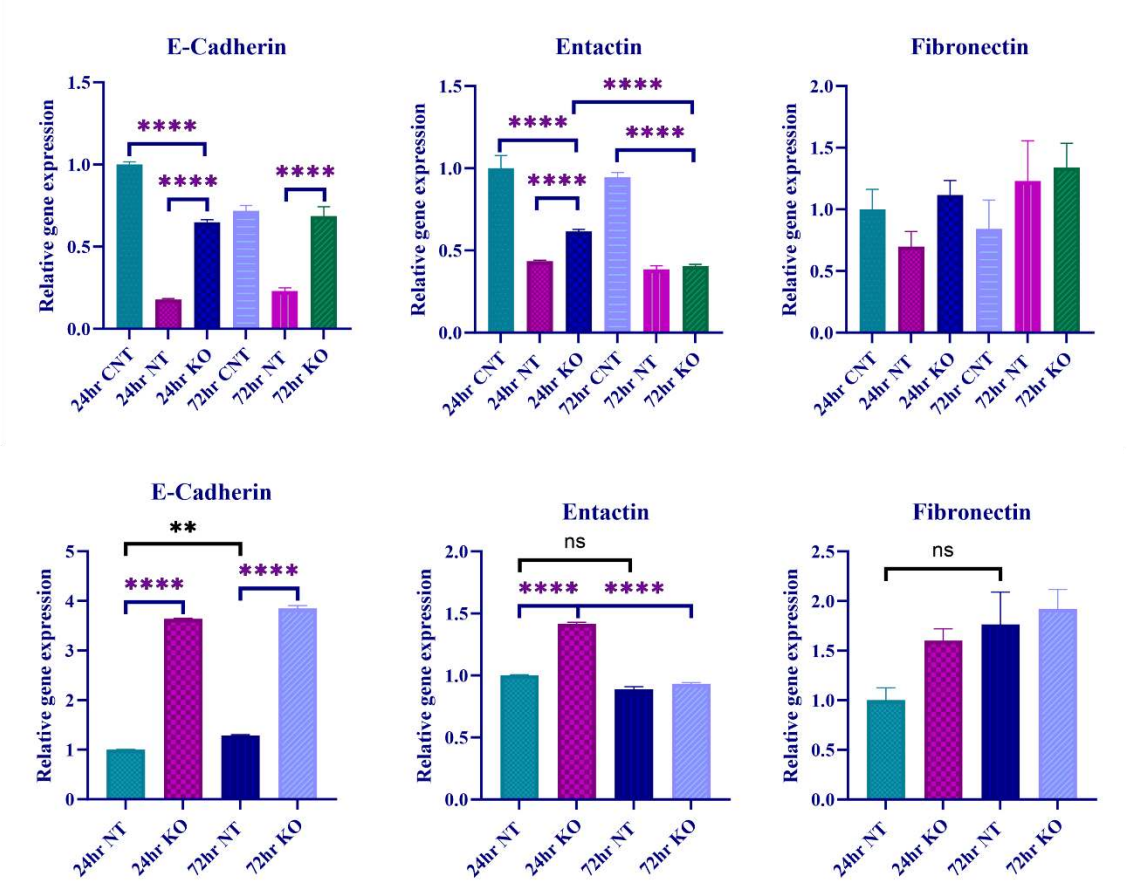

Figure 60. Expression of adhesion marker genes in coculture groups after Gm15452 Knockout. CNT: Control; NT: Non-targeted; KO: Knock out. Significance; (*) p<0.05, (**) p<0.001, (***) p<0.0001, (****) p<0.00001

While there was no significance in ***LIF*** expression between the control groups and the KO groups, the KO groups showed an increase compared to NT in both the 24 and 72 hour culture groups. Time-dependent expression was also found to increase significantly in the KO groups towards the 72nd hour. While no significance was detected between the groups in ***Esr1*** expression, a significant decrease in ***PR*** expression was detected between the control group and the KO group at the 24th hour, and a significant increase was detected between the NT group and the KO groups at the 72nd hour of incubation.

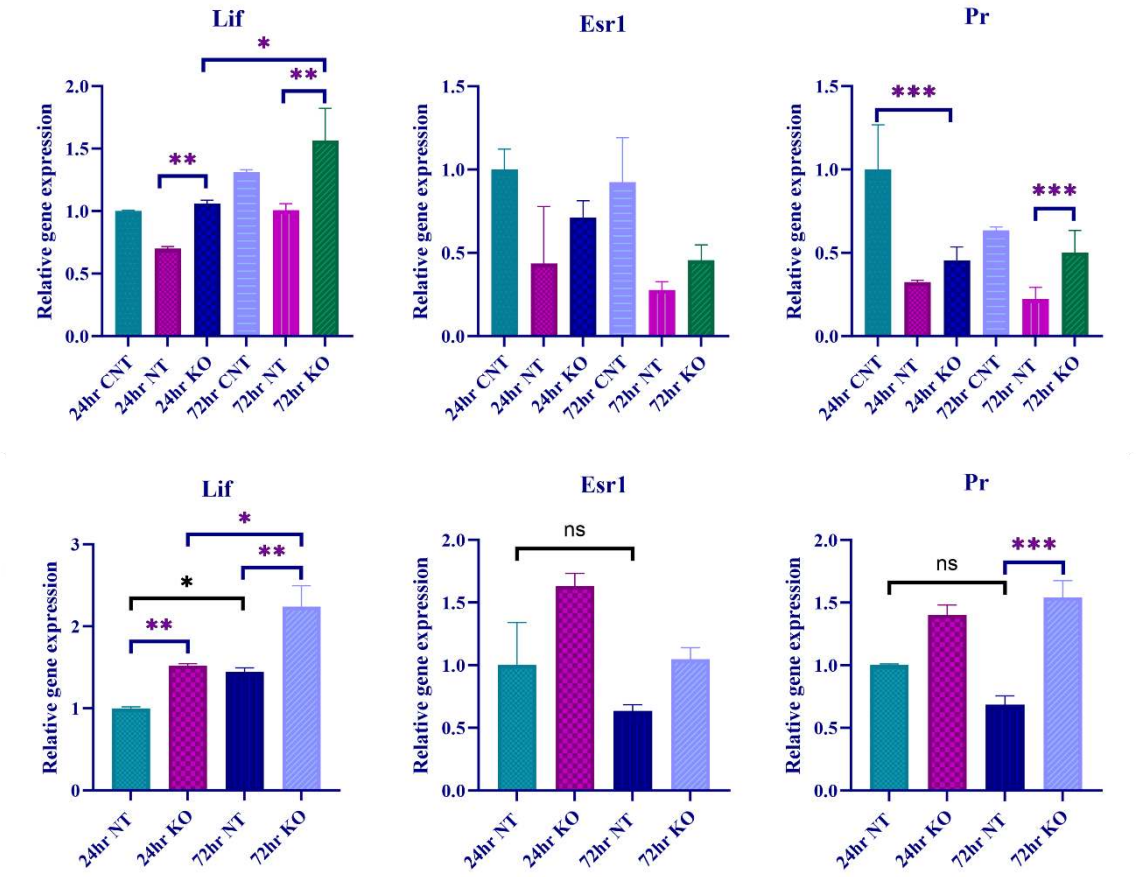

Figure 61. Expression of genes, that play a functional role during implantation, in coculture groups after Gm15452 Knockout. CNT: Control; NT: Non-targeted; KO: Knock out. Significance; (*) p<0.05, (**) p<0.001, (***) p<0.0001, (****) p<0.00001

Mmp9 expressions increased significantly in KO groups compared to control and NT groups in both 24 and 72 hours of culture. When looking at the time-dependent change, a significant increase was observed in the KO groups at the 72nd hour compared to the 24th hour. A significant decrease in ***Wnt4*** expression was observed in both the 24th and 72nd hours in the KO groups compared to the control group, while the opposite result was detected in the NT groups. When the time-dependent change between KO groups was examined, a significant decrease was observed at the 72nd hour. When ***Hoxa10*** expression was considered, a significant decrease was observed in the KO groups compared to the control at both times. Compared to the NT groups, the KO group showed a significant increase only at the 72nd hour. No significant gene changes were detected between KO groups at two different times.

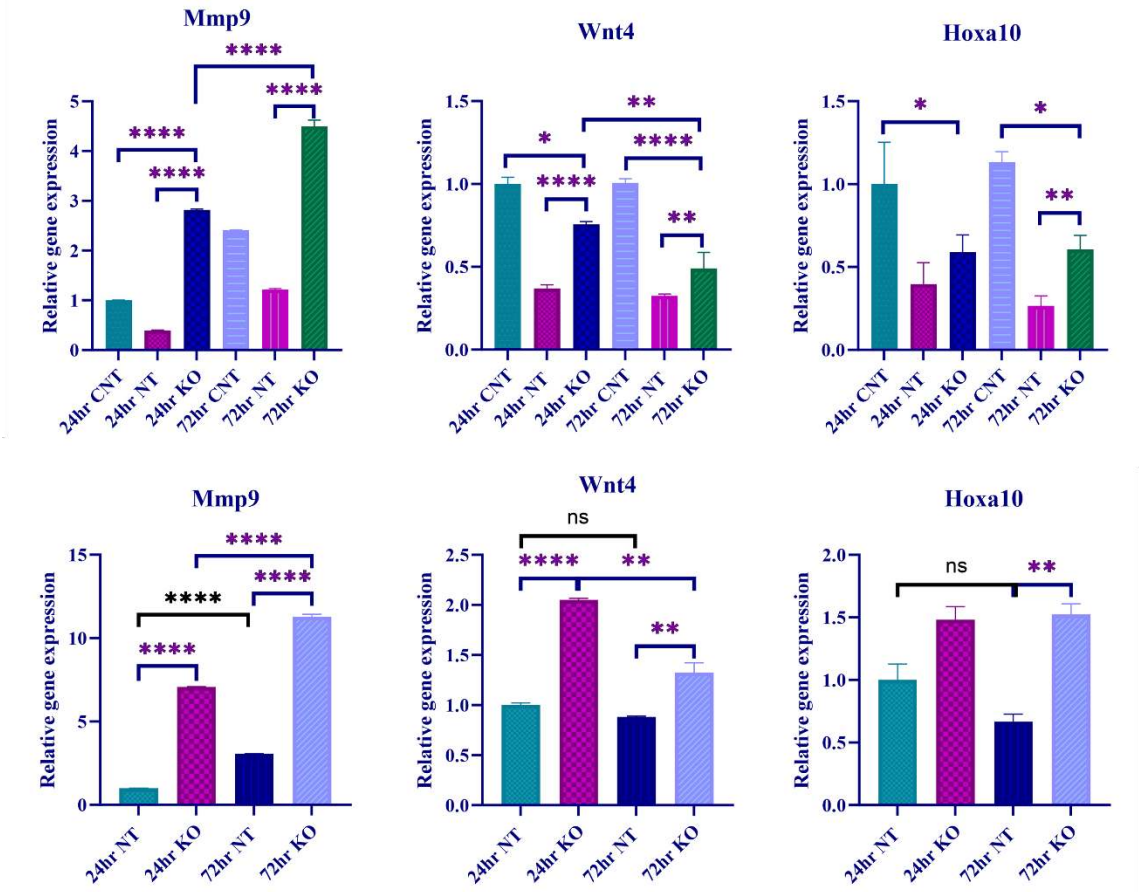

Figure 62. Expression of invasion and development marker genes in coculture groups after Gm15452 Knockout. CNT: Control; NT: Non-targeted; KO: Knock out. Significance; (*) p<0.05, (**) p<0.001, (***) p<0.0001, (****) p<0.00001

IF stainings mostly show correlation with gene expression analysis as, e-cadherin has showed slight increase, entactin has shown significant and MMP9 showed increased expression (Figure 63).

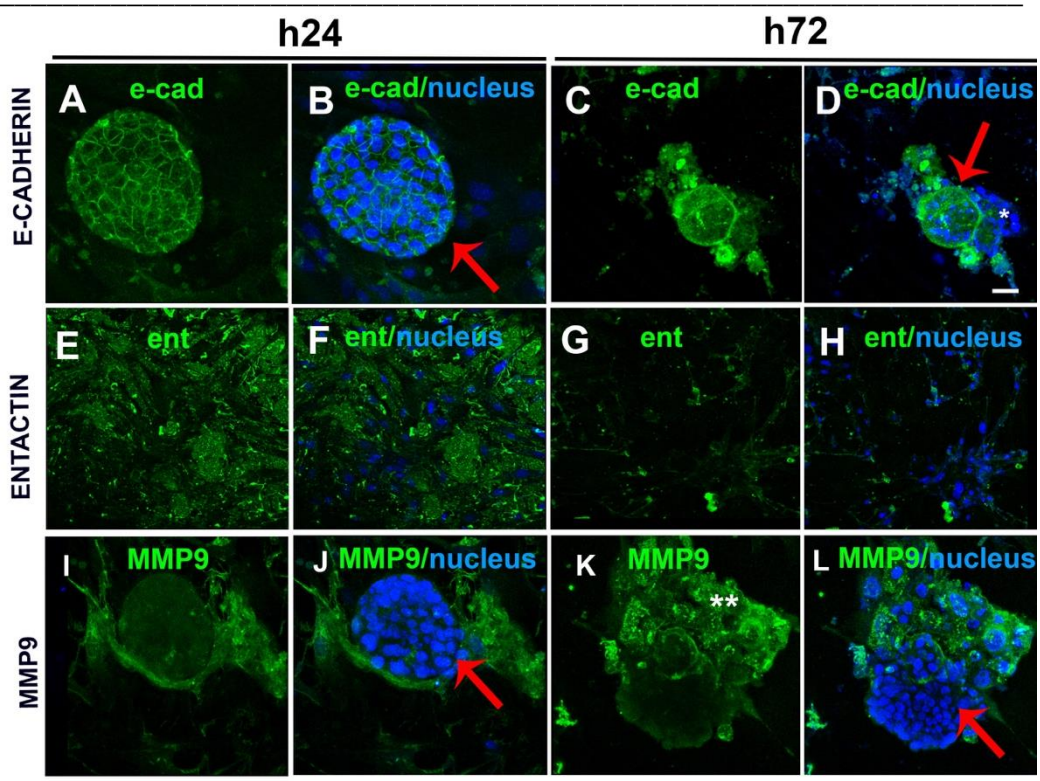

Figure 63. IF staining of GM15452 in KO stroma cell group. Some implantation markers that showed significant difference in expression has also been stained for protein expression. E-cadherin has showed slight increase, although it was non significant. Still, the invasion pattern (asterisk, D) and the blastocyst itself (red arrow, B, D) can be discriminated clearly. The decoration of e-cadherin has also been revealed satisfactorily (A). Entactin has shown significant decrease in correlation with gene expression analysis. MMP9 showed increased expression (K, double asterisk) just beneath the blastocyst (L, red arrow). Red arrows: blastocysts. Scale bar for all images has been represented in D and it is 50 µm., except for A-B, at which it represents 25 µm. The images are constructed as maximum projection of 10 z-stacks.

3.13 Live/Dead Cell Assay Results

As a result of the live/dead cell assay, the amount of live and dead cells in the coculture groups was determined. There was no statistical difference in live/dead cells between the Hmga2 and Gm15452 KO endometrial epithelial groups and the control and NT groups Figure 64. This analysis was accomplished by calculation of fluorescence intensity.

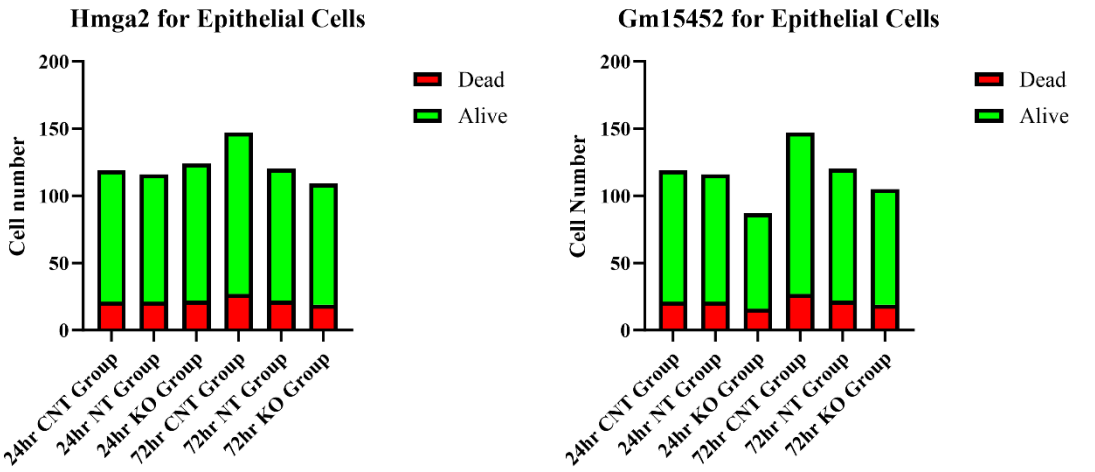

Figure 64. Live/Dead Cell Assay Results for epithelial cell KO groups. Green represents live, red color represents dead cells. CNT: Control; NT: Non-targeted; KO: Knock out. Significance; (*) $p<0.05$, (**) $p<0.001$, (***) $p<0.0001$, (****) $p<0.00001$; no significant difference was seen fort his group.

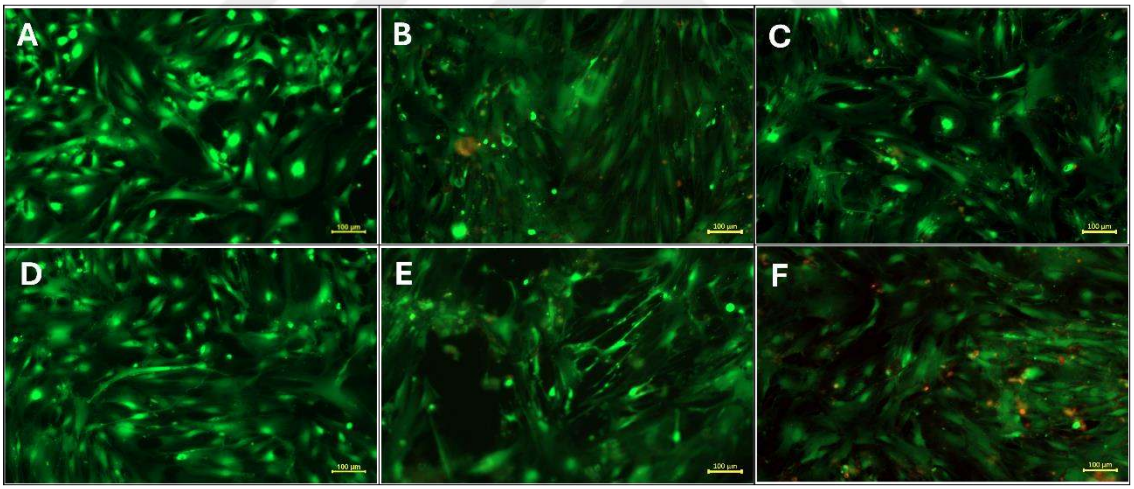

Figure 65. Live/Dead Cell Imaging of endometrial coculture groups. Green represents live, red color represents dead cells. A. 24hr Control Group; B. 24hr NT Group; C. 24hr Hmga2 KO Group; D. 72hr Control Group; E. 24hr NT Group; F. 72hr Hmga2 KO Group. Scale bars represent 100 µm.

In the Uxs1 and Gm15452 KO study performed on endometrial stroma cells, a significant decrease was observed in the KO groups compared to the control groups in the 72-hour culture groups (Figure 66). No significance was observed in terms of cell

count between 24-hour coculture groups. However, a decrease in cell count was observed in between the 24 and 72 hour culture groups of the Uxs1 KO groups.

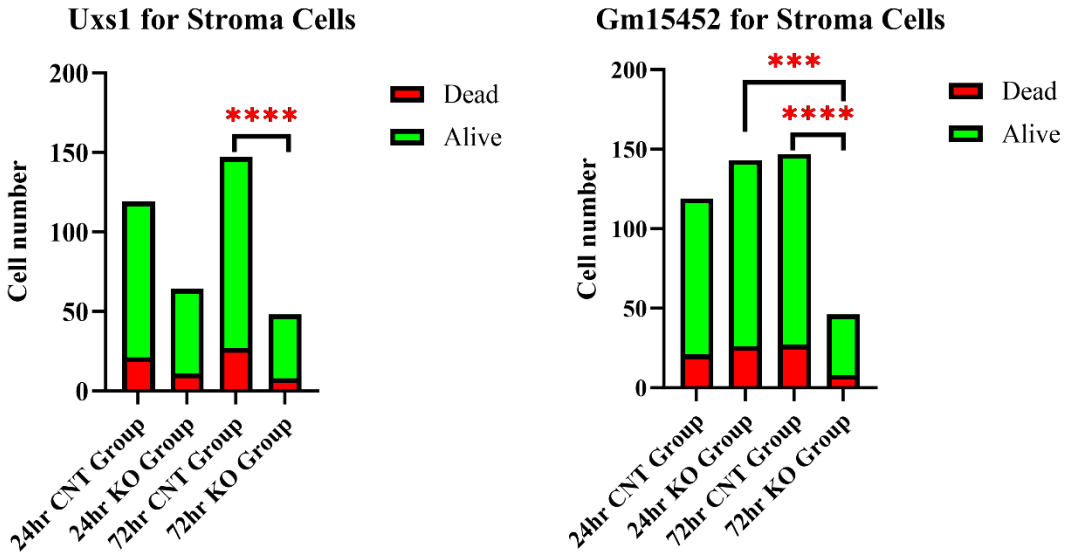

Figure 66. Live/Dead Cell Assay Results for stromal cell KO groups. Green represents live, red color represents dead cells. CNT: Control; KO: Knock out. Significance; (*) p<0.05, (**) p<0.001, (***) p<0.0001, (****) p<0.00001

Chapter 4
DISCUSSION

Various *in vitro* culture models of the endometrium have been created to examine early pregnancy processes. These models are classified in two classes: 2D and 3D culture models. In 2D models, endometrial cells are cultured as monolayers, but they exhibit limitations such as decreased biological activities and lack of cell-ECM interaction[128]. 3D models integrate the extracellular matrix (ECM) and multiple cell types, providing a more physiologically relevant environment. Cell-based 3D models include epithelial and stromal cells and can demonstrate the influence of ECM on cell behavior[71],[128]–[130].

In 3D cell cultures, the inclusion of ECM provides structural support to the established culture, helps maintain essential cell-ECM interactions, influences cell signaling and differentiation, and maintains the phenotype of cells[131]. ECM provides a three-dimensional scaffold that reflects the natural architecture of tissues, allowing cells to interact in ways that better reflect their in vivo environments[128]. It facilitates critical cell-ECM interactions, including adhesion, migration, and proliferation, allowing cells to respond appropriately to their microenvironment[72]. In addition, molecules such as integrins contained within the ECM regulate cellular behavior by providing a rich signaling environment and support functions such as survival and differentiation[132].

Matrigel is widely used in 3D culture models of the endometrium to better mimic physiological structures compared to traditional 2D models[71],[129]. Matrigel is derived from Engelbreth-Holm-Swarm (EHS) mouse sarcoma and consists predominantly of laminin, collagen IV, entactin, and growth factors. These components provide a supportive environment for cell growth, allowing cells to organize into three-dimensional structures. Various 3D culture models use Matrigel to encapsulate endometrial glandular epithelial cells and stromal cells, promoting the development of polarized structures that resemble the in vivo endometrial environment[79].

Decidualization is a critical process that prepares the endometrium for embryo implantation during pregnancy and progesterone plays a critical role in maintaining decidual gene expression. It involves morphological and functional changes in stromal cells and transforms them into specialized decidua cells. The process is initiated by signals from the embryo and involves the proliferation and differentiation of stromal cells, significant gene expression changes, and increased secretory activity. The most basic biomarkers of the process include specific genes such as prolactin (PRL) and insulin-like growth factor binding protein-1 (IGFBP-1). At the same time, these markers and morphological transformations serve as indicators of endometrial receptivity for successful implantation and early pregnancy[133]. Powerful tools have been developed to stimulate the mouse uterus to induce uterine decidualization. There are three well-established mouse models for studying decidualization: natural pregnancy decidualization, artificial decidualization, and in vitro decidualization. Decidualization, caused by natural pregnancy, occurs when fertile females mate with fertile males of the species' progeny. In the artificial decidualization model, external inducers such as sesame oil or glass beads are used, or mouse uterine scratches can be used. In the in vitro decidualization model, cultured stromal cells are induced by incubation with estrogen and progesterone[134],[135]. In this study, an attempt was made to establish a culture environment with stromal cells that were already decidualized in the culture medium. For this reason, stroma cells were isolated from uteruses obtained from previously mated females, and then cell culture medium (REPRO medium) with added estrogen and progesterone was used to support decidualization. As a result, it was observed that more PRL and IGFBP1 genes were expressed in the endometrial stromal cells induced in the experimental group without any treatment and subsequently cultured in REPRO medium. This shows that the **decidualization process can be carried out *in vitro*** in our established 3D culture.

The implantation process is governed by a complex interaction of genes and molecular pathways. Key players include the Leukemia Inhibitory Factor (LIF), which facilitates communication between the embryo and the uterus, and members of the HOX gene family, specifically HOXA10 and HOXA11, which are essential for endometrial receptivity[8],[136]. Integrins such as αvβ3 and α4β1, fibronectin, and entactin mediate blastocyst adhesion to the endometrial epithelium[42],[137]. Estrogen and progesterone

receptors (ER and PR) play important roles in endometrial preparation[138]. Insulin-like Growth Factors (IGFs), fibronectin, laminin, and various cytokines, growth factors, and chemokines contribute to angiogenesis, and tissue remodeling during implantation[32]. The coordination of these genes is crucial for the success of implantation, embryo implantation, and the onset of early pregnancy.

E-cadherin, also known as epithelial cadherin (E-Cad), is a protein that plays an important role in cell-cell adhesion, especially in the context of epithelial tissues, and is important in defining the apicobasal polarity of the epithelium[47],[48]. E-Cad, also found in the uterine endometrium, is essential for the biogenesis of epithelium. During the menstrual cycle, dynamic changes in E-Cad expression occur depending on hormone expression[43],[45]. Some studies suggest that changes in E-Cad expression or function may be associated with implantation failure and infertility. However, there is some controversy regarding E-Cad expressed during embryo implantation. Some studies report loss of E-Cad in endometrial epithelial cells at the site of implantation[139]. In previous studies it was showed that there is a dramatic cell loss in the mouse luminal epithelium after normal estrus, and if pregnancy occurs, this cell loss is prevented in the first 3 days until embryo invasion begins. Tiwari et. al.'s observation of E-Cadherin (E-Cad) distribution in the early stages of embryo implantation revealed dynamic changes in its localization in the luminal epithelial cells of the endometrium. In particular, the study suggested that one day before the beginning of embryo invasion, when the epithelial cell layer remained intact, the apical staining of E-Cad decreased from the basolateral membrane of the luminal epithelial cells, while the apical staining was preserved. They also reported that when the embryo is in the implantation window, E-Cad expression becomes stronger apico-laterally and no basal expression is observed[46]. In our study, we found that in control groups E-cad expression decreased in the 3D endometrial coculture area at 72 hours of blastocyst implantation compared to 24 hours. This result is in line with previous studies and is an indication of the **E-cadherin expression decrease in the endometrium during the invasion phase in our proposed culture model,** as *in vivo* counterparts.

Nidogen is a basement membrane glycoprotein found in almost all basement membranes[33]. Nidogen-1 contributes to the fusion of basement membranes by acting

as a bridge between laminin-1 and type IV collagen[37],[140] but it also binds fibronectin[141]. It is known that decidual cells express nidogen-1 as part of the pericellular basement membrane that arises during decidualization[142]. Changes in nidogen mRNA levels have been reported during the formation of the placenta in the mouse. It revealed highly restricted expression in decidua and maternal endothelial cells[143]. In their study, White et al. showed that there was much earlier nidogen-1 protein expression in decidual cells, glandular epithelial cells, and epithelial basement membrane in artificially induced decidua, and they found that the expression of the NID1 gene increased abnormally during faulty decidualization[144]. In the 3D endometrial coculture we established, it was observed that entactin expression occurred and did not change between the 24th and 72nd hours. This shows that the continuity of the created culture is maintained at the 72nd hour and **decidualization continues to be supported**.

Fibronectin is an extracellular matrix (ECM) protein that plays an important role in the implantation process. Studies have revealed the importance of fibronectin-integrin interactions in blastocyst attachment and growth. Kayışlı et al. reported that extracellular matrix molecules laminin and fibronectin and their receptor subunits integrin β4 and α5 play an active role in decidual tissue formation and implantation in rats[145]. Fibronectin facilitates implantation by bridging integrins on the endometrium with those on the blastocyst. During blastocyst attachment, trophoblast cells gain the ability to adhere through the accumulation of integrins on their apical surfaces. Integrins, especially α5β1 subunits, increase on the apical surface of adhesive blastocysts, facilitating their ability to bind to fibronectin[31]. Fibronectin is most prominent at the site of implantation, and this fibronectin expression corresponds to the expression of integrin 5 in invading cytotrophoblast cells[42]. Fibronectin expression was also observed in the culture medium created at the 24th hour, and a decrease, although not significant, was observed at the 72nd hour of incubation. Based on previous studies, this can be interpreted as ***fibronectin expression in the implantation area to increase embryo and endometrial attachment, and after the attachment occurs, the expression tends to decrease***. It is thought that significance in the decrease can be achieved if the culture period is extended.

Leukemia inhibitory factor (LIF) is a member of the interleukin-6 family and plays an important role in the regulation of various cellular functions by binding to membrane-bound LIF receptors (LIFR) and gp130[146]. In mice, uterine LIF exhibits biphasic expression, with peaks in the glands and the stroma surrounding the implanting blastocyst during uterine receptivity preparation[147]. LIF is involved in uterine luminal epithelial changes during the implantation window, including increased synthesis of growth factors, cytokines, and adhesion molecules[148]–[150]. In mice, the highest expression of LIF in the glands is observed before implantation[151],[152]. Epithelial-derived LIF acts as an autocrine regulator of endometrial priming. LIF-deficient female mice experience implantation failure[152]. In humans, LIF expression is highest in uterine glands during the mid-luteal phase and is detected in uterine luminal fluid during the luteal phase and the expected period of implantation[153]–[155]. LIF induce the synthesis of growth factors and implantation genes such as Msx-1 and Wnt-4 by binding to LIFR on blastocyst or endometrial surfaces during receptivity[156]. LIF is required for the differentiation of stromal cells into primary decidual cells in mice. Furthermore, the interaction of LIF with adhesion molecules (L-selectins, E-cadherins) and tight junction proteins during endometrial receptivity remains unclear[157]. During implantation, invasion is facilitated through interaction with basement membranes and various extracellular matrix proteins controlled by LIF, MMPs (2, 9, and 14), and TIMPs[158],[159]. In our study, it was observed that LIF expression increased significantly at the 72nd hour of coculture. This shows that **LIF expression is directly proportional to the increase in invasion** and shows that the **3D coculture** culture environment we created already **supports LIF expression** following the literature.

ER (estrogen receptors) and PR (progesterone receptors) are steroid hormone receptors that play an important role in regulating the implantation process during pregnancy[160]. There are two different estrogen receptors, ERα and ERβ, which are expressed in the epithelium and stroma of the human endometrium. ER-α has a broad spectrum of expression, whereas ER-β exhibits a more restricted pattern. Disruption of ER-α leads to infertility and reproductive abnormalities[161]. Although ER-β plays a role in ovulation efficiency, it is not crucial for fertility[162]. ERα is upregulated during the proliferative phase, and its downregulation during the implantation window is driven primarily by the progesterone hormone. ERs, through their expression patterns and

interactions with progesterone, are involved in preparing the endometrium for embryo implantation[163]. High ERα levels at implantation have been associated with decreased β3 integrin expression in certain conditions, such as polycystic ovary syndrome and endometriosis[164]. Progesterone is considered the pregnancy hormone and acts through PR, which consists of two isoforms (PRA and PRB). It is expressed in endometrial epithelium and stroma. The expression patterns of ER-α, ER-β, and PR differ in different uterine cell types during early pregnancy[165]. ER-α expression in the uterine epithelium is associated with epithelial cell proliferation. Stromal cell expression of ER-α and PR is associated with stromal cell proliferation during implantation. Stromal cells undergo differentiation into progesterone-sensitive peristaltic cells during the perforation process, which is characterized by morphological changes. Endometrial receptivity to embryo implantation is a transient process driven by the duration of exposure to progesterone following adequate exposure to estrogen[166]–[169]. ER and PR expressions were also observed in the endometrial coculture we created. As a result, although not significant, there was a slight decrease in ER expression in the 72nd hour of culture compared to 24 hours, while a significant decrease in PR expression was observed. The ER result is consistent with previous literature. PR expression is expected to be maintained throughout implantation process. Diao and colleagues demonstrated that progesterone receptor (PR) in the mouse uterus exhibits distinct temporal expression patterns during early pregnancy, especially during the peri-implantation period. As a result of the study, initially, PR expression was found in the uterine luminal epithelium (LE) at 0.5 weeks of pregnancy. 1.5 from the day. increased until day 2 and preimplantation 2.5. and 3.5. They found that it was upregulated in both the LE and the stroma on days 15. However, PR is 3.5 and 4.5. They reported the complete disappearance of LE between gestational days. This disappearance coincides with multiple complex processes of embryo implantation, including apposition, attachment, and invasion, highlighting the potential importance of PR in these events[170]. Accordingly, the amounts of endometrial and stromal cells used during the co-culture setup may have caused us to obtain this result. The fact that **half of the epithelial and stroma cells were used when creating culture and the loss of progesterone receptors** in epithelial cells due to implantation may have caused us to obtain this result. For this reason, it may be necessary to use a certain proportion of cells in such a culture setup.

Matrix metalloproteinase-9 (MMP-9) is a protein involved in the invasion of trophoblast cells during the implantation process. MMPs, including MMP-9, are required for erosion of the extracellular matrix (ECM) in the uterine epithelium and accelerate implantation[171]. Expression of MMP-9 and MMP-2 is particularly notable during implantation, with the highest expression observed on day 3 of pregnancy. In vitro studies involving trophoblast cells show that MMP-9 significantly increases cell invasion. Dysregulated expression of MMPs has been associated with infertility and early pregnancy loss in women[172],[173]. Lower concentration of MMP-9 in uterine fluid has been observed in women with idiopathic infertility and recurrent miscarriages[173]. MMP-9 deficiency in mice is associated with reduced litter size and an increased percentage of infertile mice[174]. Both qRT-PCR and immunofluorescence staining show that **mmp9 expression increases significantly from hour 24 to hour 72** in the coculture groups we created. The increase in Mmp9 according to the literature shows that the created culture positively supports invasion.

Wnt4, a member of the Wnt ligand family, is regulated by estrogen in the pregnant mouse uterus[175]. During early pregnancy, from day 0.5 to day 4.5, Wnt4 mRNA is weakly expressed in the luminal epithelium and decreases by day 4.5[174]. Wnt4 then localizes to the stromal cells surrounding the implanting embryo and remains in the decidua. WNT4 plays a critical role in stromal cell survival during decidualization, which is an integral part of embryo implantation[176]. Conditional ablation of Wnt4 in uterus causes deficiency in embryo implantation and subsequent decidualization and associated severe infertility. It is characterized by a reduction in uterine glands in $Wnt4^{d/d}$ mice, contributing to the implantation defect. It also negatively affects the expression of leukemia inhibitory factor (LIF), which is a very important factor for preimplantation processes. Wnt4 is subject to hormonal regulation, particularly by estrogen. Long-term exposure to estrogen induces squamous cell metaplasia in $Wnt4^{d/d}$ mice[177]. Ablation of Wnt4 leads to reduced stromal cell proliferation during decidualization and mislocalization of FOXO1, a protein associated with apoptosis regulation[178]. No difference was observed in WNT4 expression obtained from 24- and 72-hour endometrial coculture samples created in the study. In this case, we can say that

WNT4 expression is preserved in the 3D created in vitro implantation zone for 72 hours.

Homeobox A10 (HOXA10) is a gene belonging to the HOX gene family that plays a role in the regulation of embryonic development. In particular, HOXA10 is a member of the HOXA cluster, which plays a crucial role in the development of the female reproductive system[179]. Expression of HOXA10 fluctuates during the menstrual cycle and reaches highest levels during the mid-secretory phase. This timing is important because it corresponds to the implantation window when the uterus is open to the embryo[58]. Studies have shown that disruptions in HOXA10 expression can lead to uterine-induced infertility in animal models. It has been observed in previous studies that mice carrying HOXA10 mutations show implantation failure. HOXA10 expression is reduced in conditions associated with endometrial receptivity (ER) damage, such as endometriosis, adenomyosis, and hydrosalpinx[59]–[61]. Downregulation of HOXA10 in women with recurrent implantation failure and recurrent miscarriages demonstrates its importance in successful pregnancies. Studies reveal that HOXA10 regulates E-cadherin expression by binding it to its promoter region. In addition, HOXA10 acts as a transcriptional regulator of receptivity markers such as integrin αvβ3 and insulin-like growth factor binding protein 1[62]. Considering the 72-hour culture environment, HOXA10 expression appears to increase compared to the 24-hour culture environment, although it is not significant. As a gene that is important for the continuity of implantation and development, it is thought that the expression of HOXA10 will continue to increase if the culture is continued.

The overall results related to expression profile of 3D culture model mostly supported its counterparts in vivo and can be used to mimic an implantation model with certain limitations.

The ***Gm15452*** gene or "***predicted gene 15452***" is a pseudogene located on chromosome 1 in the mouse (Ncbi Gene ID: 100039474). As a result of RNA sequencing, it was observed that this gene was expressed at high levels in both epithelial and stromal cells, and its effectiveness in the field of implantation was investigated. There is currently no study on this gene in the literature. However, as a result of the knockout of related part,

significant changes were detected in the implantation parameters. By using the Crispr/cas9 method, approximately 70% reduction in the expression of the gene at the mRNA level was achieved. It was determined that E-Cad expression, which was expected to decrease at the 72nd hour compared to the control group, continued to increase in the KO group. The LIF gene showed a normal pattern compared to the control groups, but the amount of expression was higher in the KO groups compared to the control. There is no expected decrease in PR, on the contrary, there is an increase in the KO groups. There is also an increase in MMP9, higher than the expected MMP9 increment. As all groups including NT are also considers changes in Esr1, Pr, Fibronectin, WNT and Hoxa10 were less of notice. In this case, **silencing the Gm15452 gene in endometrial stroma cells affects implantation through E-Cad, LIF and MMP9** genes.

Gm15452 pseudogene was knocked out in endometrial epithelial cells. It appears to reduce E-Cad expression at the 24th hour of cocultures compared to the control group. It increases in the 72nd hour. This is the opposite of the normally expected pattern, and E-cad expression, which should decrease, is observed to increase. In this case, it can be argued that the **knockout of Gm15452 in the epithelium can be related to E-Cad**. For Entactin expression, the KO groups, which decreased at 24 and 72 hours compared to the control groups, do not show a significant difference when evaluated with the NT groups. For this reason, it can be said that the decrease in entactin is not due to the knockout of the gene, but rather the change can be able to seen as a result of the process performed. While fibronectin expression should have decreased compared to the control group pattern, the opposite situation was reflected in the KO groups. In this case, it can be said that adherence, which should decrease at the 72nd hour, continues to increase with Gm15452 KO. When LIF, one of the function-related genes, is evaluated, there is an increase among the KO groups. There is a decrease in PR and ER expressions specifically in KOs compared to the control groups. However, there is a similar expression with NT groups, therefore it cannot be said that ER and PR are affected by Gm Epi KO. Mmp9 expression in the KO group caught up with the control pattern at 24 and 72 hours, but expression in the NT groups overshadowed the KO specificity. Other invasion parameters, Wnt4 and Hoxa10, show decreasing pattern compared to the control, but since the expression values are close to the NT groups, the results cannot be said to be reliable. In this case, it seems that **Gm15452 knockout performed in**

endometrial epithelial cells is generally more effective on E-cad and fibronectin expressions.

High mobility group AT-hook 2 (***HMGA2***) is a well-conserved transcription factor belonging to the non-histone chromosomal high mobility group (HMG) protein family[180],[181]. Its expression and biochemical modifications affect various biological processes by affecting transcriptional regulation of downstream targets[181]. HMGA2, which is highly expressed during embryonic development and in rapidly proliferating cells, exhibits low expression in most adult tissues except the testes[182],[183]. It is classified as an "oncofetal" gene associated with tumor progression in humans[184]. In the knockout Hmga2 mouse model produced using CRISPR/Cas9, it was determined that HMGA2 was effective in body and organ size, fertility and behavior by specifically disrupting the coding sequence[185]. In a study on cancer cells, Shi and colleagues found that HMGA2 disruption inhibited cell proliferation. Also, it was reported that silencing HMGA2 significantly inhibited cell migration and invasion by reducing the expression of matrix metalloproteinase-2 (MMP-2) and matrix metalloproteinase-9 (MMP-9) and increasing the expression of the epithelial marker E-cadherin[186]. In our study, it was determined that the Hmga2 gene was also expressed in endometrial epithelial cells in the implantation area. The 70% decrease in the Hmga2 gene in CRISPR/Cas9 treated epithelial cells compared to the control and non-targeted groups shows that our procedure works at the gene expression level. When the general gene distribution of NT groups is examined, there is an expression closer to the control group. In this case, it seems that the effects that can be defined as off targeted are lower in Hmga2 KO. Although E-cad has a normal pattern in the KO groups compared to the control group, it is expressed at a much lower level than the control groups. While an increase in LIF is expected at the 72nd hour, there is a decrease. This shows that Hmga2 knockout in epithelial cells may have an effect on LIF. When Mmp9 expression is examined, there is an extreme increase in the KO groups at the 24th hour and a sharp decrease is observed at the 72nd hour. In addition, a decrease in Wnt4 and Hoxa10 was detected in the KO groups both between the 24th and 72nd hours and in comparison, with the control groups. This shows that **epithelial knock out of Hmga2 has a negative interaction on both adherence, invasion and functional genes**.

UDP-glucuronic acid decarboxylase 1 (***UXS1***) is an enzyme involved in cellular metabolism. It plays a role in the detoxification and conversion of UDP-glucuronic acid (UDPGA) to UDP-xylose. UDPGA is an intermediate in the metabolic pathway produced by UDP-glucose 6-dehydrogenase (UGDH). UXS1 is located in the Golgi apparatus and participates in glycosylation processes. Doshi et al. in a recent study highlighted the therapeutic potential of UDP-glucuronic acid decarboxylase 1 (UXS1), a detoxifying enzyme. The authors identified UXS1 as being involved in the production of the toxic intermediate UDP-glucuronic acid (UDPGA) by UDP-glucose 6-dehydrogenase (UGDH). Knockdown of UXS1 appeared to be detrimental to cancer cell lines with high UGDH expression due to the accumulation of UDPGA in the medium. RNA sequencing revealed that loss of UXS1 alters Golgi structure and function, affecting glycosylation and protein trafficking. Loss of UXS1 led to defective glycosylation, increased protein degradation, and decreased overall protein levels. Also, doxycycline-inducible knockout of of UXS1 in xenograft tumors inhibited growth in UGDH high cell lines[187]. Teoh and colleagues reported a significant increase in fibronectin, identified with epithelial-mesenchymal transition (EMT), in their study on Ugdh-KO created with CRISPR/Cas9 for breast cancer cells[188]. In our study, it was determined that the Uxs1 gene was expressed in the stromal cells in the implantation area. With CRISP/Cas9 application, a decrease of around 40% was achieved in gene expression compared to the control and non-targeted groups. Since RNA expression can be seen as a result of this process, it must also be tested at the protein level in order to show the success of the applied process. E-cad also decreased in the UXS1 KO groups with a proportional decrease in the control of 24 and 72 hour in vitro culture. However, at the 24-hour evaluation, a very significant amount of E-Cad expression is seen in the KO groups. In terms of LIF expression, the increase observed from 24 to 72 in the control groups was not achieved in the KO groups. This shows the effect of the Uxs1 gene on LIF expression. PR decreases at the 72nd hour in the control, there is a decrease in the KO groups compared to the 24-hour groups. However, it is clearly observed that PR expression is greatly reduced in the KO groups. Mmp9 expression is also seriously affected by KO formation. Towards the 72nd hour, the gene that should increase decreases and this seriously affects blastocyst invasion. Although entactin appears to be at lower levels in genome edited groups compared to control groups, it increases at 24 hours compared to NT groups. It is observed that fibronectin increases in the KO

groups, although it should show a decreasing pattern compared to the control and NT groups. It was determined that Uxs1 KO stroma caused intense fibronectin expression in co-culture. When ER expression is examined, a reduction in the amount of receptors is observed in the transition from 24 hours to 72 hours. In this case, KO of the Uxs1 gene in endometrial stroma cells downregulates ER expression at implantation. Since the results in 24-hour processes give different results compared to the control and NT groups, the KO expression result obtained is not considered reliable. In this case, it may be necessary to fully support the gene expression results by detecting protein expression. On the other hand, when Wnt4 and Hoxa10 are examined, although an expression pattern similar to the control group pattern is observed, WNT4 and Hoxa10 gene expressions generally decreased compared to the control group. In Live Dead cell analysis, the decrease in the amount of live and dead cells in Uxs1 KO groups shows that the **implantation area is not sustainable in the absence of Uxs1**.

CONCLUSION

The endometrial coculture model, created in vitro can represent implantation. The decrease of E-Cad and the decrease of entactin and fibronectin, even if they are non-significant, suggest that adhesion is occurring, and invasion is starting from the 24th hour to the 72nd hour. The increase in LIF indicates that it is functionally compatible with its in vivo counterpart in both the embryo and the endometrium. It is also estimated that the invasion phase was manipulated very well. The significant increase in Mmp9 is an indicator of the invasion. There were no significant changes in Hoxa10 and WNT4, probably due to the limited duration of the culture. In particular, the apparent, although not significant, increase in Hox10 appears to be compatible with the culture's in vivo counterparts. Of course, in addition to the short cultural period, the cultural environment created may not be conducive for development. It may be possible to understand this with longer-term culture and more detailed studies.

In broad terms, the knockout of **Hmga2** in endometrial epithelial cells has a remarkable impact on implantation, influencing key genes such as **E-Cadherin, Fibronectin, LIF, Mmp9, and Wnt4**. Meanwhile, the knockout of **Uxs1** in endometrial stroma cells significantly affects implantation by modulating the **E-Cadherin, LIF, and Mmp9** genes.

Intriguingly, the knockout of the **Gm15452** gene, categorized as a pseudogene, within the endometrial epithelium particularly influences the expression of **E-Cadherin and LIF** in the implantation area. Similarly, its knockout in stromal cells affects E-Cadherin, LIF, and Mmp9.

In conclusion, the expression of Hmga2, Uxs1, and Gm15452 (a pseudogene) plays an essential role in endometrial receptivity, decidualization, and implantation. The potential significance of these genes in these processes needs further exploration

through comprehensive studies, promising to enrich and deepen our understanding of the literature.

BIBLIOGRAPHY

1. Standring S. *Gray`s Anatomy: The Anatomical Basics of Clinical Practice*. 41st ed. Elsevier Limited; 2016. Accessed December 20, 2023. https://search.worldcat.org/title/920806541
2. Ross MH, Pawlina W. *Histology A Text and Atlas With Correlated Cell and Molecular Biology*. 6th ed.; 2010. Accessed September 19, 2023. https://www.scirp.org/(S(351jmbntvnsjt1aadkozje))/reference/referencespapers.aspx?referenceid=933254
3. Moore KL. *The Developing Human: Clinically Oriented Embryology*. 10th ed.; 2016. Accessed December 20, 2023. https://search.worldcat.org/title/1198440372
4. Kierszenbaum A, Tres L. *Hisyology and Cell Biology: An Introduction to Phatology*. 4th ed. (Elsevier, ed.).; 2020. Accessed December 20, 2023. https://www.nobelkitabevi.com.tr/histoloji-ve-embriyoloji/23618-histology-and-cell-biology-an-introduction-to-pathology-5th-edition.html
5. Mescher AL. *Junqueira's Basic Histology: Text and Atlas*. 15th ed.; 2018. Accessed December 21, 2023. https://www.nobelkitabevi.com/junqueiras-basic-histology-text-and-atlas-fifteenth-edition-
6. Gilbert SF. An Introduction to Early Developmental Processes. Published online 2000. Accessed January 24, 2024. https://www.ncbi.nlm.nih.gov/books/NBK9992/
7. Ochoa-Bernal MA, Fazleabas AT. Physiologic Events of Embryo Implantation and Decidualization in Human and Non-Human Primates. *International Journal of Molecular Sciences 2020, Vol 21, Page 1973*. 2020;21(6):1973. doi:10.3390/IJMS21061973
8. Sehring J, Jeelani R. Human implantation: The complex interplay between endometrial receptivity, inflammation, and the microbiome. *Placenta*. 2022;117:179-186. doi:10.1016/j.placenta.2021.12.015
9. Cha J, Sun X, Dey SK. Mechanisms of implantation: strategies for successful pregnancy. *Nature Medicine 2012 18:12*. 2012;18(12):1754-1767. doi:10.1038/nm.3012

10. Liu D, Chen Y, Ren Y, et al. Primary specification of blastocyst trophectoderm by scRNA-seq: New insights into embryo implantation. *Sci Adv*. 2022;8(32):3725. doi:10.1126/SCIADV.ABJ3725/SUPPL_FILE/SCIADV.ABJ3725_TABLES_S1_TO_S10.ZIP
11. Ruane PT, Garner T, Parsons L, et al. Trophectoderm differentiation to invasive syncytiotrophoblast is promoted by endometrial epithelial cells during human embryo implantation. *Human Reproduction*. 2022;37(4):777-792. doi:10.1093/HUMREP/DEAC008
12. Paria BC, Song H, Dey SK. Implantation: molecular basis of embryo-uterine dialogue. *Int J Dev Biol*. 2001;45(3):597-605.
13. Llen A, Ilcox JW, Onna D, et al. Time of Implantation of the Conceptus and Loss of Pregnancy. *https://doi.org/101056/NEJM199906103402304*. 1999;340(23):1796-1799. doi:10.1056/NEJM199906103402304
14. Martín J, Domínguez F, Ávila S, et al. Human endometrial receptivity: gene regulation. *J Reprod Immunol*. 2002;55(1-2):131-139. doi:10.1016/S0165-0378(01)00140-1
15. Rashid NA, Lalitkumar S, Lalitkumar PG, Gemzell-Danielsson K. Endometrial receptivity and human embryo implantation. *American Journal of Reproductive Immunology*. 2011;66(SUPPL. 1):23-30. doi:10.1111/J.1600-0897.2011.01048.X
16. Klonos E, Katopodis P, Karteris E, Papanikolaou E, Tarlatzis B, Pados G. Endometrial changes in estrogen and progesterone receptor expression during implantation in an oocyte donation program. *Exp Ther Med*. 2020;20(6):1-1. doi:10.3892/etm.2020.9308
17. Holmberg JC, Haddad S, Wünsche V, et al. An In Vitro Model for the Study of Human Implantation. *American Journal of Reproductive Immunology*. 2012;67(2):169-178. doi:10.1111/J.1600-0897.2011.01095.X
18. Brosens JJ, Hayashi N, White JO. Progesterone receptor regulates decidual prolactin expression in differentiating human endometrial stromal cells. *Endocrinology*. 1999;140(10):4809-4820. doi:10.1210/ENDO.140.10.7070
19. Salleh N, Giribabu N. Leukemia Inhibitory Factor: Roles in Embryo Implantation and in Nonhormonal Contraception. *The Scientific World Journal*. 2014;2014. doi:10.1155/2014/201514

20. Fouladi-Nashta AA, Jones CJP, Nijjar N, et al. Characterization of the uterine phenotype during the peri-implantation period for LIF-null, MF1 strain mice. *Dev Biol*. 2005;281(1):1-21. doi:10.1016/J.YDBIO.2005.01.033
21. Su RW, Jia B, Ni H, et al. Junctional adhesion molecule 2 mediates the interaction between hatched blastocyst and luminal epithelium: induction by progesterone and LIF. *PLoS One*. 2012;7(4):e34325. doi:10.1371/JOURNAL.PONE.0034325
22. Aghajanova L, Stavreus-Evers A, Nikas Y, Hovatta O, Landgren BM. Coexpression of pinopodes and leukemia inhibitory factor, as well as its receptor, in human endometrium. *Fertil Steril*. 2003;79(3 SUPPL. 1):808-814. doi:10.1016/S0015-0282(02)04830-6
23. Rutanen EM. Insulin-like growth factors in endometrial function. *Gynecol Endocrinol*. 1998;12(6):399-406. doi:10.3109/09513599809012842
24. Fowler DJ, Nicolaides KH, Miell JP. Insulin-like growth factor binding protein-1 (IGFBP-1): a multifunctional role in the human female reproductive tract. *Hum Reprod Update*. 2000;6(5):495-504. doi:10.1093/HUMUPD/6.5.495
25. Rajkumar K, Dheen T, Krsek M, Murphy LJ. Impaired estrogen action in the uterus of insulin-like growth factor binding protein-1 transgenic mice. *Endocrinology*. 1996;137(4):1258-1264. doi:10.1210/ENDO.137.4.8625897
26. Matsumoto H, Sakai K, Iwashita M. Insulin-like growth factor binding protein-1 induces decidualization of human endometrial stromal cells via α5β1 integrin. *Mol Hum Reprod*. 2008;14(8):485-489. doi:10.1093/MOLEHR/GAN038
27. Kim SM, Kim JS. A Review of Mechanisms of Implantation. *Dev Reprod*. 2017;21(4):351. doi:10.12717/DR.2017.21.4.351
28. Sperandio M, Smith ML, Forlow SB, et al. P-selectin glycoprotein ligand-1 mediates L-selectin-dependent leukocyte rolling in venules. *J Exp Med*. 2003;197(10):1355-1363. doi:10.1084/JEM.20021854
29. Feng Y, Ma X, Deng L, et al. Role of selectins and their ligands in human implantation stage. *Glycobiology*. 2017;27(5):385-391. doi:10.1093/GLYCOB/CWX009
30. Genbacev OD, Prakobphol A, Foulk RA, et al. Trophoblast L-selectin-mediated adhesion at the maternal-fetal interface. *Science*. 2003;299(5605):405-408. doi:10.1126/SCIENCE.1079546

31. Wang J, Mayernik L, Armant DR. Integrin signaling regulates blastocyst adhesion to fibronectin at implantation: Intracellular calcium transients and vesicle trafficking in primary trophoblast cells. *Dev Biol*. 2002;245(2):270-279. doi:10.1006/dbio.2002.0644

32. Green CJ, Fraser ST, Day ML. Insulin-like growth factor 1 increases apical fibronectin in blastocysts to increase blastocyst attachment to endometrial epithelial cells in vitro. *Human Reproduction*. 2015;30(2):284-298. doi:10.1093/HUMREP/DEU309

33. Erickson AC, Couchman JR. Still more complexity in mammalian basement membranes. *J Histochem Cytochem*. 2000;48(10):1291-1306. doi:10.1177/002215540004801001

34. Carlin B, Jaffe R, Bender B, Chung AE. Entactin, a novel basal lamina-associated sulfated glycoprotein. *Journal of Biological Chemistry*. 1981;256(10):5209-5214. doi:10.1016/S0021-9258(19)69388-9

35. Kimura N, Toyoshima T, Kojima T, Shimane M. Entactin-2: a new member of basement membrane protein with high homology to entactin/nidogen. *Exp Cell Res*. 1998;241(1):36-45. doi:10.1006/EXCR.1998.4016

36. Kohfeldt E, Sasaki T, Göhring W, Timpl R. Nidogen-2: a new basement membrane protein with diverse binding properties. *J Mol Biol*. 1998;282(1):99-109. doi:10.1006/JMBI.1998.2004

37. Pujuguet P, Simian M, Liaw J, Timpl R, Werb Z, Bissell MJ. Nidogen-1 regulates laminin-1-dependent mammary-specific gene expression. *J Cell Sci*. 2000;113 (Pt 5)(Pt 5):849-858. doi:10.1242/JCS.113.5.849

38. Chakravarti S, Tam MF, Chung AE. The basement membrane glycoprotein entactin promotes cell attachment and binds calcium ions. *Journal of Biological Chemistry*. 1990;265(18):10597-10603. doi:10.1016/S0021-9258(18)86988-5

39. Senior RM, Gresham HD, Griffin GL, Brown EJ, Chung AE. Entactin stimulates neutrophil adhesion and chemotaxis through interactions between its Arg-Gly-Asp (RGD) domain and the leukocyte response integrin. *J Clin Invest*. 1992;90(6):2251-2257. doi:10.1172/JCI116111

40. Yelian FD, Edgeworth NA, Dong LJ, Chung AE, Armant DR. Recombinant entactin promotes mouse primary trophoblast cell adhesion and migration through the Arg-Gly-Asp (RGD) recognition sequence. *J Cell Biol*. 1993;121(4):923-929. doi:10.1083/JCB.121.4.923

41. Nicosia RF, Bonanno E, Smith M, Yurchenco P. Modulation of Angiogenesis in Vitro by Laminin-Entactin Complex. *Dev Biol*. 1994;164(1):197-206. doi:10.1006/DBIO.1994.1191

42. Öner H, Öner J, Demir R. Expression of nidogens in rat uterus and embryo during decidualization and implantation. *J Morphol*. 2006;267(7):822-830. doi:10.1002/JMOR.10449

43. Reardon SN, King ML, II JAML, et al. Cdh1 is essential for endometrial differentiation, gland development, and adult function in the mouse uterus. *Biol Reprod*. 2012;86(5):141-142. doi:10.1095/BIOLREPROD.112.098871/2541565

44. Sancakli Usta C, Turan G, Bulbul CB, Usta A, Adali E. Differential expression of Oct-4, CD44, and E-cadherin in eutopic and ectopic endometrium in ovarian endometriomas and their correlations with clinicopathological variables. *Reproductive Biology and Endocrinology*. 2020;18(1):1-10. doi:10.1186/S12958-020-00673-1/FIGURES/5

45. Matsuzaki S, Darcha C, Maleysson E, Canis M, Mage G. Impaired Down-Regulation of E-Cadherin and β-Catenin Protein Expression in Endometrial Epithelial Cells in the Mid-Secretory Endometrium of Infertile Patients with Endometriosis. *J Clin Endocrinol Metab*. 2010;95(7):3437-3445. doi:10.1210/JC.2009-2713

46. Tiwari A, Ashray N, Singh N, Sharma S, Modi D. Modulation of endometrial E-Cadherin and N-Cadherin by ovarian steroids and embryonic stimuli. *bioRxiv*. Published online April 8, 2021:2021.04.08.438921. doi:10.1101/2021.04.08.438921

47. Piprek RP, Kloc M, Mizia P, Kubiak JZ. The Central Role of Cadherins in Gonad Development, Reproduction, and Fertility. *International Journal of Molecular Sciences 2020, Vol 21, Page 8264*. 2020;21(21):8264. doi:10.3390/IJMS21218264

48. Fujimoto J, Ichigo S, Hori M, Tamaya T. Alteration of E-cadherin, α-and β-catenin mRNA expression in human uterine endometrium during the menstrual cycle. *Gynecological Endocrinology*. 1996;10(3):187-191. doi:10.3109/09513599609027987

49. Qiong Z, Jie H, Yonggang W, Bin X, Jing Z, Yanping L. Clinical validation of pinopode as a marker of endometrial receptivity: a randomized controlled trial. *Fertil Steril*. 2017;108(3):513-517.e2. doi:10.1016/J.FERTNSTERT.2017.07.006

50. Nikas G. Endometrial receptivity: changes in cell-surface morphology. *Semin Reprod Med*. 2000;18(3):229-235. doi:10.1055/S-2000-12561

51. Nilsson O. Ultrastructure of mouse uterine surface epithelium under different estrogenic influences. 3. Late effect of estrogen administered to spayed animals. *J Ultrastruct Res*. 1958;2(2):185-199. doi:10.1016/S0022-5320(58)90017-0

52. Psychoyos A, Mandon P. Scanning electron microscopy of the surface of the rat uterine epithelium during delayed implantation. *J Reprod Fertil*. 1971;26(1):137-138. doi:10.1530/JRF.0.0260137

53. Nardo LG, Sabatini L, Rai R, Nardo F. Pinopode expression during human implantation. *European Journal of Obstetrics and Gynecology and Reproductive Biology*. 2002;101(2):104-108. doi:10.1016/S0301-2115(01)00523-1

54. Harper MJK. 10 The implantation window. *Baillieres Clin Obstet Gynaecol*. 1992;6(2):351-371. doi:10.1016/S0950-3552(05)80092-6

55. Hawkins SM, Matzuk MM. The Menstrual Cycle. *Ann N Y Acad Sci*. 2008;1135(1):10-18. doi:10.1196/ANNALS.1429.018

56. Harper MJK. The implantation window. *Baillieres Clin Obstet Gynaecol*. 1992;6(2):351-371. doi:10.1016/S0950-3552(05)80092-6

57. Lim HJ, Dey SK. HB-EGF: A unique mediator of embryo-uterine interactions during implantation. *Exp Cell Res*. 2009;315(4):619-626. doi:10.1016/j.yexcr.2008.07.025

58. Bagot CN, Troy PJ, Taylor HS. Alteration of maternal Hoxa10 expression by in vivo gene transfection affects implantation. *Gene Ther*. 2000;7(16):1378-1384. doi:10.1038/SJ.GT.3301245

59. Daftary GS, Kayisli U, Seli E, Bukulmez O, Arici A, Taylor HS. Salpingectomy increases peri-implantation endometrial HOXA10 expression in women with hydrosalpinx. *Fertil Steril*. 2007;87(2):367-372. doi:10.1016/J.FERTNSTERT.2006.06.041

60. Celik O, Unlu C, Otlu B, Celik N, Caliskan E. Laparoscopic endometrioma resection increases peri-implantation endometrial HOXA-10 and HOXA-11 mRNA expression. *Fertil Steril*. 2015;104(2):356-365. doi:10.1016/J.FERTNSTERT.2015.04.041

61. Tiberi F, Tropea A, Romani F, Apa R, Marana R, Lanzone A. Prokineticin 1, homeobox A10, and progesterone receptor messenger ribonucleic acid expression in primary cultures of endometrial stromal cells isolated from endometrium of

healthy women and from eutopic endometrium of women with endometriosis. *Fertil Steril*. 2010;94(7):2558-2563. doi:10.1016/J.FERTNSTERT.2010.03.006

62. Bi Y, Huang W, Yuan L, et al. HOXA10 improves endometrial receptivity by upregulating E-cadherin. *Biol Reprod*. 2022;106(5):992-999. doi:10.1093/BIOLRE/IOAC007
63. Huelsken J, Vogel R, Brinkmann V, Erdmann B, Birchmeier C, Birchmeier W. Requirement for beta-catenin in anterior-posterior axis formation in mice. *J Cell Biol*. 2000;148(3):567-578. doi:10.1083/JCB.148.3.567
64. Lloyd S, Fleming TP, Collins JE. Expression of Wnt genes during mouse preimplantation development. *Gene Expression Patterns*. 2003;3(3):309-312. doi:10.1016/S1567-133X(03)00046-2
65. Hatta K, Chen Z, Carter AL, et al. Orphan Receptor Kinase ROR2 is Expressed in the Mouse Uterus. *Placenta*. 2010;31(4):327-333. doi:10.1016/J.PLACENTA.2010.01.012
66. Aoki K, Taketo MM. Tissue-specific transgenic, conditional knockout and knock-in mice of genes in the canonical Wnt signaling pathway. *Methods Mol Biol*. 2008;468:307-331. doi:10.1007/978-1-59745-249-6_24
67. Koler M, Achache H, Tsafrir A, Smith Y, Revel A, Reich R. Disrupted gene pattern in patients with repeated in vitro fertilization (IVF) failure. *Hum Reprod*. 2009;24(10):2541-2548. doi:10.1093/HUMREP/DEP193
68. Larsen EC, Christiansen OB, Kolte AM, Macklon N. New insights into mechanisms behind miscarriage. *BMC Med*. 2013;11(1). doi:10.1186/1741-7015-11-154
69. Ban Z, Knöspel F, Schneider MR. Shedding light into the black box: Advances in in vitro systems for studying implantation. *Dev Biol*. 2020;463(1):1-10. doi:10.1016/J.YDBIO.2020.04.003
70. Lee KY, Jeong JW, Tsai SY, Lydon JP, DeMayo FJ. Mouse models of implantation. *Trends Endocrinol Metab*. 2007;18(6):234-239. doi:10.1016/J.TEM.2007.06.002
71. Wang H, Pilla F, Anderson S, et al. A novel model of human implantation: 3D endometrium-like culture system to study attachment of human trophoblast (Jar) cell spheroids. *Mol Hum Reprod*. 2012;18(1):33-43. doi:10.1093/MOLEHR/GAR064

72. Li X, Kodithuwakku SP, Chan RWS, et al. Three-dimensional culture models of human endometrium for studying trophoblast-endometrium interaction during implantation. *Reproductive Biology and Endocrinology 2022 20:1*. 2022;20(1):1-19. doi:10.1186/S12958-022-00973-8

73. Carson DD, Tang JP, Gay S. Collagens support embryo attachment and outgrowth in vitro: Effects of the Arg-Gly-Asp sequence. *Dev Biol*. 1988;127(2):368-375. doi:10.1016/0012-1606(88)90323-5

74. Wu TC, Wan Y, Damjanov I. Positioning of inner cell mass determines the development of mouse blastocysts in vitro. *Development*. 1981;65(1):105-117. doi:10.1242/DEV.65.1.105

75. Hsu YC. Differentiation in vitro of mouse embryos to the stage of early somite. *Dev Biol*. 1973;33(2):403-411. doi:10.1016/0012-1606(73)90145-0

76. Kauma SW, Matt DW. Coculture cells that express leukemia inhibitory factor (LIF) enhance mouse blastocyst development in vitro. *J Assist Reprod Genet*. 1995;12(2):153-156. doi:10.1007/BF02211386/METRICS

77. Harrison SE, Sozen B, Christodoulou N, Kyprianou C, Zernicka-Goetz M. Assembly of embryonic and extraembryonic stem cells to mimic embryogenesis in vitro. *Science (1979)*. 2017;356(6334). doi:10.1126/SCIENCE.AAL1810/SUPPL_FILE/HARRISON.SM.PDF

78. Fernando SR, Chen X, Cheng KW, et al. ACE inhibitors on ACE1, ACE2, and TMPRSS2 expression and spheroid attachment on human endometrial Ishikawa cells. *Reprod Biol*. 2022;22(3):100666. doi:10.1016/J.REPBIO.2022.100666

79. Kleinman HK, Martin GR. Matrigel: Basement membrane matrix with biological activity. *Semin Cancer Biol*. 2005;15(5):378-386. doi:10.1016/J.SEMCANCER.2005.05.004

80. Park DW, Choi DS, Ryu HS, Kwon HC, Joo H, Min CK. A well-defined in vitro three-dimensional culture of human endometrium and its applicability to endometrial cancer invasion. *Cancer Lett*. 2003;195(2):185-192. doi:10.1016/S0304-3835(03)00131-9

81. Bodke V V., Burdette JE. Advancements in Microfluidic Systems for the Study of Female Reproductive Biology. *Endocrinology*. 2021;162(10). doi:10.1210/ENDOCR/BQAB078

82. De Bem THC, Tinning H, Vasconcelos EJR, Wang D, Forde N. Endometrium On-a-Chip Reveals Insulin- and Glucose-induced Alterations in the

Transcriptome and Proteomic Secretome. *Endocrinology*. 2021;162(6). doi:10.1210/ENDOCR/BQAB054

83. Nikolakopoulou K, Turco MY. Investigation of infertility using endometrial organoids. *Reproduction*. 2021;161(5):R113-R127. doi:10.1530/REP-20-0428
84. Yu L, Wei Y, Duan J, et al. Blastocyst-like structures generated from human pluripotent stem cells. *Nature 2021 591:7851*. 2021;591(7851):620-626. doi:10.1038/s41586-021-03356-y
85. Vander Borght M, Wyns C. Fertility and infertility: Definition and epidemiology. *Clin Biochem*. 2018;62:2-10. doi:10.1016/J.CLINBIOCHEM.2018.03.012
86. Mascarenhas MN, Flaxman SR, Boerma T, Vanderpoel S, Stevens GA. National, Regional, and Global Trends in Infertility Prevalence Since 1990: A Systematic Analysis of 277 Health Surveys. *PLoS Med*. 2012;9(12):e1001356. doi:10.1371/JOURNAL.PMED.1001356
87. WHO Scientific Group on Recent Advances in Medically Assisted Conception. Recent advances in medically assisted conception : report of a WHO Scientific Group. Published online 1992:111.
88. Coughlan C, Ledger W, Wang Q, et al. Recurrent implantation failure: definition and management. *Reprod Biomed Online*. 2014;28(1):14-38. doi:10.1016/J.RBMO.2013.08.011
89. Rinehart J. Recurrent implantation failure: definition. *J Assist Reprod Genet*. 2007;24(7):284-287. doi:10.1007/S10815-007-9147-4
90. Salumets A, Suikkari AM, Mäkinen S, Karro H, Roos A, Tuuri T. Frozen embryo transfers: implications of clinical and embryological factors on the pregnancy outcome. *Hum Reprod*. 2006;21(9):2368-2374. doi:10.1093/HUMREP/DEL151
91. Zinaman MJ, Clegg ED, Brown CC, O'Connor J, Selevan SG. Reprint of: Estimates of human fertility and pregnancy loss. *Fertil Steril*. 2019;112(4):e229-e235. doi:10.1016/j.fertnstert.2019.08.096
92. Larsen EC, Christiansen OB, Kolte AM, Macklon N. New insights into mechanisms behind miscarriage. *BMC Med*. 2013;11(1). doi:10.1186/1741-7015-11-154
93. Zeyneloglu HB, Onalan G. Remedies for recurrent implantation failure. *Semin Reprod Med*. 2014;32(4):297-305. doi:10.1055/S-0034-1375182
94. Zeadna A, Son WY, Moon JH, Dahan MH. A comparison of biochemical pregnancy rates between women who underwent IVF and fertile controls who

conceived spontaneously†. *Hum Reprod*. 2015;30(4):783-788. doi:10.1093/HUMREP/DEV024

95. Orvieto R, Meltcer S, Nahum R, Rabinson J, Anteby EY, Ashkenazi J. The influence of body mass index on in vitro fertilization outcome. *Int J Gynaecol Obstet*. 2009;104(1):53-55. doi:10.1016/J.IJGO.2008.08.012
96. Waylen AL, Metwally M, Jones GL, Wilkinson AJ, Ledger WL. Effects of cigarette smoking upon clinical outcomes of assisted reproduction: a meta-analysis. *Hum Reprod Update*. 2009;15(1):31-44. doi:10.1093/HUMUPD/DMN046
97. Nepomnaschy PA, Welch KB, McConnell DS, Low BS, Strassmann BI, England BG. Cortisol levels and very early pregnancy loss in humans. *Proceedings of the National Academy of Sciences*. 2006;103(10):3938-3942. doi:10.1073/PNAS.0511183103
98. Pasch LA, Gregorich SE, Katz PK, et al. Psychological distress and in vitro fertilization outcome. *Fertil Steril*. 2012;98(2):459-464. doi:10.1016/J.FERTNSTERT.2012.05.023
99. Kwak-Kim JYH, Chung-Bang HS, Ng SC, et al. Increased T helper 1 cytokine responses by circulating T cells are present in women with recurrent pregnancy losses and in infertile women with multiple implantation failures after IVF. *Hum Reprod*. 2003;18(4):767-773. doi:10.1093/HUMREP/DEG156
100. Yamada H, Morikawa M, Kato EH, Shimada S, Kobashi G, Minakami H. Pre-conceptional natural killer cell activity and percentage as predictors of biochemical pregnancy and spontaneous abortion with normal chromosome karyotype. *Am J Reprod Immunol*. 2003;50(4):351-354. doi:10.1034/J.1600-0897.2003.00095.X
101. Geva E, Amit A, Lerner-Geva L, et al. Prednisone and aspirin improve pregnancy rate in patients with reproductive failure and autoimmune antibodies: a prospective study. *Am J Reprod Immunol*. 2000;43(1):36-40. doi:10.1111/J.8755-8920.2000.430107.X
102. Azem F, Many A, Yovel I, Amit A, Lessing JB, Kupferminc MJ. Increased rates of thrombophilia in women with repeated IVF failures. *Hum Reprod*. 2004;19(2):368-370. doi:10.1093/HUMREP/DEH069
103. Cicinelli E, Matteo M, Tinelli R, et al. Prevalence of chronic endometritis in repeated unexplained implantation failure and the IVF success rate after

antibiotic therapy. *Hum Reprod*. 2015;30(2):323-330. doi:10.1093/HUMREP/DEU292

104. Moreno I, Codoñer FM, Vilella F, et al. Evidence that the endometrial microbiota has an effect on implantation success or failure. *Am J Obstet Gynecol*. 2016;215(6):684-703. doi:10.1016/J.AJOG.2016.09.075
105. Raziel A, Friedler S, Schachter M, Kasterstein E, Strassburger D, Ron-El R. Increased frequency of female partner chromosomal abnormalities in patients with high-order implantation failure after in vitro fertilization. *Fertil Steril*. 2002;78(3):515-519. doi:10.1016/S0015-0282(02)03298-3
106. Sutter P De, Stadhouders R, Dutré M, Gerris J, Dhont M. Prevalence of chromosomal abnormalities and timing of karyotype analysis in patients with recurrent implantation failure (RIF) following assisted reproduction. *Facts Views Vis Obgyn*. 2012;4(1):59. Accessed January 18, 2024. /pmc/articles/PMC3991441/
107. Lambalk CB, Banga FR, Huirne JA, et al. GnRH antagonist versus long agonist protocols in IVF: a systematic review and meta-analysis accounting for patient type. *Hum Reprod Update*. 2017;23(5):560-579. doi:10.1093/HUMUPD/DMX017
108. Saccone G, Schoen C, Franasiak JM, Scott RT, Berghella V. Supplementation with progestogens in the first trimester of pregnancy to prevent miscarriage in women with unexplained recurrent miscarriage: a systematic review and meta-analysis of randomized, controlled trials. *Fertil Steril*. 2017;107(2):430-438.e3. doi:10.1016/J.FERTNSTERT.2016.10.031
109. Jansen R, Van Embden JDA, Gaastra W, Schouls LM. Identification of genes that are associated with DNA repeats in prokaryotes. *Mol Microbiol*. 2002;43(6):1565-1575. doi:10.1046/J.1365-2958.2002.02839.X
110. Ishino Y, Shinagawa H, Makino K, Amemura M, Nakatura A. Nucleotide sequence of the iap gene, responsible for alkaline phosphatase isozyme conversion in Escherichia coli, and identification of the gene product. *J Bacteriol*. 1987;169(12):5429-5433. doi:10.1128/JB.169.12.5429-5433.1987
111. Wiedenheft B, Sternberg SH, Doudna JA. RNA-guided genetic silencing systems in bacteria and archaea. *Nature 2012 482:7385*. 2012;482(7385):331-338. doi:10.1038/nature10886

112. Deltcheva E, Chylinski K, Sharma CM, et al. CRISPR RNA maturation by trans-encoded small RNA and host factor RNase III. *Nature 2011 471:7340*. 2011;471(7340):602-607. doi:10.1038/nature09886

113. Cai R, Lv R, Shi X, Yang G, Jin J. CRISPR/dCas9 Tools: Epigenetic Mechanism and Application in Gene Transcriptional Regulation. *International Journal of Molecular Sciences 2023, Vol 24, Page 14865*. 2023;24(19):14865. doi:10.3390/IJMS241914865

114. Wang H, Yang H, Shivalila CS, et al. One-Step Generation of Mice Carrying Mutations in Multiple Genes by CRISPR/Cas-Mediated Genome Engineering. *Cell*. 2013;153(4):910-918. doi:10.1016/J.CELL.2013.04.025

115. Long C, Li H, Tiburcy M, et al. Correction of diverse muscular dystrophy mutations in human engineered heart muscle by single-site genome editing. *Sci Adv*. 2018;4(1). doi:10.1126/SCIADV.AAP9004/SUPPL_FILE/AAP9004_SM.PDF

116. Chavez M, Chen X, Finn PB, Qi LS. Advances in CRISPR therapeutics. *Nature Reviews Nephrology 2022 19:1*. 2022;19(1):9-22. doi:10.1038/s41581-022-00636-2

117. Xiong B, Zhao Y, Beall S, Sadusky AB, Dean J. A Unique Egg Cortical Granule Localization Motif Is Required for Ovastacin Sequestration to Prevent Premature ZP2 Cleavage and Ensure Female Fertility in Mice. *PLoS Genet*. 2017;13(1). doi:10.1371/JOURNAL.PGEN.1006580

118. Wu Y, Liang D, Wang Y, et al. Correction of a genetic disease in mouse via use of CRISPR-Cas9. *Cell Stem Cell*. 2013;13(6):659-662. doi:10.1016/J.STEM.2013.10.016

119. Chemello F, Bassel-Duby R, Olson EN. Correction of muscular dystrophies by CRISPR gene editing. *J Clin Invest*. 2020;130(6):2766-2776. doi:10.1172/JCI136873

120. Zhang C, Lu T, Zhang Y, et al. Rapid generation of maternal mutants via oocyte transgenic expression of CRISPR-Cas9 and sgRNAs in zebrafish. *Sci Adv*. 2021;7(32). doi:10.1126/SCIADV.ABG4243

121. Ma H, Marti-Gutierrez N, Park SW, et al. Correction of a pathogenic gene mutation in human embryos. *Nature*. 2017;548(7668):413-419. doi:10.1038/NATURE23305

122. Fogarty NME, McCarthy A, Snijders KE, et al. Genome editing reveals a role for OCT4 in human embryogenesis. *Nature*. 2017;550(7674):67-73. doi:10.1038/NATURE24033

123. Whyte JJ, Meyer AE, Spate LD, et al. Inactivation of porcine interleukin-1β results in failure of rapid conceptus elongation. *Proc Natl Acad Sci U S A*. 2018;115(2):307-312. doi:10.1073/PNAS.1718004115

124. Johns DN, Lucas CG, Pfeiffer CA, et al. Conceptus interferon gamma is essential for establishment of pregnancy in the pig†. *Biol Reprod*. 2021;105(6):1577-1590. doi:10.1093/BIOLRE/IOAB186

125. Taskin AC, Akkoc T, Caputcu AT, Arat S, Bagis H. Optimal Method of Mouse Blastomere Biopsy: In vitro Developmental Potential of the Biopsied Embryo to Blastocyst Stage after Aspirated Eight-Cell Mouse Embryos. Published online January 1, 2011. doi:10.81043/APERTA.89551

126. Balaban B, Brison D, Calderón G, et al. The Istanbul consensus workshop on embryo assessment: proceedings of an expert meeting. *Hum Reprod*. 2011;26(6):1270-1283. doi:10.1093/HUMREP/DER037

127. Gardner DK, Lane M, Stevens J, Schlenker T, Schoolcraft WB. Blastocyst score affects implantation and pregnancy outcome: towards a single blastocyst transfer. *Fertil Steril*. 2000;73(6):1155-1158. doi:10.1016/S0015-0282(00)00518-5

128. Fitzgerald HC, Schust DJ, Spencer TE. In vitro models of the human endometrium: evolution and application for women's health +. *Biol Reprod*. 2021(2):282-293. doi:10.1093/biolre/ioaa183

129. Arnold JT, Kaufman DG, Seppälä M, Lessey BA. Endometrial stromal cells regulate epithelial cell growth in vitro: a new co-culture model. *Human Reproduction*. 2001;16(5):836-845.

130. Govindasamy N, Long H, Jeong HW, et al. 3D biomimetic platform reveals the first interactions of the embryo and the maternal blood vessels. *Dev Cell*. 2021;56(23):3276-3287.e8. doi:10.1016/J.DEVCEL.2021.10.014

131. Bentin-Ley U, Pedersen B, Lindenberg S, Falck Larsen J, Hamberger L, Horn T. Isolation and culture of human endometrial cells in a three-dimensional culture system. *J Reprod Fertil*. 1994;101(2):327-332. doi:10.1530/JRF.0.1010327

132. Lalitkumar PGL, Lalitkumar S, Meng CX, et al. Mifepristone, but not levonorgestrel, inhibits human blastocyst attachment to an in vitro endometrial

three-dimensional cell culture model. *Hum Reprod*. 2007;22(11):3031-3037. doi:10.1093/HUMREP/DEM297

133. Gellersen B, Brosens JJ. Cyclic decidualization of the human endometrium in reproductive health and failure. *Endocr Rev*. 2014;35(6):851-905. doi:10.1210/ER.2014-1045
134. Lee KY, Jeong JW, Tsai SY, Lydon JP, DeMayo FJ. Mouse models of implantation. *Trends Endocrinol Metab*. 2007;18(6):234-239. doi:10.1016/J.TEM.2007.06.002
135. Wang C, Zhao M, Zhang WQ, et al. Comparative Analysis of Mouse Decidualization Models at the Molecular Level. *Genes (Basel)*. 2020;11(8):1-12. doi:10.3390/GENES11080935
136. Xu B, Sun X, Li L, et al. Pinopodes, leukemia inhibitory factor, integrin-b3, and mucin-1 expression in the peri-implantation endometrium of women with unexplained recurrent pregnancy loss. Published online 2012. doi:10.1016/j.fertnstert.2012.04.032
137. Marsh C, Schumacher K, Nothnick WB, et al. Secretory Phase and Implantation. *Menstrual Cycle*. Published online December 28, 2018. doi:10.5772/INTECHOPEN.81304
138. Ding YB, He JL, Liu XQ, Chen XM, Long CL, Wang YX. Expression of DNA methyltransferases in the mouse uterus during early pregnancy and susceptibility to dietary folate deficiency. *Reproduction*. 2012;144(1):91-100. doi:10.1530/REP-12-0006
139. Jha RK, Titus S, Saxena D, Kumar PG, Laloraya M. Profiling of E-cadherin, β-catenin and Ca2+ in embryo–uterine interactions at implantation. *FEBS Lett*. 2006;580(24):5653-5660. doi:10.1016/J.FEBSLET.2006.09.014
140. Fox JW, Mayer U, Nischt R, et al. Recombinant nidogen consists of three globular domains and mediates binding of laminin to collagen type IV. *EMBO J*. 1991;10(11):3137-3146. doi:10.1002/J.1460-2075.1991.TB04875.X
141. Hsieh JC, Wu C, Chung AE. The binding of fibronectin to entactin is mediated through the 29 kDa amino terminal fragment of fibronectin and the G2 domain of entactin. *Biochem Biophys Res Commun*. 1994;199(3):1509-1517. doi:10.1006/bbrc.1994.1402

142. Wewer UM, Damjanov A, Weiss J, Liotta LA, Damjanov I. Mouse endometrial stromal cells produce basement-membrane components. *Differentiation*. 1986;32(1):49-58. doi:10.1111/J.1432-0436.1986.TB00555.X

143. Thomas T, Dziadek M. Expression of laminin and nidogen genes during the postimplantation development of the mouse placenta. *Biol Reprod*. 1993;49(6):1251-1259. doi:10.1095/BIOLREPROD49.6.1251

144. White CA, Robb L, Salamonsen LA. Uterine extracellular matrix components are altered during defective decidualization in interleukin-11 receptor α deficient mice. *Reproductive Biology and Endocrinology*. 2004;2(1):1-15. doi:10.1186/1477-7827-2-76/FIGURES/4

145. Ali Kayişli Ü, Asar M, Demir R. Distributions and Possible Roles of Laminin, Fibronectin and TheirReceptor Subunits Integrin \beta4 and \alpha5 in Remodelling of ExtracellularMatrix during Decidualization in Rats. *Turkish Journal of Biology*. 2000;24(3):379-396. doi:-

146. Mathieu ME, Saucourt C, Mournetas V, et al. LIF-dependent signaling: new pieces in the Lego. *Stem Cell Rev Rep*. 2012;8(1):1-15. doi:10.1007/S12015-011-9261-7

147. Song H, Lim H. Evidence for heterodimeric association of leukemia inhibitory factor (LIF) receptor and gp130 in the mouse uterus for LIF signaling during blastocyst implantation. *Reproduction*. 2006;131(2):341-349. doi:10.1530/REP.1.00956

148. Lecce L, Kaneko Y, Madawala RJ, Murphy CR. ICAM1 and fibrinogen-γ are increased in uterine epithelial cells at the time of implantation in rats. *Mol Reprod Dev*. 2011;78(5):318-327. doi:10.1002/MRD.21307

149. Noda N, Minoura H, Nishiura R, et al. Expression of tenascin-C in stromal cells of the murine uterus during early pregnancy: induction by interleukin-1 alpha, prostaglandin E(2), and prostaglandin F(2 alpha). *Biol Reprod*. 2000;63(6):1713-1720. doi:10.1095/BIOLREPROD63.6.1713

150. Wang X, Wang H, Matsumoto H, Roy SK, Das SK, Paria BC. Dual source and target of heparin-binding EGF-like growth factor during the onset of implantation in the hamster. *Development*. 2002;129(17):4125-4134. doi:10.1242/DEV.129.17.4125

151. Bhatt H, Brunet LJ, Stewart CL. Uterine expression of leukemia inhibitory factor coincides with the onset of blastocyst implantation. *Proc Natl Acad Sci U S A*. 1991;88(24):11408. doi:10.1073/PNAS.88.24.11408

152. Stewart CL, Kaspar P, Brunet LJ, et al. Blastocyst implantation depends on maternal expression of leukaemia inhibitory factor. *Nature*. 1992;359(6390):76-79. doi:10.1038/359076A0

153. Licht P, Lösch A, Dittrich R, Neuwinger J, Siebzehnrübl E, Wildt L. Novel insights into human endometrial paracrinology and embryo-maternal communication by intrauterine microdialysis. *Hum Reprod Update*. 1998;4(5):532-538. doi:10.1093/HUMUPD/4.5.532

154. Laird SM, Tuckerman EM, Dalton CF, Dunphy BC, Li TC, Zhang X. The production of leukaemia inhibitory factor by human endometrium: presence in uterine flushings and production by cells in culture. *Hum Reprod*. 1997;12(3):569-574. doi:10.1093/HUMREP/12.3.569

155. Chen DB, Hilsenrath R, Yang ZM, et al. Leukaemia inhibitory factor in human endometrium during the menstrual cycle: cellular origin and action on production of glandular epithelial cell prostaglandin in vitro. *Hum Reprod*. 1995;10(4):911-918. doi:10.1093/OXFORDJOURNALS.HUMREP.A136060

156. Daikoku T, Song H, Guo Y, et al. Uterine Msx-1 and Wnt4 Signaling Becomes Aberrant in Mice with the Loss of Leukemia Inhibitory Factor or Hoxa-10: Evidence for a Novel Cytokine-Homeobox-Wnt Signaling in Implantation. *Molecular Endocrinology*. 2004;18(5):1238-1250. doi:10.1210/ME.2003-0403

157. Sharma A, Kumar P. Understanding implantation window, a crucial phenomenon. *J Hum Reprod Sci*. 2012;5(1):2. doi:10.4103/0974-1208.97777

158. Bai SX, Wang YL, Qin L, Xiao ZJ, Herva R, Piao YS. Dynamic expression of matrix metalloproteinases (MMP-2, -9 and -14) and the tissue inhibitors of MMPs (TIMP-1, -2 and -3) at the implantation site during tubal pregnancy. *Reproduction*. 2005;129(1):103-113. doi:10.1530/REP.1.00283

159. Staun-Ram E, Shalev E. Human trophoblast function during the implantation process. *Reproductive Biology and Endocrinology*. 2005;3(1):1-12. doi:10.1186/1477-7827-3-56/METRICS

160. Young SL. Oestrogen and progesterone action on endometrium: a translational approach to understanding endometrial receptivity. *Reprod Biomed Online*. 2013;27(5):497-505. doi:10.1016/J.RBMO.2013.06.010

161. Kuiper GGJM, Carlsson B, Grandien K, et al. Comparison of the ligand binding specificity and transcript tissue distribution of estrogen receptors alpha and beta. *Endocrinology*. 1997;138(3):863-870. doi:10.1210/ENDO.138.3.4979

162. Krege JH, Hodgin JB, Couse JF, et al. Generation and reproductive phenotypes of mice lacking estrogen receptor beta. *Proc Natl Acad Sci U S A*. 1998;95(26):15677-15682. doi:10.1073/PNAS.95.26.15677

163. Lessey BA, Killam AP, Metzger DA, Haney AF, Greene GL, McCarty KS. Immunohistochemical analysis of human uterine estrogen and progesterone receptors throughout the menstrual cycle. *J Clin Endocrinol Metab*. 1988;67(2):334-340. doi:10.1210/JCEM-67-2-334

164. Gregory CW, Wilson EM, Apparao KBC, et al. Steroid receptor coactivator expression throughout the menstrual cycle in normal and abnormal endometrium. *J Clin Endocrinol Metab*. 2002;87(6):2960-2966. doi:10.1210/JCEM.87.6.8572

165. Tan J, Paria BC, Dey SK, Das SK. Differential Uterine Expression of Estrogen and Progesterone Receptors Correlates with Uterine Preparation for Implantation and Decidualization in the Mouse. *Endocrinology*. 1999;140(11):5310. doi:10.1210/ENDO.140.11.7148

166. Huet-Hudson YM, Andrews GK, Dey SK. Cell type-specific localization of c-myc protein in the mouse uterus: modulation by steroid hormones and analysis of the periimplantation period. *Endocrinology*. 1989;125(3):1683-1690. doi:10.1210/ENDO-125-3-1683

167. Paria BC, Huet-Hudson YM, Dey SK. Blastocyst's state of activity determines the "window" of implantation in the receptive mouse uterus. *Proc Natl Acad Sci U S A*. 1993;90(21):10159-10162. doi:10.1073/PNAS.90.21.10159

168. Dunn CL, Kelly RW, Critchley HOD. Decidualization of the human endometrial stromal cell: an enigmatic transformation. *Reprod Biomed Online*. 2003;7(2):151-161. doi:10.1016/S1472-6483(10)61745-2

169. Klonos E, Katopodis P, Karteris E, Papanikolaou E, Tarlatzis B, Pados G. Endometrial changes in estrogen and progesterone receptor expression during implantation in an oocyte donation program. *Exp Ther Med*. 2020;20(6):1-1. doi:10.3892/ETM.2020.9308

170. Diao H, Paria BC, Xiao S, Ye X. Temporal expression pattern of progesterone receptor in the uterine luminal epithelium suggests its requirement during early

events of implantation. *Fertil Steril*. 2011;95(6):2087-2093. doi:10.1016/J.FERTNSTERT.2011.01.160

171. Bischof P, Martelli M, Campana A, Itoh Y, Ogata Y, Nagase H. Importance of matrix metalloproteinases in human trophoblast invasion. *Early Pregnancy*. 1995;1(4):263-269. Accessed January 23, 2024. https://europepmc.org/article/med/9363258
172. Tang M, Xu Y, Julian JA, Carson D, Tabibzadeh S. Lefty is expressed in mouse endometrium in estrous cycle and peri-implantation period. *Human Reproduction*. 2005;20(4):872-880. doi:10.1093/HUMREP/DEH717
173. Skrzypczak J, Wirstlein P, Mikołajczyk M, Ludwikowski G, Zak T. TGF superfamily and MMP2, MMP9, TIMP1 genes expression in the endometrium of women with impaired reproduction. *Folia Histochem Cytobiol*. 2007;45(I):143-148. Accessed January 23, 2024. https://journals.viamedica.pl/folia_histochemica_cytobiologica/article/view/4474
174. Dubois B, Arnold B, Opdenakker G. Gelatinase B deficiency impairs reproduction. *J Clin Invest*. 2000;106(5):627-628. doi:10.1172/JCI10910
175. Hou X, Tan Y, Li M, Dey SK, Das SK. Canonical Wnt signaling is critical to estrogen-mediated uterine growth. *Mol Endocrinol*. 2004;18(12):3035-3049. doi:10.1210/ME.2004-0259
176. Li Q, Kannan A, Wang W, et al. Bone morphogenetic protein 2 functions via a conserved signaling pathway involving Wnt4 to regulate uterine decidualization in the mouse and the human. *J Biol Chem*. 2007;282(43):31725-31732. doi:10.1074/JBC.M704723200
177. Franco HL, Dai D, Lee KY, et al. WNT4 is a key regulator of normal postnatal uterine development and progesterone signaling during embryo implantation and decidualization in the mouse. *The FASEB Journal*. 2011;25(4):1176-1187. doi:10.1096/FJ.10-175349
178. Labied S, Kajihara T, Madureira PA, et al. Progestins regulate the expression and activity of the forkhead transcription factor FOXO1 in differentiating human endometrium. *Mol Endocrinol*. 2006;20(1):35-44. doi:10.1210/ME.2005-0275
179. Du H, Taylor HS. The Role of Hox Genes in Female Reproductive Tract Development, Adult Function, and Fertility. *Cold Spring Harb Perspect Med*. 2015;6(1). doi:10.1101/CSHPERSPECT.A023002

180. Ozturk N, Singh I, Mehta A, Braun T, Barreto G. HMGA proteins as modulators of chromatin structure during transcriptional activation. *Front Cell Dev Biol*. 2014;2(MAR). doi:10.3389/FCELL.2014.00005

181. Colombo DF, Burger L, Baubec T, Schübeler D. Binding of high mobility group A proteins to the mammalian genome occurs as a function of AT-content. *PLoS Genet*. 2017;13(12). doi:10.1371/JOURNAL.PGEN.1007102

182. Liu J, Schiltz JF, Shah PC, Benson KF, Chada KK. Genomic structure and expression of the murine Hmgi(y) gene. *Gene*. 2000;246(1-2):197-207. doi:10.1016/S0378-1119(00)00073-1

183. Hirning-Folz U, Wilda M, Rippe V, Rn Bullerdiek J, Hameister H. The Expression Pattern of the Hmgic Gene During Development. *Genes Chromosomes Cancer*. 1998;23:350-357. doi:10.1002/(SICI)1098-2264(199812)23:4

184. Cattaruzzi G, Altamura S, Tessari MA, et al. The second AT-hook of the architectural transcription factor HMGA2 is determinant for nuclear localization and function. *Nucleic Acids Res*. 2007;35(6):1751-1760. doi:10.1093/NAR/GKL1106

185. Lee MO, Li J, Davis BW, et al. Hmga2 deficiency is associated with allometric growth retardation, infertility, and behavioral abnormalities in mice. *G3: Genes|Genomes|Genetics*. 2022;12(2). doi:10.1093/G3JOURNAL/JKAB417

186. Shi Z, Li X, Wu D, et al. Silencing of HMGA2 suppresses cellular proliferation, migration, invasion, and epithelial–mesenchymal transition in bladder cancer. *Tumor Biology*. 2016;37(6):7515-7523. doi:10.1007/S13277-015-4625-2/FIGURES/4

187. Brewer G. UXS1: a sweet spot for cell death. *Nature Reviews Cancer 2023 24:1*. 2023;24(1):3-3. doi:10.1038/s41568-023-00646-7

188. Teoh ST, Ogrodzinski MP, Lunt SY. UDP-Glucose 6-Dehydrogenase Knockout Impairs Migration and Decreases in vivo Metastatic Ability of Breast Cancer Cells. *bioRxiv*. Published online May 31, 2020:2020.05.30.125419. doi:10.1101/2020.05.30.125419

RNA SEQ DATA

Matrigel Enhel 24h [1, 2, 3]
UP-Regulated Ensembl Gene IDs (ranked based on Adj p-value)

	Ensembl Gene ID	padj	log2FoldChange	pvalue	stat	foldChange	log10padj	Gene Name	Type	Species	Chr	Position (Mbp)
DESeq2	ENSMUSG00000000031	1.97915E-08	8.117575601	1.03401E-11	46.26294664	277.7370051	7.716897147	H19	lncRNA	Mouse	7	142.1293
	ENSMUSG00000056758	0.017032137	2.900781367	3.67077E-06	17.03447689	7.468307795	1.768730687	Hmga2	coding	Mouse	10	120.1972

edgeR No significant differentially expressed genes were found (logFc > 1, <-1, padj < 0.05)

limma	ENSMUSG00000051285	9.21473E-10	10.51580548	2.20715E-13	9.214731E-10	5886.743393	9.035510452	Pcmtd1	coding	Mouse	1	7.1591
	ENSMUSG00000057363	0.019926864	4.137852963	1.43187E-05	0.019926864	17.60436346	1.700661046	Ubxn1	coding	Mouse	1	43.7861
	ENSMUSG00000084353	0.043193655	11.74576481	4.13031E-05	0.043193655	3434.215396	1.364580046	Gm15452	pseudo	Mouse	1	8.6621

Transwell Enhel 24h [7, 8, 9]
UP-Regulated Ensembl Gene IDs (ranked based on Adj p-value)

	Ensembl Gene ID	padj	log2FoldChange	pvalue	stat	foldChange	log10padj	Gene Name	Type	Species	Chr	Position (Mbp)
DESeq2	No significant differentially expressed genes were found (logFc > 1, padj < 0.05)											
edgeR	No significant differentially expressed genes were found (logFc > 1, <-1, padj < 0.05)											
limma	No significant differentially expressed genes were found (logFc > 1, <-1, padj < 0.05)											

Matrigel Stroma 24h vs 72h [4, 5, 6 vs 16, 17, 18]
UP-Regulated Ensembl Gene IDs (ranked based on Adj p-value)

	Ensembl Gene ID	padj	log2FoldChange	pvalue	stat	foldChange	log10padj	Gene Name	Type	Species	Chr	Position (Mbp)
DESeq2	ENSMUSG00000060026	0.000711431	5.406472687	5.62103E-07	25.03804099	42.4141169	3.144219964	Tpt1	coding	Mouse	14	76.0825
	ENSMUSG00000025980	0.004643564	4.004231587	8.64474E-06	19.61193581	16.06925998	2.184185629	Hspa8	coding	Mouse	1	55.1170
	ENSMUSG00000020064	0.032079911	1.004855638	5.02689E-05	16.43794388	2.006215436	1.49376685	Hars	coding	Mouse	10	62.0796
	ENSMUSG00000054871	0.040423809	1.67100662	0.000105857	15.0343837	3.184680484	1.393372515	Tmem158	coding	Mouse	9	123.0683
	ENSMUSG00000027358	0.040423809	2.087280611	0.000102373	15.09042391	4.162001688	1.393372515	Bmp2	coding	Mouse	2	133.3943
edgeR	ENSMUSG00000051285	1.00011E-07	9.083677702	2.44644E-11	1.00011E-07	531.4083592	6.999490557	Pcmtd1	coding	Mouse	1	7.1591
	ENSMUSG00000048538	3.82636E-06	7.374990791	1.73788E-09	3.82636E-06	165.9953239	5.440529311	Gm9825	pseudo	Mouse	1	7.2480
	ENSMUSG00000057363	0.000686184	5.628245764	5.00258E-07	0.000686184	49.46190034	3.157276217	Ubxn1	coding	Mouse	1	43.7861
	ENSMUSG00000084353	0.001755431	2.935624007	9.45867E-06	0.001755431	7.599076001	2.055772245	Gm15452	pseudo	Mouse	1	8.6621
	ENSMUSG00000026374	0.009541969	6.357675735	0.000103397	0.009541969	82.00703288	2.020362002	Tm	coding	Mouse	1	118.2225
	ENSMUSG00000041763	0.016880733	3.388260443	4.44762E-05	0.016880733	10.25503482	1.772606888	Tpp2	coding	Mouse	1	43.9729
	ENSMUSG00000025912	0.016880733	9.27071491	4.28044E-05	0.016880733	665.6920717	1.772606888	Myh11	coding	Mouse	1	9.7376
	ENSMUSG00000026463	0.017796776	4.809357499	5.15562E-05	0.017796776	30.0513417	1.749609671	Nbeal1	coding	Mouse	1	151.4469
	ENSMUSG00000019699	0.01827461	6.503386817	5.69031E-05	0.01827461	90.73497238	1.738151894	Akt3	coding	Mouse	1	176.6476
	ENSMUSG00000063659	0.034217479	3.1372231263	8.63259E-05	0.034217479	8.737584678	1.615671073	Zbtb18	coding	Mouse	1	177.2699
	ENSMUSG00000032666	0.034217479	9.190272063	9.28099E-05	0.034217479	564.1181177	1.615671073	1700025G04Rik	coding	Mouse	1	151.7202
	ENSMUSG00000015961	0.052592896	2.297867362	0.000103397	0.052592896	4.917644017	1.595206219	Adm	coding	Mouse	1	177.5905
	ENSMUSG00000026635	0.066881543	6.780003544	0.000114603	0.066881543	109.6996458	1.575418008	Epha4	coding	Mouse	1	77.3438
	ENSMUSG00000026402	0.028895121	9.387681631	0.000131499	0.028895121	669.8443372	1.539175483	Rgl1	coding	Mouse	1	152.3925
	ENSMUSG00000026475	0.032623911	2.933399388	0.000157093	0.032623911	5.253930045	1.486437348	Arpc5	coding	Mouse	1	152.6423
	ENSMUSG00000056870	0.032623911	5.684446237	0.000164106	0.032623911	51.4272951	1.486437348	Gulp1	coding	Mouse	1	44.5907
	ENSMUSG00000042772	0.038125155	6.575716335	0.000220294	0.038125155	95.38670781	1.418788394	Smg7	coding	Mouse	1	152.7127
	ENSMUSG00000026491	0.047078039	9.399680845	0.000259181	0.047078039	675.4048109	1.327188634	Abcf1	coding	Mouse	1	179.5725

limma No significant differentially expressed genes were found (logFc > 1, <-1, padj < 0.05)

Matrigel Epitel 72h [13, 14, 15]
DOWN-Regulated Ensembl Gene IDs (ranked based on Adj p-value)

	Ensembl Gene ID	padj	log2FoldChange	pvalue	stat	foldChange	log10padj	Symbol	Gene Name	Species	Chr	Position (Mbp)
DESeq2	ENSMUSG00000051855	0,039378507	-1,604621354	0,000190952	13,91808978	0,32882198	1,40474075	Met	coding	Mouse	6	30.7235
	ENSMUSG00000032116	0,013636988	-1,530185699	1,88274E-05	18,3043751	0,346232798	1,865281533	Stt3a	coding	Mouse	9	36.6406
	ENSMUSG00000040952	0,030210188	-1,48312931	0,000113939	14,89043429	0,357712066	1,519846574	Rpn1	coding	Mouse	7	24.5838
	ENSMUSG00000025151	0,029066862	-1,29493962	8,07778E-05	15,539999	0,407553166	1,536601857	Maged1	coding	Mouse	X	93.5791
	ENSMUSG00000028703	0,013636988	-1,216489873	2,20425E-05	18,00413667	0,43032845	1,865281533	Lrrc41	coding	Mouse	4	115.9325
	ENSMUSG00000015750	0,029066862	-1,036689719	9,39661E-05	15,25422849	0,487444639	1,536601857	Aph1a	coding	Mouse	3	95.8013
edgeR	ENSMUSG00000048538	0,019926864	-2,225480699	1,00477E-05	0,019926864	0,213827498	1,700561046	Gm9826	pseudo	Mouse	1	7.2480
	ENSMUSG00000066693	0,044598121	-2,158865917	5,37947E-05	0,044598121	0,223932229	1,350683437	Gm7493	pseudo	Mouse	1	9.0332
	ENSMUSG00000026374	0,044598121	-1,775257914	6,40931E-05	0,044598121	0,292142061	1,350683437	Tsn	coding	Mouse	1	118.2225
limma												

Transwell Epitel 72h [19, 20, 21]
DOWN-Regulated Ensembl Gene IDs (ranked based on Adj p-value)

	Ensembl Gene ID	padj	log2FoldChange	pvalue	stat	foldChange	log10padj	Gene Name	Type	Species	Chr	Position (Mbp)
DESeq2	ENSMUSG00000051855	0,018347105	-1,528658209	4,67561E-06	20,96577734	0,346599575	1,736432462	Met	coding	Mouse	1	30.7235
edgeR												
limma												

Matrigel Stroma 72h [4, 5, 6 vs 16, 17, 18]
DOWN-Regulated Ensembl Gene IDs (ranked based on Adj p-value)

	Ensembl Gene ID	padj	log2FoldChange	pvalue	stat	foldChange	log10padj	Gene Name	Type	Species	Chr	Position (Mbp)
DESeq2	ENSMUSG00000069495	0,000323273	-1,09721973	8,44274E-08	28,70174943	0,467416403	3,49043107	Epc2	coding	Mouse	2	49.3415
	ENSMUSG00000032366	0,000621067	-1,556124005	3,24402E-07	26,09870347	0,340063482	3,206861408	Tpm1	coding	Mouse	9	66.9299
	ENSMUSG00000033863	0,006147198	-1,563517595	6,42173E-06	20,35820132	0,338325167	2,211322823	Klf9	coding	Mouse	19	23.1186
	ENSMUSG00000051855	0,040422809	-1,631388203	0,000103404		0,322777472	1,393373515	Met	coding	Mouse	6	30.7235
	ENSMUSG00000034640	0,040422809	-1,322840986	0,000104086	15,06109744	0,399746973	1,393373515	Tiparp	coding	Mouse	3	65.4358
edgeR	ENSMUSG00000066693	0,008755431	-2,263830402	1,04855E-05	0,008755431	0,208218419	2,05772245	Gm7493	pseudo	Mouse	1	9.0332
	ENSMUSG00000081441	0,013944465	-3,351047496	2,37218E-05	0,013944465	0,09800182	1,855596146	Gm6161	pseudo	Mouse	1	9.6448
	ENSMUSG00000057335	0,013944465	-2,274054695	2,67199E-05	0,013944465	0,206748004	1,855596146	Cep170	coding	Mouse	1	176.5612
	ENSMUSG00000045210	0,016880733	-4,157214191	4,34854E-05	0,016880733	0,056047188	1,772608688	Vcpip1	coding	Mouse	1	9.7888
	ENSMUSG00000043019	0,024217479	-1,600746002	8,72934E-05	0,024217479	0,329706446	1,615871073	Edem3	coding	Mouse	1	151.6311
	ENSMUSG00000039630	0,033862268	-1,924633739	0,000178436	0,033862268	0,263407122	1,470283964	Hnrnpu	coding	Mouse	1	178.1487
	ENSMUSG00000025915	0,034655309	-2,047769803	0,000190915	0,034655309	0,24185767	1,460230219	Sgk3	coding	Mouse	1	9.8683
	ENSMUSG00000099377	0,038125155	-2,371876403	0,000219572	0,038125155	0,193194188	1,418788384	Gm6159	pseudo	Mouse	1	78.7609

Transwell Stroma 72h [22, 23, 24]

DOWN-Regulated Ensembl Gene IDs (ranked based on Adj p-value)

	Ensembl Gene ID	padj	log2FoldChange	pvalue	stat	foldChange	log10padj	Gene Name	Type	Species	Chr	Position (Mbp)
	ENSMUSG00000051855	2,55827E-05	-1,366632951	5,46056E-08	29,54598657	0,387795253	4,592053172	Mast	coding	Mouse	6	30.7235
	ENSMUSG00000003038	0,005222921	-1,387038063	3,62385E-05	17,0588804	0,382348982	2,282003414	Hmgn2	coding	Mouse	4	133.6920
	ENSMUSG00000025151	0,007191906	-1,057930164	6,14037E-05	16,05865887	0,480320682	2,143156013	Maged1	coding	Mouse	X	93.5791
	ENSMUSG00000118866	0,008191838	-1,348546033	7,43122E-05	15,69775568	0,392687605	2,086618666	Metazoa_SRP	misc_RNA	Mouse	12	69.2061
	ENSMUSG00000062014	0,014277724	-1,401343402	0,000182852	13,99957056	0,378576456	1,845341013	Cmfb	coding	Mouse	14	47.0456
	ENSMUSG00000062248	0,017237237	-1,719338087	0,000271801	13,25536077	0,303688022	1,763532335	Cks2	coding	Mouse	13	51.7993
	ENSMUSG00000038965	0,023677981	-1,023738688	0,00045486	12,29218121	0,491840115	1,625655332	Uba2l3	coding	Mouse	16	16.9699
	ENSMUSG00000000355	0,024268611	-1,265422272	0,000492106	12,1453415	0,415977594	1,614955084	Mctl1	coding	Mouse	X	37.6895
	ENSMUSG00000047045	0,029650553	-1,025538033	0,000844881	11,13995135	0,491227069	1,527967201	Tmem164	coding	Mouse	X	141.4644

DESeq2

	ENSMUSG00000066693	0,000643766	-2,00160737	7,70978E-07	0,000643766	0,249721619	3,191271706		pseudo	Mouse	1	9.0332
	ENSMUSG00000026483	0,00518750I	-6,267096218	1,49102E-05	0,005187501	0,012984226	2,285041796	Nibanl	coding	Mouse	1	151.4469
	ENSMUSG00000063659	0,010897325	-2,046020189	3,65419E-05	0,010897325	0,242151159	1,96268009	Zbtb18	coding	Mouse	1	177.2699
	ENSMUSG00000026235	0,013526432	-2,031741991	5,83175E-05	0,013526432	0,244859601	1,868816762	Epha4	coding	Mouse	1	77.3438
	ENSMUSG00000015961	0,013526432	-1,223103053	5,64074E-05	0,013526432	0,428360378	1,868816762	Adss	coding	Mouse	1	177.5905
	ENSMUSG00000026482	0,015393251	-5,482756143	7,71008E-05	0,015393251	0,022362788	1,812669643	Rgl1	coding	Mouse	1	152.3925
	ENSMUSG00000008475	0,015393251	-1,971389823	7,94031E-05	0,015393251	0,255007251	1,812669643	Arpc5	coding	Mouse	1	152.6423
	ENSMUSG00000042772	0,023362886	-2,507517685	0,000143714	0,023362886	0,175857932	1,631473515	Smg7	coding	Mouse	1	152.7127
	ENSMUSG00000026491	0,023362886	-1,851438689	0,000145493	0,023362886	0,277115884	1,631473515	Ahctf1	coding	Mouse	1	179.5725
	ENSMUSG00000025917	0,028541023	-1,555045371	0,000184577	0,028541023	0,340317826	1,544530465	Copt5	coding	Mouse	1	10.0948
	ENSMUSG00000025986	0,038452884	-1,182811524	0,000286419	0,038452884	0,440492227	1,41507108	Slc39a10	coding	Mouse	1	46.8467
edgeR	ENSMUSG00000064943	0,038452884	-1,141008951	0,000294729	0,038452884	0,453442351	1,41507108	Gm23240	snRNA	Mouse	1	48.5013
	ENSMUSG00000056763	0,042096567	-5,670981954	0,000335173	0,042096567	0,01962747	1,375753316	Cpped1	coding	Mouse	1	10.1082

Transwell Stroma 24h [10, 11, 12]

UP-Regulated Ensembl Gene IDs (ranked based on Adj p-value)

	Ensembl Gene ID	padj	log2FoldChange	pvalue	stat	foldChange	log10padj	Gene Name	Type	Species	Chr	Position (Mbp)
	ENSMUSG00000003545	7,479035-12	2,410740257	2,990945-15	61,7043667	5,317470987	11,12615493	Fosb	coding	Mouse	7	19.0366
	ENSMUSG00000026826	9,013315-06	2,311610831	9,619335-09	32,91670264	4,964370641	5,045115797	Nr4a2	coding	Mouse	2	56.9968
	ENSMUSG00000052684	0,00036813	1,927467055	1,14558E-06	23,66652864	3,803867662	3,433998904	Jun	coding	Mouse	4	94.9373
	ENSMUSG00000092341	0,002167152	2,354796371	8,095025-06	19,91529357	5,115220288	2,664110709	Malat1	lncRNA	Mouse	19	5.8457
	ENSMUSG00000091243	0,002362835	1,146757267	1,00868E-05	19,49491011	2,214156606	2,626566559	Vgll3	coding	Mouse	16	65.6121
	ENSMUSG00000107462	0,00294503	2,648159081	1,47251E-05	18,77281309	6,268668682	2,530910232	Gm7384	pseudo	Mouse	6	141.0838
	ENSMUSG00000000567	0,003100785	1,679451126	1,82015E-05	18,36884524	3,203060673	2,508528357	Sox9	coding	Mouse	11	112.6731
	ENSMUSG00000025025	0,005680815	1,782205243	4,24394E-05	16,75904862	3,439515229	2,245589317	Mxi1	coding	Mouse	19	53.2989
	ENSMUSG00000022528	0,007191906	1,682629273	6,01502E-05	16,09791642	3,210124548	2,143156013	Hes1	coding	Mouse	16	29.8832
	ENSMUSG00000056758	0,010663243	5,70760569	0,000108112	14,98948608	52,25893034	1,972110713	Hmga2	coding	Mouse	10	120.1972
	ENSMUSG00000117176	0,016107692	2,222302559	0,000214884	13,69624392	4,666376	1,792966685	Gm49879	pseudo	Mouse	17	56.5459
	ENSMUSG00000008398	0,016275732	1,206626576	0,000225811	13,60311454	2,307973367	1,788459475	Elk3	coding	Mouse	10	93.0833
	ENSMUSG00000017677	0,018204083	1,277552314	0,000301135	13,06332257	2,424273229	1,73983201	Wbp1	coding	Mouse	11	79.1302
	ENSMUSG00000021250	0,019660917	1,355501106	0,000346217	12,80217406	2,558859802	1,706396235	Fos	coding	Mouse	12	85.5207
DESeq2	ENSMUSG00000063015	0,02479048	1,071693945	0,000532737	11,99744094	2,101899871	1,605715062	Ceni	coding	Mouse	5	90.3298
	ENSMUSG00000025283	0,02479048	1,107650509	0,000542374	11,96402977	2,154944194	1,605715062	Setl	coding	Mouse	X	153.9961
	ENSMUSG00000029580	0,025723997	1,501504816	0,000631432	11,68095202	2,83137888	1,589661553	Actb	coding	Mouse	5	142.8889
	ENSMUSG00000026728	0,025723997	1,512736966	0,000622843	11,70643699	2,853508708	1,589661553	Vim	coding	Mouse	2	13.5787
	ENSMUSG00000032402	0,025723997	1,656793109	0,000628747	11,68888053	3,153148485	1,589661553	Smad3	coding	Mouse	9	63.5540
	ENSMUSG00000092505	0,027742948	1,539277922	0,000735482	11,39736895	2,906489954	1,556847397	Gm19246	pseudo	Mouse	7	42.1382
	ENSMUSG00000061288	0,029407743	1,128950945	0,000800317	11,24049649	2,186996551	1,531528305	Tesk3	coding	Mouse	5	117.2582
	ENSMUSG00000031740	0,029650553	2,497977004	0,000826524	11,18070351	5,648927576	1,527967201	Mmp2	coding	Mouse	8	93.5539
	ENSMUSG00000020827	0,031433489	1,252259889	0,000922541	10,97691044	2,382142783	1,502607416	Mink1	coding	Mouse	11	70.4537
	ENSMUSG00000031972	0,035314539	1,718627754	0,001074135	10,69520645	3,291232063	1,452046458	Acta1	coding	Mouse	8	124.6185
	ENSMUSG00000054871	0,038770903	1,024085772	0,001310348	10,32789165	2,03367025	1,411494079	Tmem158	coding	Mouse	9	123.0881
	ENSMUSG00000082874	0,04596907	1,362852149	0,001766154	9,777967665	2,571931375	1,337534282	Rpl15-ps1	pseudo	Mouse	11	21.9031
	ENSMUSG00000028060	0,0474326	1,072633363	0,001974249	9,57332485	2,103268979	1,323923068	Khdc4	coding	Mouse	3	88.5931
	ENSMUSG00000062235	0,0474326	1,196566373	0,001972277	9,57515956	2,291935387	1,323923068	Btf3-ps6	pseudo	Mouse	7	89.7567
	ENSMUSG00000032238	0,0474326	1,592429731	0,001931647	9,613380613	3,015567922	1,323923068	Rora	coding	Mouse	9	68.5611
	ENSMUSG00000039220	0,049318381	1,068858959	0,002315911	9,280619283	2,097773562	1,306991187	Ppplr10	coding	Mouse	17	36.2273
	ENSMUSG00000051285	1,85864E-18	7,869539018	4,46182E-22	1,85864E-18	233,8661124	17,73080549	Pcmtd1	coding	Mouse	1	7.1591
	ENSMUSG00000048538	1,79991E-09	3,447845723	8,62233E-13	1,79991E-09	10,91201572	8,744748965	Gm9826	pseudo	Mouse	1	7.2480
	ENSMUSG00000057363	8,949E-06	3,298931709	6,43042E-09	8,949E-06	9,841864879	5,048225693	Usp1	coding	Mouse	1	43.7861
	ENSMUSG00000084353	0,000643766	2,741280363	6,22236E-07	0,000643766	6,68663498	3,191271706	Gm15452	pseudo	Mouse	1	8.8621
	ENSMUSG00000081441	0,002483722	3,769258559	4,16432E-06	0,002483722	13,63514898	2,604897067	Gm6161	pseudo	Mouse	1	9.6448
	ENSMUSG00000026374	0,002483722	5,687226786	3,76043E-06	0,002483722	51,52593184	2,604897067	Tsn	coding	Mouse	1	118.2225
	ENSMUSG00000041763	0,005187501	2,382807857	1,46739E-05	0,005187501	5,215508277	2,285041796	Top2	coding	Mouse	1	43.9728
	ENSMUSG00000057335	0,005187501	3,348246023	1,01305E-05	0,005187501	10,18409603	2,285041796	Cep170	coding	Mouse	1	176.5612
	ENSMUSG00000025912	0,005187501	3,741327694	1,15353E-05	0,005187501	13,3737087	2,285041796	Mybl1	coding	Mouse	1	9.7376
	ENSMUSG00000045210	0,005187501	11,50896942	1,42554E-05	0,005187501	2914,372211	2,285041796	Vcpip1	coding	Mouse	1	9.7888
	ENSMUSG00000019699	0,008800012	6,099982908	2,74012E-05	0,008800012	68,59268898	2,055516721	Akt3	coding	Mouse	1	176.8476
edgeR	ENSMUSG00000043019	0,011417562	9,256839485	4,10212E-05	0,011417562	611,7674277	1,942426609	Edem3	coding	Mouse	1	151.6311
	ENSMUSG00000032666	0,013526432	8,665258948	5,49549E-05	0,013526432	405,9783401	1,868816762	1700025G04Rik	coding	Mouse	1	151.7282
	ENSMUSG00000039630	0,015393251	1,619581525	8,11141E-05	0,015393251	3,072858905	1,812669643	Hnrnpu	coding	Mouse	1	178.1487
	ENSMUSG00000056870	0,015393251	2,538524463	8,10045E-05	0,015393251	5,809985099	1,812669643	Culp1	coding	Mouse	1	44.5907
	ENSMUSG00000099377	0,023362886	1,182974837	0,000139473	0,023362886	2,270444604	1,631473515	Gm6159	pseudo	Mouse	1	78.7609
	ENSMUSG00000025915	0,023362886	2,400647415	0,000130271	0,023362886	5,280400712	1,631473515	Sgk3	coding	Mouse	1	9.8683
	ENSMUSG00000026478	0,036863619	1,921981663	0,000256059	0,036863619	3,789432117	1,433402027	Lamc1	coding	Mouse	1	153.0947
	ENSMUSG00000004364	0,036863619	2,125291164	0,000254097	0,036863619	4,362911363	1,433402027	Cul3	coding	Mouse	1	80.2426
	ENSMUSG00000042699	0,037871472	3,15056957	0,00027213	0,037871472	8,880060898	1,421687818	Dhx9	coding	Mouse	1	153.3315
	ENSMUSG00000026109	0,042096567	1,706657985	0,000345332	0,042096567	3,264038298	1,375753316	Tmeff2	coding	Mouse	1	50.9398
	ENSMUSG00000067851	0,042096567	2,697896123	0,000352905	0,042096567	6,486550039	1,375753316	Arfgef1	coding	Mouse	1	10.2078
	ENSMUSG00000026473	0,047342094	2,196479346	0,000408219	0,047342094	4,551933075	1,324752533	Glul	coding	Mouse	1	153.7757

limma

No significant differentially expressed genes were found (log2fc > 1, < -1, padj < 0.05)

ETHICS COMMITTEE DECISION

KOÇ
ÜNİVERSİTESİ

HAYVAN DENEYLERİ YEREL ETİK KURUL KARARI

Toplantı Tarihi:	29.12.2016
Protokol No:	2016.HADYEK.033
Sorumlu Araştırıcı:	Serçin Karahüseyinoğlu
Araştırma Başlığı:	CRISPR/Cas9 genom düzenleme teknolojisi kullanılarak fare modelinde implantasyon sürecini kontrol eden genlerin ortaya çıkarılması
Başlangıç tarihi:	30.12.2016
Hayvan türü ve sayıları:	342 Adet B6 CBAF1 Dişi Fare, 15 Adet B6 CBAF1 Erkek Fare, 24 Adet CD1 Dişi Fare, 15 Adet CD1 Erkek Fare

Koç Üniversitesi Etik Kurulu'na değerlendirilmek üzere başvuruda bulunduğunuz yukarıda künyesi yazılı projenizin başvuru dosyası ve ilgili belgeleri, Üniversitemiz "Hayvan Deneyleri Yerel Etik Kurulu" tarafından araştırmanın gerekçe, amaç, yaklaşım ve yöntemleri dikkate alınarak incelenmiştir.

Üniversite Senatosunun 5 Şubat 2016 tarih ve 2016/2 sayılı oturumunda kabul edilen "Hayvan Deneyleri Yerel Etik Kurulu (HADYEK) yönergesi" uyarınca yapılan inceleme sonucunda çalışmanın gerçekleştirilmesinde etik ve bilimsel sakınca bulunmadığına karar verilmiştir. Araştırmaya yukarıda verilen başlangıç tarihi itibariyle başlayabilirsiniz.

Notlar:

- Araştırma başlangıç tarihinin gecikmesi durumunda Etik Kurul'a başvurularak tarihlerin değiştirilmesi gereklidir.
- Etik Kurul incelemesi ve onayı olmadan bu araştırmada kullanılan prosedürler, formlar ya da protokollerde herhangi bir değişiklik yapılamaz.

Saygılarımla,

Prof. Dr. Hakan S. Orer
Başkan

VITA

Gizem Söyler . She completed her undergraduate education at Department of Biology. Later, she pursued her master's degree specializing in Histology and Embryology. Her master's thesis, titled "Comparison of Age-Related Anti-Müllerian Hormone, Inhibin-B Levels, and Follicle Reserve in Rat Ovaries," reflected her research interests during this period.

Subsequently, she furthered her academic journey by undertaking doctoral studies at Koç University, Institute of Health Sciences, in the Reproductive Medicine program. Her doctoral thesis primarily focuses on implantation, 3D endometrial coculture, in vitro embryo culture, and the CRISPR/Cas9 system.